Chemical, Material and Metallurgical Engineering III

Edited by
Jianmin Zeng, Jiahao Li and Hongxi Zhu

TRANS TECH PUBLICATIONS

Chemical, Material and Metallurgical Engineering III

Edited by
Jianmin Zeng
Jiahao Li
Hongxi Zhu

Chemical, Material and Metallurgical Engineering III

Selected, peer reviewed papers from the
2013 3rd International Conference on
Chemical, Metallurgical Engineering
(ICCMME 2013),
December 10-11, 2013, Zhuhai, China

Edited by

Jianmin Zeng, Jiahao Li and Hongxi Zhu

Trans Tech Publications Ltd
Kreuzstrasse 10
CH-8635 Durnten-Zurich
Switzerland
http://www.ttp.net

Volumes 881-883 of
Advanced Materials Research
ISSN print 1022-6680
ISSN cd 1022-6680
ISSN web 1662-8985

Full text available online at *http://www.scientific.net*

***Distributed** worldwide by*

Trans Tech Publications Ltd
Kreuzstrasse 10
CH-8635 Durnten-Zurich
Switzerland

Fax: +41 (44) 922 10 33
e-mail: sales@ttp.net

and in the Americas by

Trans Tech Publications Inc.
PO Box 699, May Street
Enfield, NH 03748
USA

Phone: +1 (603) 632-7377
Fax: +1 (603) 632-5611
e-mail: sales-usa@ttp.net

Preface

ICCMME series provides a forum for accessing to the most up-to-date and authoritative knowledge from both industrial and academic worlds, sharing best practice in the field of Chemical Engineering, Chemistry, Materials and Materials Processing, Metallurgical Engineering. The meeting provides an opportunity to highlight recent developments and to identify emerging and future areas of growth in this exciting field. The 1st International Conference on Chemical, Material and Metallurgical Engineering (ICCMME 2011) was successfully taken place in Beihai, China, December 23-25, 2011. Following the success of the inaugural conference, the 2nd International Conference on Chemical, Material and Metallurgical Engineering (ICCMME 2012) was held in Kunming, China, from December 15 to December 16. The 3rd International Conference on Chemical, Material and Metallurgical Engineering (ICCMME 2013) taken place in Zhuhai, China from December 10 to December 11, 2013. ICCMME 2013 brought together leaders from industry and academia to exchange and share their experiences, present research results, explore collaborations and to spark new ideas, with the aim of developing new projects and exploiting new technology in this field.

We would like to express our thanks to all the authors for their time and genuine efforts and to the reviewers for their fruitful comments during the preparation of this volume. We also take this opportunity to thank the many people and organizations who have supported this conference.

The editors

The 2013 International Conference on

Chemical, Material and Metallurgical Engineering

(ICCMME 2013)

Conference Organization

Co-Chairmen

Prof. Jianyi Kong, Wuhan University of Science and Technology, China

Prof. Olaf Diegel, Auckland University of Technology, NTZ

Prof. Zhi Lv, Nonferrous Metals Society of Guangxi, China

Prof. Jianmin Zeng, Guangxi University, China

Technical and Organizing Committee

Prof. Yanfeng Chen, Nanjing University, China

Prof. Xun Cai, Shanghai Jiaotong University, China

Prof. Laifei Cheng, Northwestern Polytechnical University, China

Prof. Yuan Gao, Guilin University of Electronic Technology, China

Prof. Hongzhen Guo, Northwestern Polytechnical University, China

Prof. Weihao Xiong, Huazhong University of Science and Technology, China

Prof. Yongping Lei, Beijing University of Technology, China

Prof. Xiang Xiong, Central South University, China

Prof. Zhanyi Cao, Jilin University, China

Prof. Deguang Cao, Guangxi University, China

Prof. Hongxi Zhu, Wuhan University of Science and Technology

Prof. Zhong Cao, Changsha University of Science and Technology, China

Prof. Xinsheng Chai, South China University of Technology, China

Prof. Mingqing Chen, Jiangnan University, China

Prof. Wenbo Du, Beijing University of Technology, China

Prof. Chenji Deng, Wuhan University of Science and Technology

Prof. Yunsheng Ding, Hefei University of Technology,China

Prof. Kaimin Liang, Tsinghua University, China

Prof. Hongliang Li, Qingdao University, China

Prof. Dehong Lu, Kunming Univ. of Science of Technology, China

Prof. Yanxuan Wen, Guangxi university, China

Prof. Kaiming Wu, Wuhan University of Science and Technology

Prof. Jiannan Xiang, Hunan University, China

Prof. Huiming Xiao, University of New Brunswick, Canada

Prof. Qianwei Xu, Tongji University, China

Prof. Anping Xu, Hebei University of Technology,China

Prof. Qiaoqin Yang, University of Saskatchewan, Canada

Prof. Mingshan Yang, Beijing Institute of Petrochemical Technology

Prof. Lin Yu, Guangdong University of Technology, China

Prof. Zhen'ou Zeng, South China University of Technology, China

Prof. Xuejun Zhang, Beijing University of Chemical Technology, China

Prof. Jianwei Guo, Guangdong University of Technology, China

Prof. Fuhou Lei, Guangxi University for Nationalities, China

Prof. Zili Liu, Guangzhou University, China

Prof. Lihe Qian, Yanshan University, China

Prof. Shahrum Abdullah, University Kebangsaan Malaysia, Malaysia

Prof. Katsuyuki Aoki, Toyohashi University of Technology, Japan

Prof. AKM Nurul Amin, International Islamic University, Malaysia

Dr. Geng Chen, University of Washington, Seattle, USA

Prof. Carlos Caceres, The University of Queensland, Australia

Dr. Mark Fong, Hong Kong Industrial Technology Research Centre

Dr. Yuantong Gu, Queensland University of Technology, Australia

Prof. Geun Jo Han, Dong-A Univeristy, Korea

Prof. Yinghe He, James Cook University, Australia

Dr. Xinjiang Hao, University of Birmingham, UK

Prof. Toshio Haga, Osaka Institute of Technology, Japan

Prof. Yun-Hae Kim, Korea Maritime University, Korea

Prof. Sagar Kamarthi, Northeastern University, USA

Prof. Jong Kook Lee, Chosun University, Korea

Prof. Jia-Horng Lin, Feng Chia University, Taiwan

Prof. Hongwei Liu, Queensland University of Technology, Australia

Dr. Zhengxin Liu, National Insti. of Adv. Ind. Sci. & Tech., Japan

Dr. Chunsheng Lu, Curtin University of Technology, Australia

Prof. Ken-ichi Manabe, Tokyo Metropolitan University, Japan

Prof. Kyung-Man Moon, Korea Maritime University, Korea

Prof. Walid Mahmoud Shewakh, Beni Suef university, Egypt

Dr. Jianjian Shi, Indiana University School of Medicine, USA

Prof. Hiroyuki Takei, Toyo University, Japan

Dr. Dongbin Wei, University of Wollongong, Australia

Dr. Gui Wang, The University of Queensland, Australia

Dr. Xingzhong Yan, South Dakota State University, USA

Prof. Raj Das, University of Auckland, New Zealand

Prof. Chuanjian Zhong, State Univ. of New York at Binghamton, USA

Prof. Huaiyong Zhu, Queensland University of Technology, Australia

Local Organizing Committee

Prof. Jitai Niu, Harbin Institute of Technology, China

Prof. Chenji Deng, Wuhan University of Science and Technology, China

Prof. Jun Hu, Shanghai Research Institute of Materials

Prof. Jianmin Zeng, Guangxi University, China

Table of Contents

Chapter 2: Catalyst and Catalytic Reaction

Chapter 3: Pharmaceutical Engineering, Biological Chemical and Biomedical

Chapter 4: Waste Disposal and Environmental Chemicals

Chapter 4: Waste Disposal and Environmental Chemicals

Chapter 5: Chemical Thermodynamics and Kinetics

Chapter 6: Food Science and Food Chemistry

Chapter 7: Composites and Polymers

Chapter 8: Micro / Nano Materials

Chapter 9: Ceramic

Chapter 10: Functional Materials

Chapter 11: Environmental Friendly Materials

Chapter 12: Building Materials

Chapter 12: Building Materials

Chapter 13: Iron, Steel and Alloys

Chapter 14: Materials Processing Technology

Chapter 15: Metallurgical Science and Technology

Chapter 16: Exploration and Extraction of Mineral Resources, Mining Engineering

Chapter 17: Measurements and Modeling in Material Science

CHAPTER 1:

Chemical Materials and Technologies

Advanced Materials Research Vols. 881-883 (2014) pp 3-8

doi:10.4028/www.scientific.net/AMR.881-883.3

Strategy in Optimization of Silicone Oil Emulsion by D-Optimal Mixture Design

Hongxin Shi [1], Shanshan Jiang [2], Haimin Shen [3], Hongke Wu[4]

Zhejiang University of Technology, State Key Laboratory Breeding Base of Green Chemistry Synthesis Technology, Hangzhou 310032, China

[1]shihxin@zjut.edu.cn, [2]718644207@qq.com , [3] hamshen@zjut.edu.cn, [4] wuhongke@zjut.edu.cn

Keywords: silicone oil emulsion; D-optimal mixture design; formulation; stability; emulsifier

Abstract: Silicon oil emulsion was prepared by mixing silicon oil with emulsifiers and water. To optimize the emulsifiers formulation, the D-optimal mixture design (DMD) in Design-Expert software was used to design the emulsifiers formulation. E-1304, AEO-3, SG-6and OP-10 were used as emulsifiers. According to the mixture design matrix given by Design Expert 8.0.5, 20 samples of silicon oil emulsion were prepared, and their stabilities were investigated. Through the establishment of the regression model, the analysis of the interaction among the variables and operating the optimization functions of the mixture design software, an optimized emulsifier formulation was given, and with which a silicon oil emulsion with high solid content (56%) and good stability was prepared.

Introduction

Silicone oil is a non-toxic polymer with unique properties such as high lubricity, excellent ability in spreading, hydrophobicity and low surface tension, thus it is widely used in personal care, leather care, fermentation industry, etc. For silicone oil is insoluble in either hydrophilic or hydrophobic solvents, a common mode of dispersing it is in the form of emulsions [1-3]. But its hydrophobicity makes it spread in water very difficultly, which limits its usage in some fields. Under the impetus of the silicone oil emulsion being used more and more widely, researchers have been paying more and more attentions to study the formulations of silicone oil emulsifiers. A large number of attempts have been made to find a good emulsifier formulation [4-6], which need much time and consume many materials. To overcome these defects, the D-optimal Mixture Design (DMD) in Design-Expert software was used to optimize the emulsifiers formulation.

DMD is an effective technique of responding surface methodology (RSM) for optimizing mixing process [7] which is different from other experiment designs, such as orthogonal design, uniform design. Its characteristic is that the total amount of components in the mixture is kept as a constant when the proportions of each component varies. Also, the number of trials needed to evaluate multiple components and their interactions are less. This method is now widely used for the formulation in metallurgical, chemical, pharmaceutical and food industries, and gives good results [8]. The mixture design can estimate the relationship between formulation and performance through regression analysis in fewer experiments. Zhang et al. studied the formulation of plant protein beverage using the mixture design, and obtained the optimized combination of walnut milk, peanut milk, and soy milk [9]. Tong and Gong optimized the blending of tea using the mixture design to obtain the lowest cost [10]. In this article, the mixture design method was used in the optimization of silicone oil emulsion with the stability as responses to explore a new optimized method of emulsifiers formulation. Through the establishment of the regression model, the analysis

of the interaction among the variables and combining the optimization functions of the mixture design software, we got an optimized emulsifiers formulation and prepared silicon oil emulsion with high solid content and good stability.

Experimental

2.1 Chemical Reagents and Instruments Dimethyl silicone oil (with a viscosity of 350cs); Non-ionic surfactants E-1304, AEO-3, SG-6and OP-10, they are all technical-grade materials; IKA agitator, TDL-50B centrifuge.

2.2 Preparation of Silicone Oil Emulsion To a 250 ml three-necked round-bottom flask equipped with a stirrer, 15 g silicon oil, 1.8 g emulsifier-mixture were added and mixed by magnetic stirring in 240r/min at room temperature for 10min. 8.5g water was added slowly to the oil phase to form a W/O emulsion with agitation in 800r/min for 10 min, then 4.7g water was added into the emulsion to make a quick phase transition to a O/W emulsion, which was still subjected to stirring until a stable silicone oil emulsion was obtained.

2.3 Testing the Stability of Emulsion The emulsion sample was added to the centrifuge tube which was then rotated in a centrifuge at the speed of 3000 r/min for 30 min. The stability of the silicon sample was valued according to its phase separation and ratio of oil floating on the emulsion surface after centrifugation. The stability standard of the emulsion was listed in Table 1.

Table 1 The stability standard of the emulsion

Oil delamination [%]	no	＜ 10	10~ 15	15~ 20	20~ 25	25~ 30	30~ 35	35~ 40	40~ 45	45~ 50	＞ 50
Stability score	10	9	8	7	6	5	4	3	2	1	0

Results and Discussion

3.1 Regression Equation The designed formulations shown in Table 2 were given by Design-Expert 8.0.5 software, in which there are 20 experiment entries of emulsifier formulations for testing the stabilities of silicon oil emulsions. The columns A, B, C and D give dosages of components E-1304, AEO-3, SG-6and OP-10 of each formulation of silicon oil emulsion, respectively. In every experiment entry or emulsifier formulation, total dosages equal to 1. Those components were mixed to a emulsifiers mixture according to Table 2, then were mixed with silicon oil in the presence of water in the ratio of W(emulsifiers mixture) : W(silicon oil) : W(water)= 6 : 50 : 44 to form silicon oil emulsion. Their stabilities were tested and recorded as actual value. Using Design-Expert 8.0.5 software, the experiment values of the stabilities in Table 2 were regressed and fitted into linear model，quadratic model and special model, respectively. Their standard variances(S), multi-correlation coefficiences(R^2), adjusted correlation coefficiences (adjusted R^2) and predicted correlation coefficiences (predicted R^2) were listed in Table 3. It was clear that $S_{\text{Special cubic model}} < S_{\text{Quadratic model}} < S_{\text{Linear model}}$, but $R^2_{\text{Special cubic model}} > R^2_{\text{Quadratic model}} > R^2_{\text{Linear model}}$, adjusted $R^2_{\text{Special cubic model}}$ > adjusted $R^2_{\text{Quadratic model}}$ > adjusted $R^2_{\text{Linear model}}$ and predicted $R^2_{\text{Special cubic model}}$ > predicted $R^2_{\text{Quadratic model}}$ > predicted $R^2_{\text{Linear model}}$. For the quadratic model, the standard deviation was 0.29 and correlation coefficient was 0.9971 respectively, so that the special cubic model was the optimized regression model with the lowest standard deviation and the highest R squared statistics. Under the help of Design-Expert 8.0.5 software, the final mathematical model of stability was given as Eq. 1.

$$Y_{\text{Stability}}=7.33A-20.99B+2.66C+5.85D+49.69AB+23.68AC+14.35AD+69.18BC+59.87BD$$
$$+9.30CD-81.44ABC-55.20ABD-45.91ACD-1.55BCD \quad \text{Eq.1}$$

According to Eq.1, every predicted valve of stabilities of 20 entries was calculated shown in Table 2, which inosculated with its actual value well.

Table 2 Mixture design matrix with the experimental and predicted values of stability

Standard no	Component dosages of each formulation				Stability	
	A	B	C	D	*Actual value*	*Predicted value*
1	0.214	0.400	0.286	0.100	10	10
2	0.148	0.480	0.261	0.111	10	10.2
3	0.236	0.477	0.186	0.102	10	9.99
4	0.229	0.400	0.100	0.271	10	10
5	0.166	0.400	0.235	0.199	8	8
6	0.100	0.568	0.232	0.100	7	6.5
7	0.100	0.424	0.300	0.176	8	8
8	0.100	0.540	0.155	0.206	9	9.01
9	0.100	0.568	0.232	0.100	6	6.5
10	0.108	0.400	0.194	0.298	7	7
11	0.300	0.400	0.155	0.145	8	8
12	0.138	0.600	0.100	0.162	0	0.000534
13	0.100	0.508	0.100	0.292	10	9.99
14	0.138	0.600	0.100	0.162	0	0.000534
15	0.261	0.533	0.106	0.100	7	7
16	0.170	0.477	0.177	0.177	10	9.98
17	0.300	0.400	0.155	0.145	10	10
18	0.108	0.400	0.194	0.298	7	7
19	0.100	0.424	0.300	0.176	8	8
20	0.181	0.480	0.100	0.238	10	10.01

A=E-1304；B=AEO-3；C=SG-6；D=OP-10；

Table 3 Regression analysis of stability

Model	S	R^2	Adjusted R^2	Predicted R^2	Remark
Linear model	2.5	0.4219	0.3135	0.0920	
Quadratic model	0.66	0.9749	0.9523	0.7903	
Special cubic model	0.29	0.9971	0.9908	0.9833	suggested

Table 4 Analysis of variance of the regression equation for stability

Source	Sum of squares	df	Mean square	F value	P-value Prob > F	
Model	172.05	13	13.23	158.47	< 0.0001	significant
Linear mixing	72.80	3	24.27	290.58	< 0.0001	
AB	4.77	1	4.77	57.17	0.0003	
AC	0.66	1	0.66	7.92	0.0306	
AD	0.18	1	0.18	2.17	0.1909	
BC	5.74		5.74	68.74	0.0002	
BD	2.27		2.27	27.22	0.0020	
CD	0.041		0.041	0.50	0.5081	
ABC	1.62		1.62	19.37	0.0046	

ABD	0.50		0.50	5.99	0.0499	
ACD	0.17		0.17	2.04	0.2030	
BCD	0.0001713		0.0001713	0.002051	0.9653	
Residual	0.50	6	0.084			
Lack of fit	0.001099		0.001099	0.011	0.9206	not significant
Pure error	0.50	5	0.100			
Cor Total	172.55	19				

The analysis of variance (ANOVA) for Special Cubic mixture Model are summarized in Table 4. The Model F-value 158.47 implies the model is significant. There is only 0.01% chance that a "Model F-Value"this large could occur due to noise. Values of "Prob > F" less than 0.0500 indicate the effect of the model condition on the response value is significant. In this case, Linear Mixture Components, AB, AC, BC, BD, ABC, ABD are significant model terms. Values greater than 0.1000 indicate the model terms are not significant. That means the interaction effect between E-1304 and AEO-3, E-1304 and SG-6, AEO-3 and SG-6, AEO-3 and OP-10, E-1304, AEO-3 and SG-6as well as E-1304, AEO-3 and OP-10 were significant for stability. The "Lack of Fit F-value" 0.01 implied the "Lack of Fit" was not significant compared to the pure error. There was a 92.06% chance that a "Lack of Fit F-value" this large could occur due to noise. Non-significant lack of fit was good to which we want the model to fit. The rationality of the model can be checked by the determination coefficient R^2. The regression models were highly significant ($p < 0.05$) for stability with satisfactory coefficient of determination (R^2= 0.9971) .

3.2 The Effect of Emulsifier Dosage on the Stability of the Silicone Oil Emulsion To obtain more detailed interrelations and interactions, contour plots were shown in Fig. 1 and Fig. 2. E-1304, AEO-3, SG-6and OP-10 were used as emulsifiers among which the dosage of one component was fixed and othe three were variable to investigate the effect of the their interaction on the stability of the silicon oil emulsion.

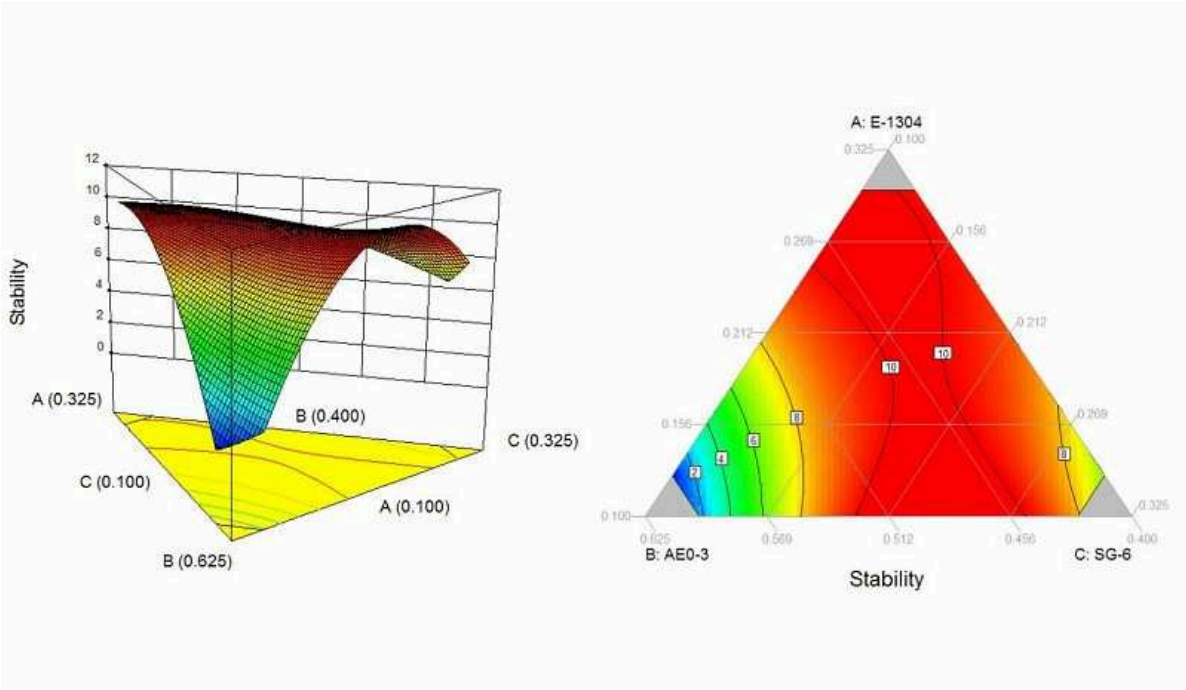

Fig. 1 Response surface plot and its contour plot of the stablity of silicone oil emulsion versus emulsifier E-1304, AEO-3 and SG-6content

Fig.1 showed the effect of the interaction of E-1304, AEO-3 and SG-6 on the stability of silicone oil emulsion when OP-10 was fixed as a constant (0.2); Fig.2 showed the effect of the interaction of E-1304 AEO-3 and OP-10 on the stability of silicone oil emulsion when SG-6 was fixed as a constant (0.1); Silicone oil emulsion would exhibit good stability in the red area in Fig.1 and Fig.2, and the ratios of E-1304, AEO-3, SG-6 and OP-10 were 0.1~0.3, 0.4~0.5, 0.1~0.25, and 0.1~0.3, respectively. If the ratios of various emulsifiers fall in the red areas in Fig.1 and Fig.2, the silicone oil emulsion prepared will give good stability. Further, if the ratios of various emulsifiers fall in the red areas between contour lines 10, silicone oil emulsion prepared will give better stability.

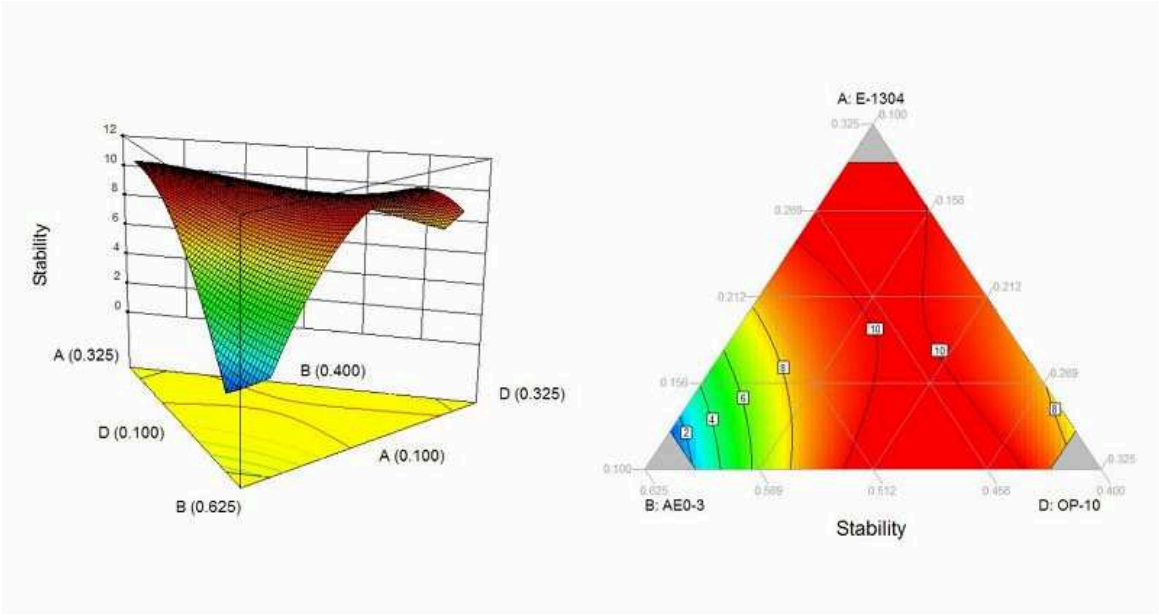

Fig. 2 Response surface plot and its contour plot of the stability of silicone oil emulsion versus emulsifier E-1304, AEO-3 and OP-10content

3.3 Optimization of the Emulsifiers Formulation The results above were obtained by changing three component dosages and fixing one component dosage, and the ratios range of E-1304, AEO-3, SG-6 and OP-10 were fixed. To meet the expectation of stability, the function of optimization in the software was used and the desired response values were set in Table 5. The software ran in a steepest climb prediction from a random combination until target stability values obtained.Three optimal emulsifiers formulations close to the target stability value were given in Table 6. The data indicated that the component ratios of three emulsifier formulations were similar，the predicted stability values were 10. So they could be used as the optimal formulations of emulsifiers for silicon oil emulsion. The three silicone oil emulsions were prepared and their stabilities were measured and listed in Table 6. The actual stabilities all were 10 and consistent with the predicted values. So that the optimal formulations of emulsifiers for silicon oil emulsion is 25%E-1304, 45% AEO-3, 10% SG-6and 20% OP-10.

Table 5 The desirable rangs for each variable and stability

Name	Target	Lowest limit	Highest limit
A(%)	In the range	0.1	0.3
B(%)	In the range	0.4	0.5
C(%)	In the range	0.1	0.25
D(%)	In the range	0.1	0.3
Stability	Maximum	0	10

Table 6 Optimal combination and predicted results

Run	E-1304	AE0-3	SG-6	OP-10	predicted Stability	Actual stability
1	0.243	0.466	0.100	0.191	10.0	10
2	0.253	0.455	0.100	0.191	10.0	10
3	0.250	0.450	0.100	0.2	10.0	10

Summary

The D-optimal mixture design in Design-Expert software was used successfully to optimize the emulsifiers formulation for preparing silicon oil emulsion. When E-1304, AEO-3, SG-6 and OP-10 were used as emulsifier mixture to prepare a silicon oil emulsion，and W(emulsifiers mixture) : W(silicon oil) : W(water)= 6 : 50 : 44 , the special cubic model is the optimal regression model, and the final mathematical model of stability obtained as :

$Y_{Stability}$=7.33A-20.99B+2.66C+5.85D+49.69AB+23.68AC+14.35AD+69.18BC+59.87BD+9.30CD -81.44ABC-55.20ABD-45.91ACD-1.55BCD.

By analyzing the interaction among the variables and operating the optimization functions of the mixture design software**,** Design Expert 8.0.5, an optimal emulsifier formulation was given as 25%E-1304, 45% AEO-3, 10% SG-6 and 20% OP-10. According to this emulsifiers formulation, a silicon oil emulsion with 56% solid content and acceptable stability was prepared.

Acknowledgements

This work was supported by the Research Fund of the Department of Science and Technology of Zhejiang Province (№ 2011R09002-10).

References

[1] S.C. Mehta, P. Somasundaran, Langmuir Vol.24 (2008), p.4558–4563.
[2] S.C. Mehta, P. Somasundaran, R. Kulkarni, J. Colloid Interface Sci. Vol. 333 (2009), p.635–640.
[3] P. Somasundaran, S.C. Mehta, P. Purohit, Adv. Colloid Interface Sci. Vol.128–130 (2006), p.103–109.
[4] D.T. Liles, F. Lin, Polymeric Delivery of Therapeutics, ACS Symp. Ser., Washington DC(2010), 207–219.
[5] K.J. Lissant, Emulsions and Emulsions Technology, Marcel Decker, New York(1974).
[6] J.M. Owen, Science and Technology of Silicones and Silicone Modified Materials, ACS. Symp. Ser., Washington DC(2007).
[7] D. Caroline, E. Marina, K. Ricardo, C. G. Hector, Chemometrics and Intelligent Laboratory Systems, Vol. 86(2007), p.1–9.
[8] Y. Wang, Q. Zhe, J. Wang, G. Fu, A Zhang, Y Chen. Journal of Jiangxi University, Vol.19(2007), p. 61-63.
[9] C. Zhang, H.R. Tong, D.M. Zhang, H.N. Li. Journal of Southwest Agricultural University (Natural Science Edition) (in Chinese), Vol.28(2) (2006), p.197-200.
[10] H. R. Tong, Z. L. Gong. Journal of Tea Science (in Chinese), Vol.24(3)(2004), p. 207-211.

Advanced Materials Research Vols. 881-883 (2014) pp 9-12

doi:10.4028/www.scientific.net/AMR.881-883.9

Wood smoke impact on Particulate Matter (PM)

Ge Peng

School of Chemical Engineering, Ningbo University of Technology, Ningbo 315016, China

gepengv@hotmail.com

Keywords: Wood combustion; Particulate matter; Smoke emission

Abstract. The emission factors and emission profiles of wood combustion tracers of different wood types were assessed. Emission profiles are additionally assessed for two advanced oven/boiler types. The emission profiles and emission ratios of wood smoke tracers to the PM emission of wood fires for the major tree species were established. From this a wood smoke profile will be derived which will be used to assess the impact of wood smoke to selected PM_{10} and $PM_{2.5}$ sampling sites. Furthermore, using the energy-normalised PM mass emission data from different types of wood combustion appliances PM reduction scenarios will be assessed with the goal of a sustainable use of wood or wood-based fuels.

Introduction

Biomass combustion is one of the recommended technologies for reducing fossil fuel consumption. Biomass combustion is performed, however, in a wide variety of fire places, oven and boiler types [1]. Biomass smoke appears to be a major primary PM source in the cold season [2]. Since $PM_{2.5}$ levels cities exceed frequently the short term standard during the cold season, an attainment of the $PM_{2.5}$ standard requires an understanding of main sources and their contributions to $PM_{2.5}$ in this time of the year [3, 4]. Results of European studies indicate that inorganic secondary constituents (ammonium, nitrate, and sulphate), wood smoke, mineral dust and traffic exhaust emissions are the major contributors to wintry $PM_{2.5}$ levels [5, 6]. Wood smoke is at rural sites the largest primary contributor to $PM_{2.5}$ levels [7, 8]. Reduction of $PM_{2.5}$ levels in rural wintry areas of Europe is thus crucially dependent on reduction plans implementing technological changes in the combustion technology of biomass fuels [9]. With the biomass impact data on rural air quality in Austria, technology based reduction scenarios of PM will be derived in order to reduce the impact of biomass smoke on atmospheric PM_{10} levels. Since biomass smoke emissions are predominantly in the "fine" size range, the data can be used also for predictionsof reductions of $PM_{2.5}$ levels [10]. The data will also allow assessing the impact of changing technology on odour levels [11]. And, on a tree species basis, specific tracers or tracer combinations will be assessed, to obtain information about the major wood species involved in the biomass derived atmospheric PM levels [12]. Considerable research on the contribution of biomass smoke to ambient aerosol levels has been performed for rainforest areas [13]. However, also at rural US sites wood combustion constitutes a major source to atmospheric PM_{10} or $PM_{2.5}$ levels [14]. Other main sources of biomass smoke in North America are wild fires and agricultural burns [15]. In Europe, a range of papers about smoke emissions from fire places appeared from Scandinavian groups [16], as well as reports about long-range transport of biomass smoke [17]. Limited data on the contribution of wood combustion to the OC using levoglucosan as a tracer are available during winter periods [18]. The energy-normalised $PM_{10}/PM_{2.5}$ emission data of different wood combustion appliances PM are important numbers to run reduction scenarios for wood or wood-based fuels.

Materials and Methods

Instrument for saccharides analysis. There are two reasons, why we apply for the saccharides analysis a HPLC-instrument: First, the analysis can be performed directly after aqueous extraction of the sample and does not require a sample preparation step. Second, the electrochemical detection has

been proven useful for many hundred samples. The instrument we used until now belonged to another group and is frequently used for other applications. Thus, for the current work, where not only the combustion samples will be analysed, but also stability studies of saccharides on aerosol filtes and extracts be performed, a dedicated analytical system is needed. Planning availability of the GC-MS instrument and oftest facility for wood stoves: Availability of the GC-MS instrument and of the oven test facility has to be arranged.

Materials and equipments. In this phase materials (dry fuel wood from specific tree species) have to be acquired, tested for humidity and stored until use. Emission profiles of saccharides and other wood smoke tracers have been determined only for a few European wood species, e.g. birch, beech, oak, spruce and larch. An overview of trees in forest stands indicates a predominance of conifers (41-99%) in the mountainous countries, and a predominance of deciduous trees in the flat terrain of Hungary (86%) [19]. Tree species with a contribution of >5% in the considered countries are: Spruce, two pines (pinus sylvestris and pinus nigra), fir (abies alba) and larch (larix decidua); Beech (fagus sylvatica), two oaks (quercus robur, quercus petraea), hornbeam (carpinus betulus), poplar (hybrids), and locust (robinia pseudoacacia) [26]. The wood smoke emission study will thus be performed with wood from 5 conifer and 6 deciduous trees. The main parameter for the quality of the fuel wood is humidity, which should be in the range of 10-20%, preferrably below 15%.

Emission testing. Emission testing is performed using a "reference" oven which has been used in a combustion test series of a variety of ovens and boilers of differentsizes. Earlier work of wood combustion tests for PM emissions revealed, that continuously fed appliances where combustion gases are directed through a combustion zone emit much lower specific PM per 7 unit of energy than ovens where logs are fired batch-wise. Thus, higher emissions of wood smoke originate from smaller appliances, which apparently dominate the wood smoke composition in the ambient air. The test combustions with fuel wood will be performed in triplicates for each wood type, with split logs, and lighted by a standardised lighter material. For each test around 10 kg of wood will be used, with PM_{10} and $PM_{2.5}$ sampling from 2 min after lightning until end of the test. The end is defined when the CO_2 level is going below 3%. PM_{10} and $PM_{2.5}$ are collected via a manifold with either PM_{10} or $PM_{2.5}$ pre-separators which allows a dilution of the stack gases in the range of 1:1 – 1:30. PM samples are collected at the manifold on eight ports, on 47mm filters (usually 6 quartz fiber filters and 2 cellulose ester filters). Residence time in the manifold is around 50 sec, temperature below 40°C. During the test flue gas temperature at the sampling port, CO, CO_2, NOx, O_2, and total gaseous hydrocarbons are determined with continuous instruments. The filters are weighed for PM mass. Components to be analysed are: carbon parameters (organic carbon - OC); elemental carbon (EC); carbonate carbon (CC)), anions, cations, cellulose, humic like substances, anhydrosugars, selected metals, selected polar and non polar organics. The data from the chemical analysis are used to derive the tracer profiles for the individual wood species.

Ambient air particulate matter analysis. Air samples will be obtained from selected sites in Ningbo. From those cities and surrounding rural sites samples have been obtained for aerosol source analysis in earlier projects. The PM_{10} (and in one case $PM_{2.5}$) aerosol filters will be determined for the same set of chemical compounds, as the emission samples.

Evaluation and discussion of data. The chemical data from the smoke samples of individual wood types have been used to derive the "emission profiles". Combining the profiles and their specific wood composition, specific profiles were obtained. The ratios of the major wood smoke tracers (e.g. levoglucosan and mannosan) in relation to OC and PM of the wood smoke emission are similar.

With the factors to derive wood smoke impact on ambient aerosol particles tracer wood smoke PM contributions on PM_{10} and $PM_{2.5}$ levels at the selected Ningbo sites were assessed. In this evaluation careful considerations of lifetimes of considered analytes have to be considered. This was be done by evaluating other measurement parameters at sites to check, whether local phenomena or larger scale phenomena are responsible for elevated PM levels at a site. The specific emission numbers of PM from wood fires from our tests in conjunction with PM emission data from other studies were used to

assess the reduction potential of biomass combustion technologies on PM levels in Austria from the combustion technology side. A wood smoke impact of around 20-40% of OC at Ningbo background levels calls for strategies to reduce the emission from biomass combustion. Our study add firm data how to influence wood smoke emissions by using different fuels. Together with newer data on PM emissions from different types of ovens ways for a sustainable use of wood fuels will be assessed.

Summary

In the current climate issue biomass combustion is one of the recommended technologies for reducing fossil fuel consumption. Biomass combustion however is not free of atmospheric emissions of particulate matter and of gaseous pollutants. The emission of particulate matter is critically dependent on wood type and combustion technology. In this research we assessed the contribution of biomass combustion to atmospheric PM levels and odours of biomass burning. By investigating PM and odour emissions of different wood types and considering available information about the impact of different combustion technologies as well as available new technologies, the ways of a sustainable development of biomass combustion were assessed. The broader implications of this study are information about ways of the sustainable use of biomass in combustion processes. Since atmospheric fine particles potentially influence cloud formation and climate forcing parameters, the results from the current research will be of importance for cloud chemistry and physics research and on aerosol impact on climate issues.

References

[1] X. Querol, A. Alastuey, C. R. Ruiz, B. Artiñano, H. C. Hansson, R. M. Harrison, E. Buringh, H. M. Brink, M. Lutz, P. Bruckmann, P. Straehl and J. Schneider: Atmos. Environ. Vol. 38 (2004), p. 6547

[2] R. V. Dingenen, F. Raes, J. Putaud, U. Baltensperger, A. Charron, M. Facchini, S. Decesari, S. Fuzzi, R. Gehrig, H. Hansson, R. M. Harrison, C. Hueglin, A. M. Jones, P. Laj, G. Lorbeer, W. Maenhaut, F. Palmgren, X. Querol, S. Rodriguez, J. Schneider, H. Brink, P. Tunved, K. Torseth, B. Wehner, E. Weingartner, A. Wiedensohler and P. Wahlin: Atmos. Environ. Vol. 38 (2004), p. 2561

[3] Z. Zdrahal, J. Oliveira, R. Vermeylen, M. Claeys and W. Maenhaut: Environ. Sci. Tech. Vol. 36 (2002), p. 747

[4] P. Formenti, W. Elbert, W. Maenhaut, J.Haywood, S. Osborne and M.O. Andreae: J. Geophys. Res. Vol. 108 (2003), p. 8488

[5] T. Novakov, M. O. Andreae, R. Gabriel, T. W. Kirchstetter, O. L. Mayol-Bracero and V. Ramanathan: Geophys. Res. Letters Vol. 27 (2000), p. 4061

[6] S. A. Guazzotti, D. T. Suess, K. R. Coffee, P. K. Quinn, T. S. Bates, A. Wisthaler, A. Hansel, W. P. Ball, R. R. Dickerson, C. Neususs, P. J. Crutzen and K. A. Prather: J. Geophys. Res. Vol. 108 (2003), ACL13/1-ACL13/14

[7] M. Zheng, G. R. Cass, J. Schauer and E. S. Edgerton: Envir. Sci. Tech. Vol. 36 (2002), p. 2361

[8] W. Liu, Y. Wang, A. Russell and E. S. Edgerton: Atmos. Environ. Vol. 39 (2005), p. 4453

[9] A. Sapkota, J. M. Symons, J. Kleissl, L. Wang, M. B. Parlange, J. Ondov, P. N. Breysse, G. B. Diette, P. A. Eggleston and T. J. Buckley: Environ. Sci. Tech. Vol. 39 (2005), p. 24

[10] T. J. Ward and G. C. Smith: Atmos. Environ. Vol. 39 (2005), p.709

[11] J. Jimenez, C. Wu, C. Claiborn, T. Gould, C. D. Simpson, T. Larson and L. J. Liu: Atmos. Environ. Vol. 40 (2006), p. 639

[12] L. S. Johansson, C. Tullin, B. Leckner and P. Sjovall: Biomass and Bioenergy Vol. 25 (2003), p. 435

[13] J. Kjaellstrand and M. Olsson: Biomass and Bioenergy Vol. 27 (2004), p. 557

[14] R. Damoah, N. Spichtinger, C. Forster, P. James, I. Mattis, U. Wandinger, S. Beirle, T. Wagner and A. Stohl: Atmos. Chem. Phys. Vol. 4 (2004), p. 1311

[15] Z. Zdrahal, J. Oliveira, R. Vermeylen, M. Claeys, W. Maenhaut: Environ. Sci. Tech. Vol. 36 (2002), p. 747

[16] V. Pashynska, R. Vermeylen, G. Vas, W. Maenhaut and M. Claeys: J. Mass Spect. Vol. 37 (2002), p. 1249

[17] K. E. Yttri, C. Dye, L. H. Sloerdal and O. A. Braathen: Journal of the Air & Waste Management Association Vol. 55 (2005), p. 1169

[18] S. Szidat, T. M. Jenk, H. A. Synal, M. Kalberer, L. Wacker, I. Hajdas, A. Kasper-Giebl and U. Baltensperger: J. Geophys. Res. Vol. 111 (2005) D07206, doi:10.1029/JD006590

[19] D. R. Oros and B. R. T. Simoneit: Appl. Geochem. Vol. 16 (2001), p. 1545

Advanced Materials Research Vols. 881-883 (2014) pp 13-16

doi:10.4028/www.scientific.net/AMR.881-883.13

Quantitative Analysis of Sn-2 Palmitic Acid Content in the Triacylglycerols from Algae Oil using Enzymatic Hydrolysis

Xi Liu, Xingyu Zhao, Xudong Wang, Na Pang, Min Wang and Jun Wang[a]*

School of Biology and Chemical Engineering, Jiangsu University of Science and Technology, Zhenjiang 212018, P.R. China

[a]wangjun@just.edu.cn

Keywords: Algae oil, Lipase, Triacylglycerols (TAGs), Sn-2 Glycerel monostearte

Abstract: The enzymatic hydrolysis parameters of triacylglycerols (TAGs) in algae oil to get sn-2 glycerel monostearte including substrate amount, lipase amount and reaction time was studied, and the products of fatty acid methyl esters (FAMEs) were detected by gas chromatography (GC). The result indicated that the optimum conditions to hydrolyze TAGs in algae oil were as follows: mass ratio of substrate to lipase of 1:1, 2 mL Tris-HCl buffer, 0.2 mL $CaCl_2$ solution, 0.5 mL sodium cholate hydrate solution were added in each 30mg substrate, and reaction time of 1.5 min with 120 rpm at 40 °C, the highest palmitic acid (PA) content accounted for 9.1% of total oil.

Introduction

The main and most preferred source of nutrients for infants is breast milk, and human milk fat (HMF) is the component which provides the highest fraction for the infant's required dietary energy. So the fatty acid composition and distribution in TAGs in infant formulas have recently gained much attention, and the human milk fat substitutes (HMFS) have been developed to mimic human milk fat composition and structure from material basically based on animal oil or from tripalmitin and vegetable oil blends [1]. There is clear evidence of the importance of TAGs composition and structure for the absorption of fats and minerals in infants and that 1, 3-dioleoyl-2-palmitoyl glycerol is absorbed and transported more effectively than 1, 2-dioleoyl-3-palmitoyl glycerol. However, animal milk fat and vegetable oil, commonly used in infant formula, contains PA located predominantly at sn-1, 3 positions; so a new human milk fat substitute (HFMS) must be designed for particular purposes in infant nutrition [2].

Algae oil is abundant oil in nature. The TAGs in algae oil contains abundant fatty acid, especially palmitic acid (PA). In addition, 91% of algae oil is TAGs, which contains ample oleic acid, palmitoleic acid, linoleic acid and linolenic acid [3]. These unsaturated fatty acids are very useful for the growth and development of infants, and are essential ingredient for the composition of lipid-coated [4]. However, the content and composition of fatty acids in the TAGs of algae oil doesn't reach the international standard of HFMS. So, the process of HMFS production using algae oil has much more difficulty and challenges.

In recent years, enzymatic interesterification has received considerable attention. The interesterification of lipids catalyzed by lipases is an alternative to the chemical interesterification [5]. Nowadays, lipases are now widely used for the chemical redesign of fat for improving physical, chemical and nutritional properties. Among these lipases, porcine pancreas lipase is a good biocatalyst used to selectively hydrolyze TAGs [6, 7]. In detail, it works as a specific hydrolase which can hydrolyze sn-1,3 position of TAGs in the organic phase, and promotes enzymatic synthesis and transesterification. However, to the best of our knowledge, no report has been published about the use of the selective hydrolysis method of TAGs from algae oil [8]. Thus, a new method should be found to hydrolyze the TAGs from algae oil to obtain sn-2 glycerel monostearte.

This present study mainly focuses on the enzymatic hydrolytic method on TAGs at sn-2 position in algae oil by determination of content and recovery of fatty acid. Fig. 1 shows the hydrolysis of TAGs in algae oil to produce sn-2 glycerel monostearte and free fatty acid. The substrate amount, lipase amount and reaction time on the effects on the PAME content were investigated.

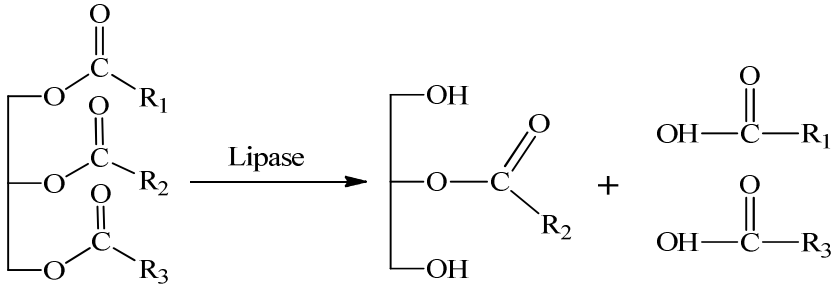

Fig. 1 Hydrolysis of TAGs from algae oil by the porcine pancreatic lipase

Materials and methods

Main materials. Porcine pancreas lipase was purchased from Sigma-Aldrich. Algae was obtained from Mertek, USA. All other solvents and reagents were purchased from Sinopharm Chemical Reagent Co., Ltd., (China), and were of analytical reagent (A. R.) grade.

The analytical method of GC. The concentration of samples was determined by GC using HP-INNOWAX (30 m×0.25 mm, id 0.25 μm). The carrier gas was nitrogen at a flow-rate of 1 mL/min with 0.5 Mpa pressure; Gas was hydrogen at flow rate of 50 mL/min with 0.5 MPa pressure. The split ratio was 50:1, injection volume: 1 μL. The injection port temperature was 250 °C, detector was 280 °C. The data was worked out correction areas normalization method [9].

Hydrolysis of sn-2 glycerel monostearte. Porcine pancreas lipase of 30 mg with 0.5 mL sodium cholate solution, 2 mL Tris-HCl buffer, and 0.2 mL $CaCl_2$ solution were performed in a centrifuge tube [10]. Then, the centrifuge tube was stirred for 2 min with 120 rpm at 40 °C, and vortexed for 1 min. N-hexane of 2 mL was added into the centrifuge tube then got supernatant. All experiments were carried out in triplicate.

Determination of sn-2 glycerel monostearte. The supernatant was coated on silica plates and make sure that it is stratified by TLC. Potassium hydroxide methanol solution of 2 mL and 2 mL n-hexane were added to the centrifuge tube at 65 °C for 1 h, it was centrifuged after adding water [11].

Calculation of fatty acid recovery. The TAGs in algae oil were used as substrate with above methods, methyl palmitate standard was added after methyl esterification. Then, GC is used to analyze composition. In addition, the triacylglycerol was process directly in the same way without adding standard [12].

$$\text{Recovery} = \frac{m_{\text{PAME with standard}} - m_{\text{PAME without standard}}}{m_{\text{standard}}} \times 100\%$$

Results and Discussion

GC chromatogram. Fig. 2 shows a gas chromatogram of fatty acid methyl esters (FAMEs) from algae oil, including lauric acid ($C_{14:0}$), PA ($C_{16:0}$), stearic acid ($C_{17:0}$), oil acid ($C_{18:0}$), linoleic acid ($C_{18:1}$), linolenic acid ($C_{18:2}$), docosapentaenoic ($C_{22:5}$), and docosahexaenoic ($C_{22:6}$).

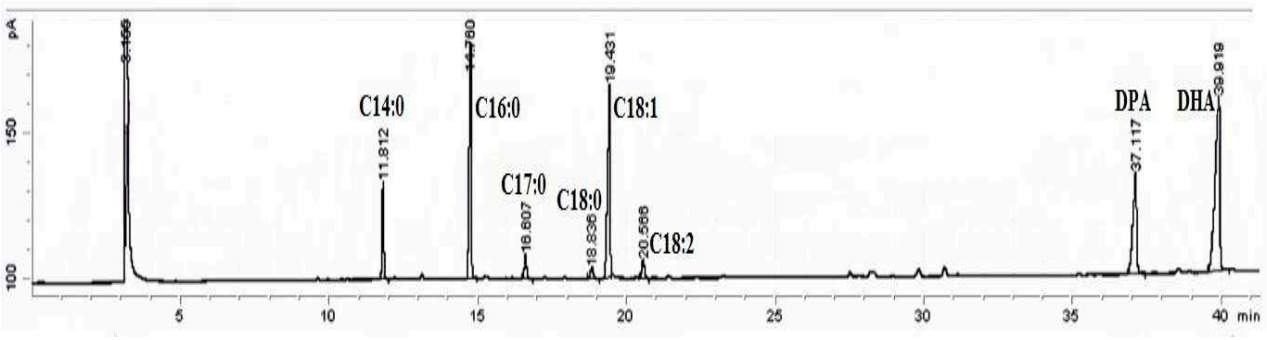

Fig. 2 The content of fatty acid methyl ester from algae oil

Effect of substrate amount. Fig. 3 shows the effect of the substrate amount on the content of PA methyl ester (PAME). Five substrate gradients were set, including 10 mg, 20 mg, 30 mg, 40 mg, and 50 mg, respectively. With the increasing substrate amount, the PAME content has a rising tend from 7.62 % to 9.03 %, the highest content of 9.03 % was gained with 30 mg substrate. The result indicates that more substrates are favorable for the reaction, but too many substrates inhibit the reaction [6]. Therefore, the suitable of substrate amount is 30 mg.

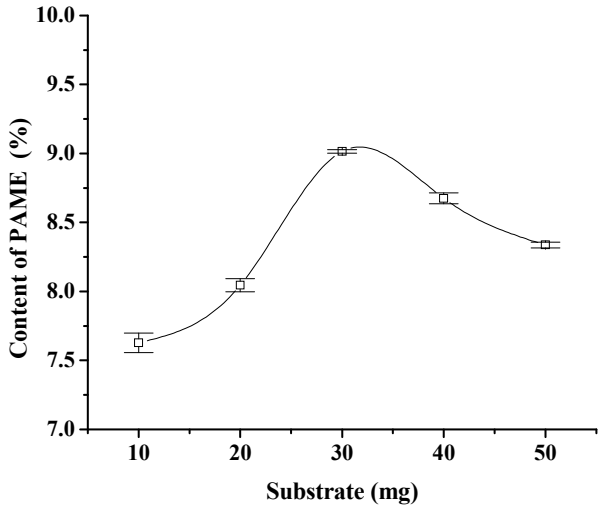

Fig. 3 Effects of substrate amount on the content of PAME

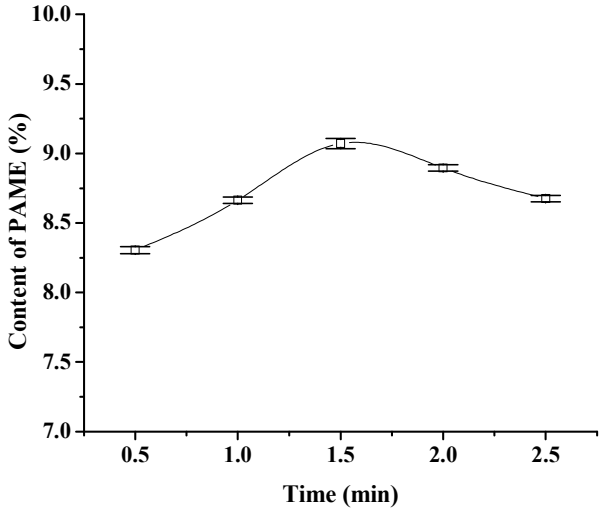

Fig. 4 Effects of lipase amount on the content of PAME

Effect of lipase amount. Fig. 4 shows the effect of lipase amount on content of PAME. Five gradients of lipase with the most suitable amount of algae oil were set, including 10 mg，20 mg，30 mg, 40 mg, and 50 mg. When the lipase amount was 30 mg, the maximum content of PAME was 9.03 %. The suitable lipase amount promotes reaction rate and more leads to substrate contacting with lipase insufficiently. Thus, the optimum lipase amount was 30 mg.

Effect of reaction time. Fig. 5 shows the effect of reaction time on the content of PAME. The most suitable algae oil amount and enzymes were mixed for five time quantum reaction, including 0.5 min, 1 min，1.5 min，2 min，and 2.5 min. When the time was 1.5 min, the PAME maximum content was achieved with 9.1 %. However, the PAME content would decrease with the increasing of reaction time. When the reaction time was extended to 2.5 min, the PAME content was decreased to 8.71 %. Too long time resulted in some glycerol monostearte decomposition which reduces the content of PAME at sn-2 position of TAGs.

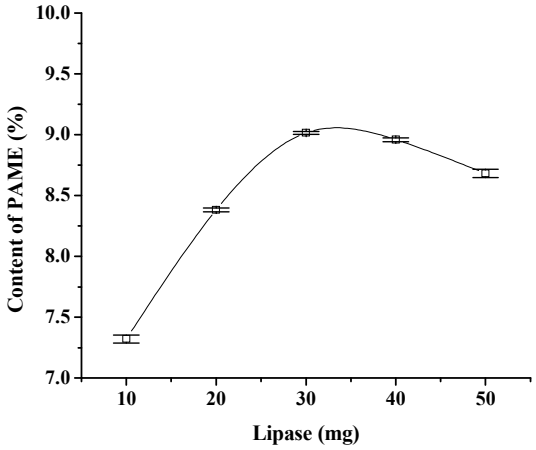

Fig. 5 Effects of time on the content of PAME.

Conclusion

Selectively enzymatic preparation of sn-2 glycerel monostearte by hydrolysising the TAGs from algae oil with porcine pancreas lipase was successfully established. The optimum conditions were as follows: the mass ratio of substrate to porcine pancreatic lipase is 1:1, and reaction time of 1.5 min. The recovery of PAME was ranging from 85.6 % to 88.3 % detected by GC. The recovery is higher than that determined by other methods.This method is a fast and efficiently way for quantitative analysising the content of sn-2 glycerel monostearte of the TAGs of algae oil.

Acknowledgements

This work was financially supported by the Undergraduate Innovation Project of China in 2013 (No. 201310289027), the Undergraduate Innovation Project of Jiangsu Province in 2013 (No. 201310289027Z), the Undergraduate Innovation Project of Jiangsu University of Science and Technology in 2013, the Graduate Innovation Project of Jiangsu University of Science and Technology in 2013, the Qing Lan Project of Jiangsu Province, and the Science and Technology Support Program of Jiangsu Province (BE2013405).

References

[1] J. Wang, J. Zhang and F. Wu: Eur. J. Lipid. Sci. Tech Vol. 115 (2013), p. 791
[2] M.F. Picciano: Pediatr. Clin. North. Am Vol. 48 (2001), p. 53
[3] Q. Zhu, J. Tang, R. Zhou , H. Gao, Y. Wang and B. Yang: China. Oil Vol. (2009), p.39
[4] H. Mu: Lipid.Tech vol. 22 (2010), p. 126
[5] Y. Wang, X. Qin, Q. Zhu, Y. Bo, R. Zhou and L. Lin: Eur. Food. Res. Tech. Vol. 230 (2010), p. 769
[6] J. Wang, G. Sun, L. Yu, F. Wu and X Guo: Bioresour. Technol. Vol. 128 (2013), p. 156
[7] J.H. Lee, J.M. Son, C.C. Akoh, M.R. Kim and K. Lee: N. Biotechnol. Vol. 27 (2010), p. 38
[8] A.M. Pina-Rodriguez and C.C. Akoh: J. Agric. Food. Chem. Vol. 57 (2009), p. 48
[9] C. Tecelão, J. Silva, E. Dubreucq, M. Ribeiro, S. Ferreira: J Mol Cat B. Vol. 65(2010), p. 122
[10] Y. Liao, R. Alvarado, B. Phinney, B. Lonnerdal: J Proteome Res. Vol. 10(2011), p. 30
[11] A. Srivastava, C. C. Akoh, Sw. Chang, G. Lee,J. Shaw: J Agric Food Chem. Vol. 54(2006), p. 51
[12] Kuratko C N, Salem N: Eur. J. Lipid Sci. Techn Vol.115(2013),p. 956

Advanced Materials Research Vols. 881-883 (2014) pp 17-20

doi:10.4028/www.scientific.net/AMR.881-883.17

Rapid Analysis of the Bisphenol A in Slips of Store receipts and ATM machine with Head-space Liquid-phase Micro-extraction Coupled to Gas Chromatography and Mass Spectrometry

Yu Ying

(Experimental Center, Liaodong University, Dandong 118000, China)

Yuying992013@163.com

Key words: head-space liquid-phase micro-extraction (HS-LPME); gas chromatography-mass spectrometry (GC-MS); shopping receipts; ATM Customer Advice; bisphenol A

Abstract: A novel method has been developed for the determination of bisphenolA in slips of store receipts and ATM machine by head-space liquid-phase micro-extraction (HS-LPME) coupled with gas chromatography-mass spectrometry (GC-MS). The variable experimental conditions for the HS-LPME extraction process were optimized. The optimal conditions were using 2ul of toluene as organic solvent drop, 0.5g of the amount of sample and 1.0cm of the depth of micro-drop from the surface of the sample. After extracting for 10 min and detection limit of 1-100mg·L-1. Detection limit (3 S/N) of the method was found to be 0.3mg·L-1, precision and recovery of these methods were tested giving values of RSD′s (n=6) less than 4.49%; and of recovery in th range of 98.80%-99.47%. The method shows advantages of simplicity, high sensitivity and high performance extraction to be in line with the analytical standard of the international organic pollutant.

Introduction

The slips of receipts in supermarkets, gas stations, fast-food restaurants，post offices and ATM machines all contain bisphenol A to increase the transparency and water-proof function. Bisphenol A(BPA), Bisphenol, can be also called Polycarbonate in industry. It is a typical synthetic endocrine disruptor, and it has been widely noticed because of its potential risk to environment and human body. BPA can be taken into human body through skin, respiratory tract and alimentary tract, and accumulate in human body. Because of its serious influence on reproductive capability and the increase of cancer cells[1], European Union has already listed it as the preferential hazardous substance.Canada is the first country that has listed BPA as a toxic chemical, and other countries, like France and Norway, also published decrees on the use of BPA in consumer goods. Though lacking of standard requirement about BPA in our country, the researchers of environmental sciences and public health all pay close attention to the pollution problems. Therefore, finding out an easy, quick and highly sensitive analytical method of BPA seems to be necessary.

The reportorial documents of analysis on BPA contain high performance liquid chromatography (HPLC), capillary.electrophoresis[2], supercritical. fluid. chromatography[3] and liquid chromatography - tandem mass spectrometry. These methods are always used with sample pre-treatment technologies, such as liquid-phase micro-extraction, solid-phase extraction[4], solid-phase micro-extraction and stirring and adsorptive extraction. The thesis chooses head-space liquid-phase micro-extraction, and this is a simple and quick sample pre-treatment technological method. This method has many advantages, it needs only bits of solvent and simple equipment, and it is easy to operate; it costs less, and it can be connected with other analytical instruments. The use of headspace sampling technology can prevent lengthy and tedious process of sample pre-treatment,

and it can also prevent organic solution from influencing analysis and reduce the pollution to chromatographic column and injection port. This can make analysis result more accurate. The thesis studies the influences of variety of extraction agent, dosage, speed of stir and height of dropper, and it also researches the influences of extract liquor and extraction time to BPA pollutant extraction efficiency. The use of head-space liquid-phase micro-extraction (HS-LPME) coupled with gas chromatography-mass spectrometry (GC-MS) gives a preferable result.

Experimental Section

Key Instrument and Reagent. Clarus500 gas chromatography/Clarus500 Quadrupole mass spectrometry instrument (Perkin Elmer Co. USA); Agilent7694E Automatic headspace sampler; PG503-S electronic balance (sensitive quality0.0001g, Mettler Toledo Co. Switzerland).

Analytical reagents are methylbenzene, n-butyl alcohol, octane, ethyl acetate, 1, 2-propylene glycol. BPA (purity 99%, Sigmc Co. USA); Water for analytical laboratory use is redistilled water.

Instrument. Chromatographic condition: PE-5MS capillary column (30m×0.25mm×0.25um); temperature of the injection port: 250℃; carrier gas: high-purity He; flow rate: 1.0mL·min^{-1} ; split ratio: 10:1; temperature programming: 50℃, keeping 1min, 5℃·min^{-1} rising to 150℃, then 15℃·min^{-1} rising to 15℃·min^{-1}, keeping 5min.

Mass spectrometry condition: ion source: EI; electron energy: 70eV; ion source temperature: 180℃; transmission line temperature: 200℃; mass spectrometry and mentioned range: 30-400amu, quadrupole temperature: 150℃, selecting ion detective model.

The configuration of Labeling Solution. Weigh up standard substance exactly 0.1g, and put it into volumetric flask. Using methylbenzene for dissolution and then diluting with it to a standard solution about both quality and concentration are 1000 mg． L^{-1}.

Experimental Method. The slips of store receipts and ATM machine are cut into pieces, and then weigh up exactly 0.5g, putting it into a bottle with polytef rubber pad, keeping 23℃ for 15min, making it be equilibrium, inserting sample injector of drawn 2.0 uL methylbenzene into the bottle, shaking for 5min, pressing the plunger of sample injector and make sure the extracting solvent being a liquid drop hanging at the point of needle, extracting for 10 min, pulling back the plunger slowly and taking out the sample injection, putting it into injection port of GC immediately and analyzing.

Results and Discussion

The Choices on Solvent Extraction. Observing and studying methylbenzene, n-butyl alcohol, octane, ethyl acetate, 1, 2-propylene glycol in the same condition, n-butyl alcohol has a strong volatility, liquid drop was damaged seriously and hard for recycling. Ethyl acetate and 1, 2-propylene glycol have high interference peaks so that the peak appears after retention time 5min. The liquid drops of octane and methylbenzene are stable, but the effect of methylbenzene is better in the same condition. It has no interference on analysis component, and it is easy for delaying and removing of effects from solvent. Methylbenzene is the choice of this experiment.

The Effect of Extraction Agent Volume. The volume of head-space liquid-phase micro-extraction liquid drop has a serious influence on extraction efficiency of analyte. Bulky liquid drop has bigger superficial area, so the extract content of analyte is bigger, too. But bulky liquid drop makes itself hard to stay stably, and it is even easy to fall off. This makes the difficulty of operation be higher, and the relative standard of deviation in experiment is much higher. When the dosage of methylbenzene increasing from 1.5uL to 2. 5uL, the extraction efficiency of BPA is enlarging as the volume of liquid drop increasing. When the dosage of methylbenzene is 3.0uL, the

extraction efficiency becomes to be the biggest efficiency, and then the efficiency reduces to be lower immediately. The dosage of methylbenzene in the experiment is 2.0uL.

The Extraction Temperature and Extraction Time. Temperature has influence on extraction process, so the control of appropriate extraction temperature is very important for the balance between solutions. Rising temperature can increase the diffusion velocity of analyte which is above solutions, and it can shorten the time to the balance. But the rising temperature can also reduce the quality of extraction and in consideration of the volatile characteristics and toxic properties of BPA, the experiment did not optimize the extraction temperature, and the experiment is chosen to proceed at room temperature.

Choosing five different time of experiment from 5 to 15min on the influence of extraction efficiency, and the gathering of samples is greatly influenced by time. As time increasing, nearer the gathering approaches balance, higher the extraction efficiency is. But after 15min, the volatility of organic solvent gives negative effects to extraction, and the repeatability of extraction reduces. In order to give consideration to both extraction efficiency and parsing time, the choice of this experimental time is 10min.

The Influence of Dosage of Samples. The experiment chooses powders of sample of 0.2g, 0.3g, 0.4g, 0.5g and 0.6g, and respectively analyzes GC-MS in the same condition in order to investigate different results from different conditions of dosage of sample on chromatographic peak area and separating effect. The result shows that 0.5g of sample satisfies the experiment because of no overlap, Trailing phenomenon, and good separating effect.

The Choices of the Speed of Stir. The speed of stir has a serious influence on extraction efficiency. Proper stir can make the concentration of analytes keep equal. The increasing of diffusion velocity not only can increase extraction efficiency, but also can shorten extraction time. The experiment shows the results of extraction efficiency at the speed of 100-400 $r \cdot min^{-1}$. The results are when the speed is quicker than 200 $r \cdot min^{-1}$, the extraction efficiency reduces because of the fast speed of stirring; when the speed reaches to 400 $r \cdot min^{-1}$, the extraction liquid drop is easy to produce bubbles, so the liquid drop which is hanging will be unstable and fall under strong external force, and this can influence the veracity and repeatability. So the choice of the speed of stir is 200 $r \cdot min^{-1}$.

The Influence of the Height of Liquid Drop. The experiment chooses methylbenzene at the height of 0.8cm, 1.0cm, 1.2cm and 1.5cm, and respectively analyzes GC-MS in the same condition. Lower the height is, higher the concentration gradient is. This can increase the extraction efficiency and help volatile matter transfer between gas phase and organic extraction agent, and chromatographic peak area will be higher. The result shows that 1.0cm height of sample satisfies the experiment.

Linearity Range and Detection Limit. Under the optimization condition, this method can measure different BPA standard solutions. The result is when the mass concentration is between 1-100 $mg \cdot L^{-1}$, it is linear relation formula is y=0.0464x+0.3141, coefficient of association is 0.9961, methodological detection limit (3S/N) is 0.3 $mg \cdot L^{-1}$.

Standard Recovery and Sample Measure. Using the experimental method to measure BPA of slips of receipts in some supermarket and ATM machine and recovering, proceeding 6 times of parallel determinations and getting standard recycle and relative standard deviation (RSD) of BPA, the results are shown in tablet 1. Comparing the results between this method and efficient liquid chromatography, five of these samples are containing high quality of BPA, and it shows that BPA pollution exist in slips of receipts in supermarket and ATM machine, and people should pay attention to it.

Tab.1 Results of recovery percentage

Sample No.	Am't of bisphenol A found in sample	Am't of bisphenol A standard added ρ (mg· L^{-1})	Total am't of bisphenolA found r	Recovery /%	RSD /%
Sample 1	1.78	2.00	3.76	99.47	3.91
Sample 2	4.67	2.00	6.59	98.80	4.49
Sample 3	2.62	2.00	4.59	99.35	4.14
Sample 4	0.83	2.00	2.81	99.29	3.02
Sample 5	1.14	2.00	3.10	98.73	3.67

References

[1] B.S. Gigerw, science,Vo1623-625 (1984).P.225
[2] P.A.Babay, R.T.Getear,andM.F.Silva, . Jchromatoger: A, Vo1 277-285 2006 (2006).P.21
[3] Z.D.Wang, M.Fings. Jchromatogrsci, 509-518 (1993).P.31
[4] A.Jain, K.K.Verma. Taranta, 684-691 (2007).P.73

Advanced Materials Research Vols. 881-883 (2014) pp 21-24

doi:10.4028/www.scientific.net/AMR.881-883.21

Chemical constituents and antibacterial activity of Euphorbia altotibetica

Ai-mei Yang[1, a], Xiao-Long Shi[1, b], Jie-li Liu[1, c], Lin Yang[1, d], Yun Men[1, e]

[1]College of Life Science and Engineering, Lanzhou University of Technology, Lanzhou, 730050, People's Republic of China, fax number: 86-931-2973924

[a]E-mail: aimeiyang@163.com, [b]E-mail: 1989sxl@163.com, [c]E-mail:liujieli888@qq.com, [d]E-mail: Yanglin-401@163.com, [e]E-mail:menyun19@163.com

Keyword: *Euphorbia altotibetica*, Chemical constitutes, Extraction and separation, Antibacterial activity

Aabstract. Five compounds were isolated from the EtOAc extract of *Euphorbia altotibetica.* The structures of these compounds were elucidated as: β-sitosterol (1), daucosterol (2), chrysophanol (3), (-)-epiafzelechin (4), 5,2′-dihydroxy-7,8,6′-trimethoxyflavanone (5) by NMR datas, the antibacterial activity of all compounds were examined on five species of bacteria *Escherichia coli, Staphylococcus aureus, Bacillus licheniformis, Pseudomonas aeruginosa* and *Streptococcus pneumoniae*.

Introduction

Euphorbia is the largest genu in the family of Euphorbiaceae, consists of more than 1000 species, there are about 80 species grow in China, about 40 species of *Euphorbia* in China have been used as herb medicine. *Euphorbia altotibetica* is an important herbal plant, distributed widely in the northwest of China, which has been used as a traditional folk medicine for the treatment of anti-cancer, antibacterial, hepatoprotective and anti-inflammatory [1,2]. As part of the continuous phytochemical research on *E. altotibetica* [3], five compounds were isolated from this plant for the first time, and the antibacterial activity on five species of bacteria, *Escherichia coli, Staphylococcus aureus, Bacillus licheniformis, Pseudomonas aeruginosa* and *Streptococcus pneumoniae*, was also examined.

Investigations, results and discussion

From the ethanol extract of the whole plant of *Euphorbia altotibetica,* five compounds: β-sitosterol (1), daucosterol (2), chrysophanol (3), (-)-epiafzelechin (4), 5,2′-dihydroxy-7,8,6′-trimethoxyflavanone (5) were isolated and purified by repeated chromatography over silica, sephadex LH-20 gel column. Every compound obtained was subjected to detail spectroscopic analys to establish their chemical structures. All of these compounds were isolated from *Euphorbia altotibetica* for the first time. The structures of these known compounds were identified by direct comparison of their spectral data (^{1}H NMRand ^{13}C NMR and DEPT) with those reported values in the literatures.

β-sitosterol (1), $C_{29}H_{50}O$, white crystal, m.p.137~138℃. ^{13}C NMR (100MHz, $CDCl_3$) δppm: 11.83 (C-18), 11.96 (C-26), 18.76 (C-21), 19.00 (C-29), 19.38 (C-19), 19.81 (C-28), 37.22 (C-1), 21.05 (C-7), 21.05 (C-11), 23.02 (C-25), 24.28 (C-15), 26.00 (C-23), 28.23 (C-27), 29.09 (C-16), 31.63(C-2), 31.87 (C-8), 33.90 (C-22), 36.12 (C-20), 36.48 (C-10), 39.74 (C-12), 42.28 (C-4),42.29 (C-13), 45.78 (C-24), 50.01 (C-9), 56.01 (C-17), 56.73 (C-14),71.78 (C-3), 140.73 (C-5),121.71 (C-6)[4].

Daucosterol (2), $C_{35}H_{60}O_6$, white powder, m.p.294~296℃, ^{13}C NMR (100MHz, $CDCl_3$) δppm: 11.85 (C-18), 11.97 (C-29), 19.03 (C-21), 19.32 (C-26), 19.80 (C-27), 19.81 (C-19), 21.03 (C-11), 23.08 (C-28), 24.30 (C-15), 25.07 (C-23), 28.24 (C-16), 29.16 (C-25), 29.70 (C-2), 31.93 (C-7), 33.95 (C-22), 33.95 (C-8), 36.15 (C-20), 36.60 (C-10), 37.01 (C-1), 38.16 (C-12), 39.73 (C-4), 42.32 (C-13), 45.85 (C-24), 50.03 (C-9), 56.04 (C-17), 56.69 (C-14), 60.39 (G-6′), 73.67 (G-2′), 73.69 (G-4′), 77.22 (C-3), 77.22 (G-3′), 77.30 (G-5′), 101.33 (G-1′), 140.90 (C-5), 122.56 (C-6)[5].

Chrysophanol (3), $C_{16}H_{10}O_4$,yellow power, m.p.185~186℃, turn red in the Borntrager reagent. IR(KBr)cm^{-1}: 3455 (OH),1682 (C=O);^{1}H NMR (400MHz, $CDCl_3$): 7.80 (1H, d, J=7.6Hz, H-5), 7.63 (1H, t, J=7.6, 8.8Hz, H-6), 7.62(1H, s, H-4), 7.26 (1H, d, J=7.2, H-7), 7.08(1H, s, H-2), 2.44 (3H, s, -CH_3), 12.09 (1H, s, -OH). ^{13}C NMR(100MHz, $CDCl_3$) δppm: 22.25 (-CH_3), 113.73 (C-9a), 115.87 (C-8a), 119.91 (C-5), 121.35 (C-4), 124.35 (C-7), 124.55 (C-2), 133.27 (C-4a), 133.64 (C-10a), 136.94 (C-6), 149.33 (C-3) 162.41 (C-8), 162.71 (C-1), 181.9 (C-10), 192.5 (C-9)[6].

(-)-epiafzelechin (4), pink neddless. The molecular formula was established as $C_{15}H_{14}O_5$. m.p.243~246℃. ^{1}H NMR (400 MHz, DMSO) δppm:7.12 (2H, d, J=8.8Hz, H-2′, 6′), 6.72 (2H, d, J=8.8Hz, H-3′, 5′), 5.90 (1H, d, J=2.4Hz, H-8), 5.66 (1H, d, J-2.4Hz, H-6), 4.89 (1H, brs, H-2), 4.03(1H, m, H-3), 2.67 (1H, dd, J=16, 5.6Hz, H-4β), 2.50 (1H, dd, J=14.0,2.0Hz, H-4α). ^{13}C NMR (100 MHz, DMSO) δppm: 28.25 (C-4), 66.26 (C-3), 80.94 (C-2), 93.77 (C-8), 95.16 (C-6), 99.05 (C-10), 114.74 (C-3′, 5′), 128.47 (C-2′, 6′), 129.85 (C-1′), 155.34 (C-9), 156.17 (4′), 156.47 (C-5), 156.95 (C-7) [7].

5, 2′-dihydroxy-7,8,6′-trimethoxyflavanone (5), yellow powder. The molecular formula was established as $C_{18}H_{18}O_7$. m.p.201~ 202 ℃, IR (KBr) cm^{-1}: 3150, 3350(OH), 1620 (C=O γ-pyrone), 1590(C=C aromatic). ^{1}H NMR (400 MHz, DMSO) δppm:12.40 (1H, s, 5-OH), 9.58 (1H, s, 2′-OH), 7.19 (1H, t, J=8.4, H-4′), 6.58 (2H, d, J=8.3Hz, H-3′, 5′), 6.22 (1H, s, H-6), 5.95 (1H, dd, J=13.5, 3.2, H-2),4.05 (1H, dd, J=16.0, 12.0, H-3) , 2.55 (1H, dd, J=16.4, 2.8, H-3), 3.84 (3H,s, 7- OCH_3), 3.85 (3H, s, 8-OCH_3), 3.38 (3H, s, 6′-OCH_3). ^{13}C NMR (100 MHz, DMSO) δppm: 40.12 (C-3), 55.80 (7, 6′- OCH_3), 61.50 (8- OCH_3), 68.2 (C-2), 95.05 (C-6), 100.26 (C-1′), 104.53 (C-10), 105.22 (C- 5′),109.1(C-3′), 129.01 (C-8), 130.59 (C-4′), 156.71 (C-2′), 156.96 (C-9), 157.05 (C-6′), 160.44 (C-5), 160.44 (C-7), 201.92 (C-4) [8].

The antibacterial activity on five species of bacteria, *Escherichia coli, Staphylococcus aureus, Bacillus licheniformis, Pseudomonas aeruginosa* and *Streptococcus pneumoniae*, was also examined, the result showed that compound 5 has weak antibacterial activity, the MIC datas were extablished as in Table.1.

Table.1 Antibacterial activity of compound 5

	E.coli /(mg/ml)	p.aeruginosa /(mg/ml)	S.pneumoniae / (mg/ml)	S.aures / (mg/ml)	Bacillaceae / (mg/ml)
5,2′-dihydroxy-7,8,6′-trimethoxyflavanone	0.20	0.20	0.40	0.20	0.20

Experimental

Equipment

Melting points: X-4 Digital Display Micro-Melting point apparatus, uncorr. Optical rotations:Perkin Elmer 241 polarimeter, solvent $CHCl_3$. IR-spectra were measured on an FTS 165-IR spectrometer (Bio-Rad, USA). ^{1}HNMR (400.13 MHz), ^{13}CNMR (100.62 MHz) and 2D NMR were recorded on a Varian INOVA-400 FT-NMR spectrometer (USA) in $CDCl_3$ with TMS as internal standard. FAB-MS was recorded on a VG ZAB-HS mass spectrometer. Separationand

purification were performed by chromatographic column (CC) over silica gel, sephadex LH-20. Silica gel (200~300 mesh) used for CC and silica gel (GF254) for TLC was obtained from the Qingdao Marine Chemical Factory, Qingdao, P. R. China. Spots were detectedonthe TLC under UV light or by heating over 110℃ after spraying with 98% H_2SO_4-EtOH (V: V = 5: 95). Sephadex LH-20 (20~150μm) was obtained from the Mitsubishi Chemical Corporation, Japan.

Plant material

Euphorbia altotibetica was bought in QingHai medicial trading center. The five species bacterias *Escherichia coli*, *Staphylococcus aureus*, *Bacillus licheniformis*, *Pseudomonas aeruginosa* and *Streptococcus pneumoniae*, were provided by Natural Medicine laboratory of Lanzhou University of Technology.

Extraction and isolation

The dried powder of *Euphorbia altotibetica* roots (5.0kg) was extracted 3 times with each 95% EtOH at room temperature. The combined extracts (820.7g) which concentrated to dryness to afford a crude extract, which was suspended in water and partitioned successively with Petroleum ether, ethyl acetate and n-butyl alcohol. The ethyl acetate extract (336.10) was subjected to column chromatography silica gel (200-300 mesh) and eluted with $CHCl_3$-MeOH (100:1 to 0:1) respectively to yield 11 fractions. Fr.1(4.0g) was subjected to silica gel column and eluted with petroleum ether-acetone(40:1 to 10:1), to obtain compound **1** (22 mg). Fr.2 (1.5 g) was eluted with MeOH (50%) on Sephadex LH-20 column to yield compound **2** (20 mg). Fr.3 (2.0 g) was retreated on MCI column and eluted with MeOH (50%~90%) and finally purified on a Sephadex LH-20 column and eluted with MeOH (50%) to yield compound **3** (15 mg). Fr.4 (2.0 g) was subjected on MCI column and eluted with MeOH (60%) and finally purified on a Sephadex LH-20 column and eluted with MeOH (50%) to yield compound **4** (15 mg). Fr.5 (5.0 g) was subjected on macroporous resin (D-101) column and eluted with H_2O, 10%, 30%, 50%, 70% and 90% EtOH, respectively, to yield compounds **5** from 50% EtOH fractions.

Antibacterial activity

The antibacterial activity were performed by oxford cup method [9]. The antibacterial activity of all these compounds were investigated on five species of bacterias, *Escherichia coli, Staphylococcus aureus, Bacillus licheniformis, Pseudomonas aeruginosa* and *Streptococcus pneumoniae*.

Acknowledgment

This research was supported by the Natural Science Foundation of Gansu Province (1212R*J*ZA032).

References

[1] Y. B. Wang, P. Ji, H. B. Wang: Chinese Journal of Natural Medicines [in Chinese]. Vol. 8, (2010). p. 94

[2] J. Xu, Y. H. Xie, X. F. Su: China tropical medicine [in Chinese]. Vol. 7, (2007). p. 106

[3] A. M. Yang, J. L. Liu, J. Sun, H. Han, H. Li, X. L. Shi: Acta Chinese Medicine and Pharmacology [in Chinese]. Vol. 40(1), (2012). p. 71

[4] W. X. Gao, X. X. Lei, M. Yu: Journal of Wenzhou University Natural Sciences [in Chinese]. Vol. 31(4), (2010). p. 11

[5] D. Y. Zhou, X. S. Yang, B. Yang: Natural Product Research and Development [in Chinese]. Vol. 19, (2007). p. 807

[6] Y. H. Lu, Z. T. Wang, L. S. Xu: Journal of Chinese Pharmaceutical Sciences [in Chinese]. Vol. 12(2), (2003). p. 112

[7] Y. J. Hu, X. P. Wu, N. Liu: Journal of Tropical and Subtropical Botany [in Chinese]. Vol. 18(5), (2010). p. 559

[8] V. M. Malikov, M. P. Yuldashev: Chemistry of Natural compounds. Vol. 38, (2002). p. 473-519.

[9] J. Z. Tang, Q. Z. Dai, W. P. Zhou, Veterinary Pharmaceuticais & Food Additives, Vol.14(5), (2009). p. 8

Advanced Materials Research Vols. 881-883 (2014) pp 25-28

doi:10.4028/www.scientific.net/AMR.881-883.25

Screening of Formulation for 5% Hexaflumuron Suspension Concentrates

Baohua Zhang

Qingdao Agricultural University, Qingdao 266109,P.R.China

zhangbaohua76@163.com

Keywords: Hexaflumuron, suspension concentrates, formulaiton

Abstract: The formulation of 5% Hexaflumuron suspension concentrates (SC) was optimized. Results showed that the optimum formulation consists of 5% Hexaflumuron, MF-5 1%, DISPERSE 1005 5%, Aluminum magnesium silicate 1.9%, 0.1% Xanthan gum (concentration is 2%), and 5% ethylene glycols, and water make up 100%. The product has good suspension stability and storage stability.

Introduction

Hexaflumuron as a benzoylphenylurea insecticide that inhibits chitin synthesis and mainly acts as a larvicide and ovicide [1] are usually used to protect the miscellaneous crops from insect damage, and specifically act on the incorporation of N-acety glucosanmine monomer into chitin in the integument resulting in the formation of abnormal new cuticle and death of the insect [2].

With many advantages, such as biological efficacy, economic viability, safety reducing environmental pollution and so on, the formulation of suspension concentrates has become widely used[3,4]. Hexaflumuron hardly dissolves in the water and melting point is far higher than the 60 ˚C, and suitable for processing into suspension concentrates. In this study, the formulation of 5% Hexaflumuron suspension concentrates has been investigated.

Materials and methods

Materials. Pesticide: Hexaflumuron (98.4%); Dispersants: MF-5, disperse 1005, 7227-A, disperse 2700, those surfactant samples were obtained from Beijing Hanmmer chem technology co, Ltd. and HUNTSMAN co, Ltd., respectively. Thickeners: xanthan gum, magnesium aluminosilicate, Sodium carboxymethyl cellulose. Antifreeze: ethylene glycol, glycerol, urea.

Experiment instrument. BT-9300H Laser Particle Size Distribution Analyzer (Bettersize Instruments LTD.), ISSMJ 0.1-1 Vertical sand mill(Shenyang Research Institute of chemical industry), 2 Ultrasonic Grinder(Shanghai Tongle CO,.LTD), JA-5003N Electronic Balance.

Methods.

(1) Preparation method of Hexaflumuron SC

Hexaflumuron, dispersing agents and wetting agent were first mixed with a mixer to homogeneity and milled in the sand Mill to target particle size D (v0.5)＜2μm. Then the thickening agents added into the S.C. continue sanding until evenly mixed. Finally, measure the dispersibility and check the stability of SC.

(2) Method for the determination of the stability of the preparation

All the additives were evaluated with particle size and dispersibility of Hexaflumuron SC. The particle size of SC was determined by BT-9300H laser particle size distribution analyzer. The

dispersibility was evaluated by observing the dispersed condition when 1mL analyte miture of SC drop into 249 mL water in the measuring cylinder.

The stability of sample SC in the hot storage and cold storage were detected by the method specified in GB/T 19136-2003 .

Results and discussion

Screening results of dispersants. The single dispersant was screened and the results are summarized in Table 1. The results showed that the SC formulation with 7227-A, DISPERSE 1005 and MF-5 were stable at (54±2) ˚C after hot storage, the particle size and dispersability did not change after at (54±2) ˚C with above three kind single dispersant. By comprehensive analyses of the results of table 1, 7227-A, DISPERSE 1005 and MF-5 are chosen as suitable dispersant to compound.

Table 1 Screening results of single dispersant

dispersant	D_{50}[μm]	dispersibility	hot storage (54±2) ˚C	
			D_{50}[μm]	dispersibility
DISPERSE2700	5.87	good	12.92	good
MF-5	1.57	excellent	1.74	good
D1001	7.29	good	4.56	good
DISPERSE 1005	1.96	good	2.0	dood
7227-A	1.56	good	1.69	good

Table 2 Screening results of compound dispersants

Dispersants	Mixture ratio	D_{50}[μm]	dispersibility	hot storage (54±2) ˚C	
				D_{50}[μm]	dispersibility
7227-A VS DISPERSE 1005	5:1	1.75	excellent	1.75	good
	4:2	1.90	good	1.88	good
	3:3	1.84	good	1.89	good
	2:4	1.69	good	1.66	good
	1:5	1.83	good	1.73	good
7227-A VS MF-5	5:1	1.51	good	1.62	good
	4:2	1.33	good	1.52	good
	3:3	1.38	good	1.60	good
	2:4	1.52	good	1.56	good
	1:5	1.98	good	1.76	good
MF-5 VS DISPERSE1005	5:1	1.45	good	1.58	good
	4:2	1.37	good	1.57	good
	3:3	1.51	good	1.60	good
	2:4	1.48	good	1.55	good
	1:5	1.36	excellent	1.41	good

The compounded of dispersants of 7227-A, DISPERSE 1005 and MF-5 are showed in the table 2, the results indicated that the particle size and dispersibility are inherited stably before and after of hot storage of all kinds of different proportion. Based on an overall consideration of various factors, MF-5 and disperse 1005 at the proportion of 1 : 5 has the optimum compound dispersants, and the content of MF-5 and disperse 1005 were 1% and 5% .

Screening results of thickener. Table 3 shows that the separate water rate and dispersibility of three kinds of thickeners as antisettling agents to keep suspension stability of SC. Date in the table 3 shows that the separate water rate is 4.8% and the smallest when adding amount 1.9% of Aluminum magnesium silicate and 0.1% Xanthan gum (concentration is 2%) in the SC formulation.

Table 3 Screening results of thickener

Aluminum magnesium silicate/%	Xanthan gum/%	dispersibility	hot storage (54±2) ˚C	
			Separate water rate	dispersibility
2	0	good	13.40	good
2.5	0	good	17.65	good
0	0.15	good	/	good
0	0.1	good	/	good
1.8	0.2	good	39.40	good
1.9	0.1	good	4.80	good

Screening results of antitreeze. Antifreeze is added in order to make the SC formulation is easy to be used in low temperature environment. Table 4 shows that the effects of ethylene glycols, glycerols and urea on the formulation. These figures suggest that the effect of ethylene glycols on the particle size and dispersibility was the smallest, and the formulation still keep good stability after cold storage.

Table 4 Screening result of antifreeze

Antifreeze[5%]	D_{50}[μm]	dispersibility	cold storage	
			D_{50}[μm]	dispersibility
ethylene glycols	1.43	good	1.44	good
glycerols	1.42	good	1.47	good
urea	1.54	good	1.47	poor

The quality control indexes of 5% Hexaflumuron suspension concentrates.

Table 5 The quality control indexes of 5% Hexaflumuron suspension concentrates

Test items	indexes
outward appearance	White and folding liquid
Dieperdibility	good
Active Component /%	⩾5
Stability of hot storage	up to standard
Stability of cold storage	up to standard
Decomposition rate /%	< 5
viscosity [30r/min]/mPa.s	126
pH	6.5~7.0
Suspension rate /%	>90

The Optimized Formula of 5% Hexaflumuron suspension concentrates were detected by the method specified in GB/T 19136-2003. The quality control indexes were showed in table 5. The data showed that the formulation of SC accorded with the requirements of SC.

Conclusion

Through the screening of additives, the optimum formula of 5% Hexaflumuron SC was obtained. The optimum formulation consists of 5% Hexaflumuron, MF-5 1%, DISPERSE 1005 5%, 1.9% Aluminum magnesium silicate, 0.1% Xanthan gum (concentration is 2%), and 5% ethylene glycols, and water make up 100%. The SC formulation has good suspension stability, particle size and distribution. 5% Hexaflumuron SC is environment friendly pesticide formulation，and has good application prospects.

Acknowledgements

This work was supported by the National Natural Science Foundation of Shandong province of China（ZR2012CQ0015）

References

[1] Retnakaran, A., and J. E. Wright. Chitin and Benzylphenyl Ureas. Junk, Dordrecht, Netherlands. (1987), p. 205-282

[2] Nakagawa Y, Ishii S, Matsumura F. Insect Biochemistry and Molecular Biology 26(1996),p. 891-898

[3] A.G. Kanellopulos: Chemistry and Industry, 12(7), (1974),p.951-955

[4] P.J Mulqueen., E.S. Paterson, G.W. Smith :Pestic Sci, 46(29) ,(1990),p.451-465

Advanced Materials Research Vols. 881-883 (2014) pp 29-34

doi:10.4028/www.scientific.net/AMR.881-883.29

Optimization of Furfural Production from Xylose by RSM Using Chromium Sulfate as Catalyst

Ye Zhang[1,a], Mingqiang Chen[1,2,b], and Jun Wang[2,b]

[1]School of Earth Science and Environmental Engineering,

Anhui University of Science and Technology, Huainan 232001, China;

[2]School of Chemical Engineering, Anhui University of Science and Technology, Huainan 232001, China

[a]zhangye0830@126.com, [b]mqchen@aust.edu.cn, [c]austwang@yahoo.com.cn

Keywords: catalytic hydrolysis, xylose, furfural, chromium sulfate, reaction conditions, response surface methodology

Abstract. Optimization of chromium sulfate catalyzed conversion conditions of xylose into furfural was studied by response surface methodology (RSM). A central composite design (CCD) was used to determine the effects of independent variables, including temperature (120-160˚C), time (30-150min), catalyst loading (1-5mmol) and moles of xylose (2.5-12.5mmol) on furfural yield, xylose conversion and solid residue. The surface response analysis revealed that temperature, time, catalyst loading and moles of xylose had a strong influence on the furfural yield, whereas moles of xylose was found to be not significant for xylose conversion. The solid residue was affected by temperature, time and moles of xylose. The maximum predicted furfural yield was 45.07% at temperature of 150˚C, time of 120min, catalyst loading of 2mmol and moles of xylose of 10mmol. Under this condition, xylose conversion could be reached 100%.

Introduction

A sustainable future for the chemical industry requires feedstock based on renewable materials rather than steadily depleting sources. Inability to effectively transform five and six-carbon carbohydrate building blocks derived from nature is a major barrier toward this challenging goal[1]. Xylose is one kind of potential feedstock for this purpose, and recent efforts have focused on converting them to furfural, a versatile furan platform compound comprised of a heteroaromatic furan ring and an aldehyde function group. Furfural is identified as one of the top 30 high-value bio-based chemicals. It is mainly used as a selective solvent for the refining of lubricating oils and diesel fuels, and as an intermediate chemical in the manufacturing of other solvents, such as tetrahydrofuran, methyl tetrahydrofuran. Besides, furfural alcohol, furoic acid, 2-methyl furan, furan, 2-acetyl furan and furfural amine are the other furan derivatives that can be produced from furfural[2].

Commercial furfural production is currently carried out by acid catalytic dehydration of pentosan-containing lignocellulosic materials from agricultural wastes(corncobs, wheat straw, rice hulls, bagasse and oat hulls), xylose is the major pentose sugar in the xylan fraction of lignocellulosic materials. A drawback with acid catalysts is that they cause various side reactions, significantly increasing the cost of further purification. Thus, the present studies of furfural production are focused on developing novel process and catalyst that will be both economically and environmentally. Many attempts were made to improve the conventional process of xylose dehydration into furfural. To overcome humin formation, the application of aqueous biphasic systems using organic solvents (such as methyl isobutyl ketone and toluene) for the extraction of furfural has been recently reported[3]. Different catalysts such as $AlCl_3$[4], $CrCl_2$[5], $FeCl_3$[6],$CrCl_3$ [7]and solid acid[8] have been assessed. It was shown that metal chlorides salts promote the formation of 1, 2-enediol, thus favoring the subsequent acid catalyzed dehydration to furfural.

To the best of our knowledge, there has few studies on the optimization of furfural from xylose catalyzed by sulfates. Thus, in this study, the temperature, time, moles of xylose and catalyst

loading were selected as variables, and the furfural yield, xylose conversion and solid residue were chosen as response values. In addition, the Response Surface Methodology (RSM) was used as an efficient tool to establish the relationship between variables and response values[9,10]. The objective was to determine the optimum process conditions for maximizing the furfural yield from xylose catalyzed by chromium sulfate in biphasic system (water/toluene).

Experimental

Materials. D-xylose(98%), furfural, phloroglucinol, chromium sulfate were obtained from Aladdin. Toluene, glacial acetic acid and hydrochloric acid were purchased from Huainan Chemical Reagent Co. Ltd. All the reagents were used as received. The distilled water was used as solvent in all treatments and analysis.

Furfural production from xylose. Xylose was used as raw material for production of furfural using chromium sulfate as catalyst in toluene/water biphasic system. 30 batch experiments (Table 1) were conducted by central composite design (CCD). The temperature(A) that ranged from 120 to 160˚C(central value=140˚C), time(B) of 30-150min(central value=90min), catalyst loading(C) of 1-5mmol(central value=3mmol) and moles of xylose(D) of 2.5-12.5mmol(central value=7.5mmol) were tested.

Analysis of furfural and xylose. The furfural obtained from xylose was detected and quantified by Select Ion Method (SIM) using a DB-17column (GC-MS, QP5050A). Helium was used as carrier gas at a flow rate of 1.3mL/min, and the initial column temperature was 80˚C for 3min, followed with a ramp of 10˚C/min to final temperature of 180˚C. The temperature of injection port and detector port were both 200˚C. Under these conditions, furfural had a retention time of 3.7min. The concentration of D-xylose in hydrolyzate was determined by colorimetric method[11]. The samples were estimated based on the absorbance at 554nm using ultraviolet-visible spectrophotometer. All analysis was performed duplicate.

The yield of furfural and conversion of xylose on initial moles of xylose were calculated using the following equation:

$$Furfural\ yield = \frac{moles\ of\ furfural\ formed}{initial\ moles\ of\ xylose} \times 100\% \quad (1)$$

$$Conversion\ of\ xylose = (1 - \frac{moles\ of\ xylose\ unreacted}{initial\ moles\ of\ xylose}) \times 100\% \quad (2)$$

Solid residue. The mass of the solid residue in the reaction was determined gravimetrically by filtration. The solid residue on the filter was precisely weighed after drying at 105˚C for 6h. The solid residue (g/100g) is expressed relative to the initial mass of xylose[12].

Results and Discussion

Fitting models. The effective variables in the hydrolysis stage were optimized, and the results of 30 batch experiments are shown in Table 1. It was indicated that the furfural yield, xylose conversion and solid residue were in the range of 10.00～48.53%, 46.34～99.75%, 2.25～13.88%, respectively. Higher values of temperature and longer reaction time tremendously enhanced the xylose conversion to 99%. This was due to the degradation of xylose into furfural. The maximum furfural yield (48.56%) was achieved at 150˚Cfor 120min, catalyst loading of 2mmol and moles of xylose of 10mmol. In addition, small amounts of solid residues were also formed.

Table 1 Experimental design and results

Standard order	Variable				Response Values		
	Temperature (˚C)	Time(min)	Catalyst loading (mmol)	Moles of xylose (mmol)	Furfural yield (%)	Xylose conversion (%)	Solid residue (%)
1	130 (-1)	60 (-1)	0.10 (-1)	0.25 (-1)	10.06	46.34	3.83
2	150 (1)	60 (-1)	0.10 (-1)	0.25 (-1)	18.31	97.24	6.27
3	130 (-1)	120 (1)	0.10 (-1)	0.25 (-1)	14.51	72.15	3.8
4	150 (1)	120 (1)	0.10 (-1)	0.25 (-1)	26.70	99.48	12.55
5	130 (-1)	60 (-1)	0.20 (1)	0.25 (-1)	29.95	72.09	6.55
6	150 (1)	60 (-1)	0.20 (1)	0.25 (-1)	30.92	99.45	6.89
7	130 (-1)	120 (1)	0.20 (1)	0.25 (-1)	31.77	95.52	7.2
8	150 (1)	120 (1)	0.20 (1)	0.25 (-1)	31.93	99.18	10.83
9	130 (-1)	60 (-1)	0.10 (-1)	0.50 (1)	21.16	51.22	2.25
10	150 (1)	60 (-1)	0.10 (-1)	0.50 (1)	36.27	95.83	3.53
11	130 (-1)	120 (1)	0.10 (-1)	0.50 (1)	31.06	75.82	4.05
12	150 (1)	120 (1)	0.10 (-1)	0.50 (1)	48.53	99.73	12.25
13	130 (-1)	60 (-1)	0.20 (1)	0.50 (1)	20.95	64.42	2.97
14	150 (1)	60 (-1)	0.20 (1)	0.50 (1)	30.57	99.75	6.07
15	130 (-1)	120 (1)	0.20 (1)	0.50 (1)	32.41	92.22	4.71
16	150 (1)	120 (1)	0.20 (1)	0.50 (1)	33.09	99.75	11.12
17	120 (-2)	90 (0)	0.15 (0)	0.375 (0)	17.03	51.73	2.69
18	160 (2)	90 (0)	0.15 (0)	0.375 (0)	23.09	99.38	13.88
19	140 (0)	30 (-2)	0.15 (0)	0.375 (0)	16.44	54.67	3.35
20	140 (0)	150 (2)	0.15 (0)	0.375 (0)	28.83	99.29	5.96
21	140 (0)	90 (0)	0.05 (-2)	0.375 (0)	25.64	73.22	4.68
22	140 (0)	90 (0)	0.25 (2)	0.375 (0)	32.68	99.56	7.04
23	140 (0)	90 (0)	0.15 (0)	0.125 (-2)	33.42	95.25	8.64
24	140 (0)	90 (0)	0.15 (0)	0.625 (2)	33.18	98.85	5.1
25	140 (0)	90 (0)	0.15 (0)	0.375 (0)	32.33	97.24	4.94
26	140 (0)	90 (0)	0.15 (0)	0.375 (0)	25.07	98.27	3.8
27	140 (0)	90 (0)	0.15 (0)	0.375 (0)	29.87	96.02	5.18
28	140 (0)	90 (0)	0.15 (0)	0.375 (0)	37.19	97.97	6.55
29	140 (0)	90 (0)	0.15 (0)	0.375 (0)	29.99	99.08	3.6
30	140 (0)	90 (0)	0.15 (0)	0.375 (0)	32.00	98.37	3.97

To evaluate the influence of these variables on the furfural yield, xylose conversion and solid residue, the regression equations were obtained as follows:

$$Furfural\ yield(\%) = 31.08 + 3.19A + 3.19B + 2.04C + 2.48D - 0.22AB - 2.60AC + 1.33AD - 1.14BC + 1.28BD - 4.69CD - 2.47A^2 - 1.82B^2 - 0.19C^2 + 0.84D^2 \quad (3)$$

$$Xylose\ conversion(\%) = 97.83 + 13.16A + 8.20B + 5.72C + 0.19D - 5.99AB - 4.55AC + 0.13AD - 0.35BC + 0.32BD - 1.09CD - 5.40A^2 - 5.04B^2 - 2.69C^2 - 0.024D^2 \quad (4)$$

$$Solid\ residue(\%) = 4.67 + 2.36A + 1.39B + 0.52C - 0.75D + 1.24AB - 0.45AC + 0.24AD - 0.34BC + 0.40BD - 0.14CD + 0.93A^2 + 0.018B^2 + 0.32C^2 + 0.57D^2 \quad (5)$$

where A, B, C, D are the coded values of temperature, reaction time, catalyst loading and moles of xylose. The regression coefficients and analysis of variance of the models for furfural, xylose and solid residue are presented in Table 2. The F-test with a low probability (p) value showed that all the models were significant. The coefficient of determination (R^2) for the models of furfural yield, xylose conversion and solid residue were found to be 0.8703, 0.9795, 0.9234, respectively, which demonstrated the agreement between the observed and predicted results. Moreover, coefficient of variations indicated a high, precision and reliability of the experiments. The probability (p) values are an indication of the order of significance of process variables affecting the response value, where smaller p value indicated higher significance. The analysis of variance showed that temperature, time, catalyst loading and moles of xylose had a significant effect on the furfural yield, and the order of significance was temperature≈time＞moles of xylose＞catalyst loading. But the

variables affecting xylose conversion and solid residue were different from furfural yield. The surface response analysis for xylose conversion indicated that temperature, time and catalyst loading were highly significant terms, whereas the moles of xylose in the studied range of 2.5-12.5mmol had a significant effect on solid residue. As shown in Table 2, lack of fit was insignificant for the furfural yield and solid residue. The study revealed that the optimal process conditions for the maximizing furfural yield as well as xylose conversion were at the same conditions: temperature of 150˚C, time of 120min, catalyst loading of 2mmol and moles of xylose of 10mmol. The maximum response value for furfural yield was predicted to be 45.07%, and the xylose conversion could be achieved 100%.

Table 2 Regression coefficients and analysis of variance of mode

Variables	Furfural		Xylose		Solid residue	
	Coefficient estimate	p Value	Coefficient estimate	p Value	Coefficient estimate	p Value
Intercept	31.08	—	97.83	—	4.67	—
A	3.19	*0.0012*	13.16	*<0.0001*	2.36	*<0.0001*
B	3.19	*0.0012*	8.20	*<0.0001*	1.39	*<0.0001*
C	2.04	*0.0223*	5.72	*<0.0001*	0.52	0.0512
D	2.48	*0.0075*	0.19	0.7985	-0.75	*0.0081*
AB	-0.22	0.8293	-5.99	*<0.0001*	1.24	*0.0009*
AC	-2.60	*0.0184*	-4.55	*0.0001*	-0.45	0.1572
AD	1.33	0.1953	0.13	0.8820	0.24	0.4400
BC	-1.14	0.2653	-0.35	0.6975	-0.34	0.2818
BD	1.28	0.2125	0.32	0.7233	0.40	0.2002
CD	-4.69	*0.0002*	-1.09	0.2341	-0.14	0.6508
A^2	-2.47	*0.0050*	-5.40	*<0.0001*	0.93	*0.0011*
B^2	-1.82	*0.0282*	-5.04	*<0.0001*	0.018	0.9380
C^2	-0.19	0.8020	-2.69	*0.0012*	0.32	0.1859
D^2	0.84	0.2787	-0.024	*0.9720*	0.57	0.0254
Model	—	*0.0002*	—	*<0.0001*	—	*<0.0001*
R^2	0.8703	—	0.9795	—	0.9234	—
Lack of fit						
Adjusted R^2	0.7492	—	0.9603	—	0.8520	—
C.V	13.95	—	4.04	—	19.65	—

Optimization of furfural yield using RSM. As shown in Fig.1(a), with increasing temperature and time, the yield of furfural increased firstly and then reduced. This was in agreement with the results of single factor experiments. The slower rise of furfural yield at higher temperatures and longer times was likely due to thermal degradation of furfural. The surface response analysis for furfural yield revealed that the interaction between temperature and catalyst loading was significant. It could be seen from Fig.1(b) that the linear increase in furfural yield was obtained with increasing catalyst loading at 120˚C. However, the furfural yield decreased drastically at temperatures above 140˚C. With increasing the catalyst loading, the maximum furfural yield was obtained at short reaction times. It may be attribute to the change of H^+ concentrations in reaction system. Fig.1(c) showed the interaction effect between catalyst loading and moles of xylose. There were two different possible regions in which furfural yield was maximized: one of low catalyst loading-high moles of xylose and another of high catalyst loading-low moles of xylose. From these results, the maximum predicted furfural yield of 45.07% could be achieved at a temperature of 150˚C, a time of 120min, catalyst loading of 2mmol and moles of xylose of 10mmol.

Optimization of xylose conversion using RSM. Xylose conversion increased with increasing temperature, time and catalyst loading. The surface response analysis showed that there was no significant interaction between variables, excepted for temperature-time and temperature-catalyst loading. It could be seen from Fig.2(a) that the rate of xylose conversion started to increase fast from 120˚C to 140˚C, and then became slow at temperatures above 140˚C. The xylose conversion could be achieved 100% in the temperature range of 140～160˚Cand a time in the range of 60～120min. The similar results could be obtained at a catalyst loading in the range of 1.4～4.8mmol,

which was shown in Fig.2(b). Therefore, highest xylose conversion could be obtained only in the proper temperature, time, catalyst loading and moles of xylose.

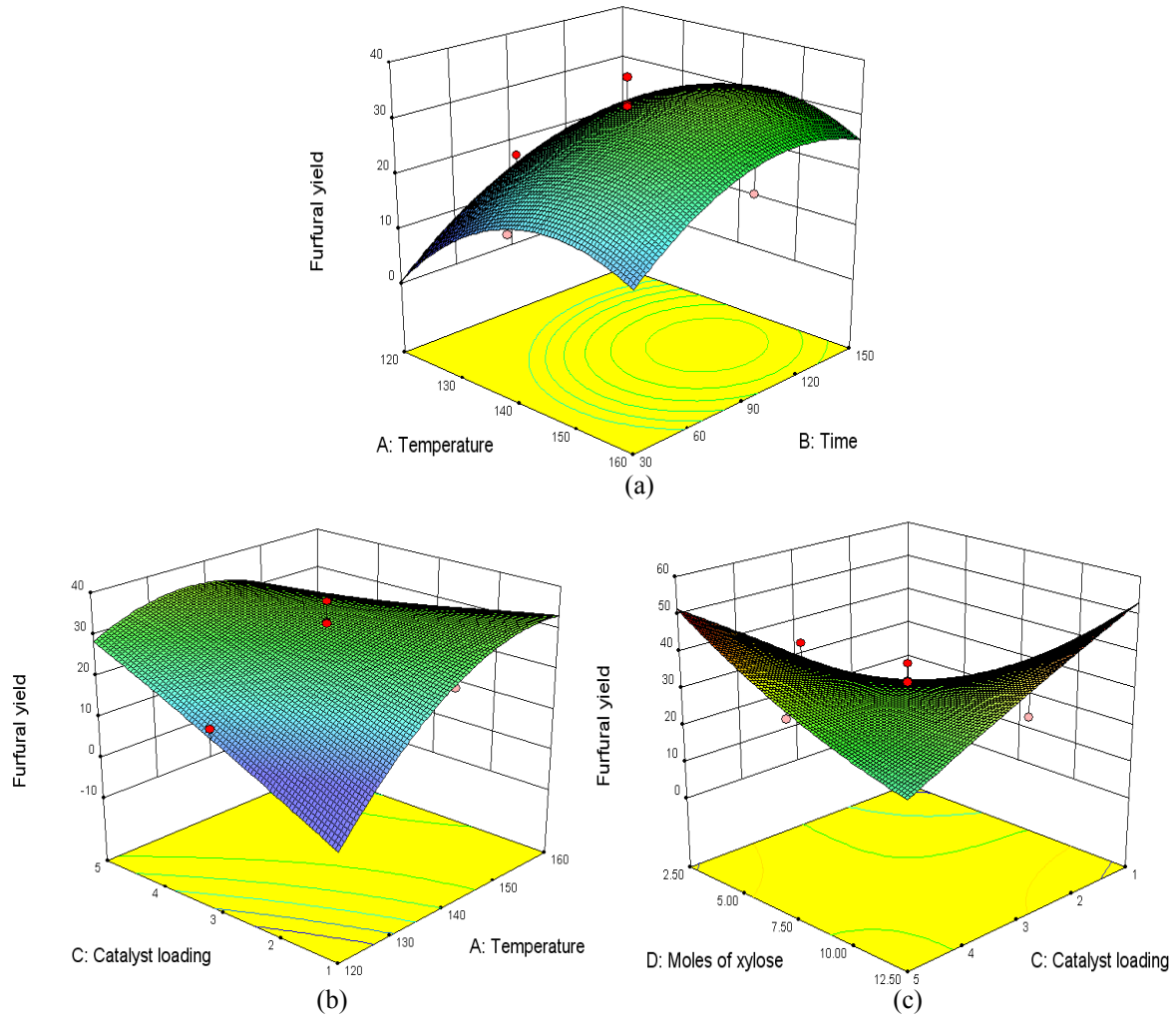

Fig.1 Response surface plots showing the effect of temperature, time, catalyst loading and moles of xylose on the furfural yield. (a) Fixed at a catalyst loading of 3mmol and moles of xylose of 7.5mmol. (b) Fixed at a time of 90min and moles of xylose of 7.5mmol. (c) Fixed at a temperature of 140˚C and a time of 90min.

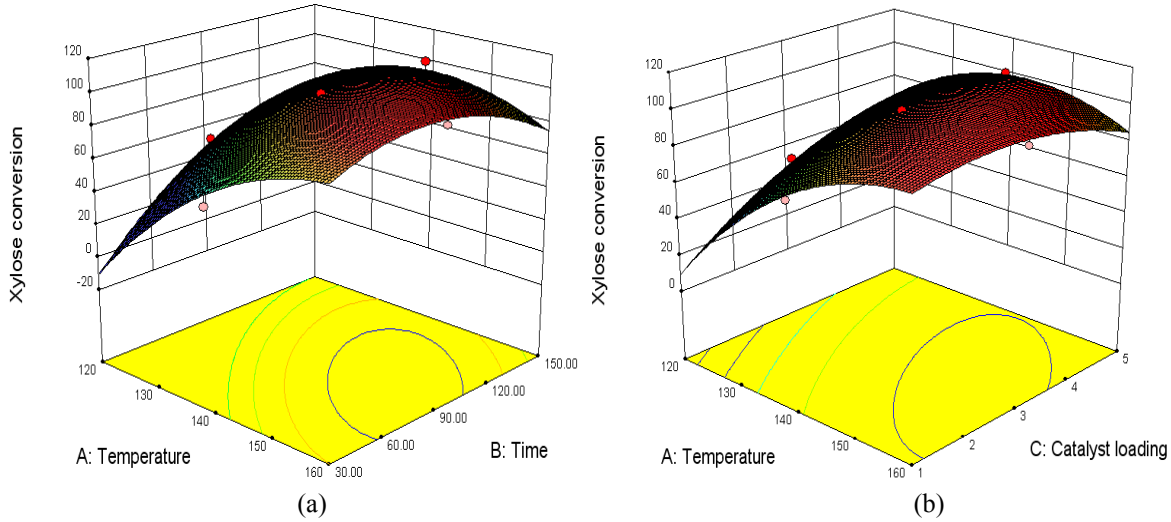

Fig.2 Response surface plots showing the effect of temperature, time and catalyst loading on the xylose conversion. (a) Fixed at a catalyst loading of 3mmol and moles of xylose of 7.5mmol. (b) Fixed at a time of 90min and moles of xylose of 7.5mmol.

Conclusions

From the studies reported in this work, it can be concluded that chromium sulfate can be used as effective catalyst for dehydration of xylose in to furfural. The results of analysis of variance and surface response plots revealed that temperature, time, catalyst loading and moles of xylose were the important variables for furfural yield. The significant order of variables was as follows: temperature, time, moles of xylose and catalyst loading. The xylose conversion was considerably affected by temperature, time and catalyst loading, while the effect of moles of xylose was not significant. The optimal conditions for achieving the highest yield of furfural was obtained, including temperature of 150˚C，time of 120min, catalyst loading of 2mmol and moles of xylose 10mmol. Under these conditions, the maximum predicted furfural yield and xylose conversion were 45.07% and 100%, respectively.

Acknowledgements

This work was supported by the Key project of Natural Science Fund of Education Department of Anhui Province (KJ2012A084).

References

[1] P. Gallezot: Chemical Society Reviews. Vol. 41(2012), p. 1538-1558.

[2] J.P. Lange, R. Price: CHEMSUSCHEM. Vol. 5(2012), p. 150-166.

[3] C. Rong, X. Ding, Y Zhu: Carbohydrate Research. Vol. 350(2010), p. 77-80.

[4] Y. Yang, C.W. Hu, M.M. Abu-Omar: CHEMSUSCHEM. Vol. 5(2012), p. 405-410.

[5] J.B. Binder, J.J. Blank, A.V. Cefali: CHEMSUSCHEM. Vol. 3(2010), p. 1268-1272.

[6] T. Vom Stein, P.M. Grande, W. Leitner: CHEMSUSCHEM. Vol. 4(2011), p. 1592-1594.

[7] Z. Zhang, Z.K. Zhao: Bioresource Technology. Vol. 101(2010), P. 1111-1114.

[8] J. Zhang, J. Zhuang, L. Lin: Biomass and Bioenergy. Vol. 39(2012), p. 73-77.

[9] O. Yemis, G. Mazza: Bioresource Technology. Vol. 109(2012), p. 215-223.

[10] W. Riansa-ngawong, P. Poonsuk: Carbohydrate Research. Vol. 346(2011), p. 103-110.

[11] T.J. Eberts, R.H. Sample, M.R. Glick: Clinical Chemistry. Vol. 25(1979), p. 1440-1443.

[12] O. Yemis, G. Mazza: Biomass and Bioenergy. Vol. 102(2012), p. 7371-7378.

Advanced Materials Research Vols. 881-883 (2014) pp 35-41

doi:10.4028/www.scientific.net/AMR.881-883.35

Lipase-catalyzed synthesis of sucrose fatty acid ester and the mechanism of ultrasonic promoting esterification reaction in non-aqueous media

Jia-Chan Zhang[1,2,a], Chan Zhang[2,b✉], Lei Zhao[1,c], Cheng-Tao Wang[1,2,d✉]

[1] Beijing Engineering and Technology Research Center of Food Additives, China

[2] Beijing Laboratory of Food Quality and Safety, Beijing Technology & Business University (BTBU),China

[a] xiaochan8787@163.com, [b✉] zhangchan@th.btbu.edu.cn, [c] zhaolei@th.btbu.edu.cn,

[d✉] wct5566@163.com (✉: Corresponding author)

Keywords: Sucrose fatty acid ester (SFAE), Novozym435, Lipase CalB, Ultrasound irradiation, Circular dichroism(CD), Scanning Electron Microscope (SEM).

Abstract. The preparation of sucrose fatty acid ester (SFAE) by lipase-catalyzing reaction using *Candida antarctica* lipase B (CalB) and its immobilized form Novozym 435 was reported in this work. The preparation was characterized in non-aqueous media with and without ultrasound irradiation treatment. A conversion rate of SFAE up to 49.60% was achieved using Novozym 435 under the optimal conditions (45.4°C; mole ratio of methyl oleate to sucrose = 6.0:1; 4.0 mL acetone; 4.0 mg/mL Novozym 435; and 24.6 h of reaction). Under optimal ultrasound conditions (50 kHz, 0.15 W/cm^2, 166.55 min), reaction time decreased by 75% approximately, compared with the control without ultrasonic irradiation, but the ultrasound irradiation treatment did not affect the SFAE yield catalyzed by Novozym 435. In the CalB-catalyzed preparation of SFAE under the same optimal reaction conditions, ultrasonic irradiation enhanced the activity of CalB during early time points and inhibited its activity after a long period of treatment. Moreover, CalB was further examined using Far-UV circular dichroism (CD) spectroscopy and scanning electron microscopy (SEM) to study the conformation and micro-morphology of CalB structural variations in various ultrasound irradiation treatments. CD results indicated that α-helical regions were increased and random coil regions remained at a similar level of proportion. SEM images showed small holes appeared on the surface of irradiated CalB. Therefore, we conclude that proper ultrasound irradiation could change the secondary structure and the surface morphology of the CalB in molecular level, and could accelerate the esterification reaction process.

Introduction

Sugar fatty acid esters (SFAE), used as emulsifying agents, are synthesized using either chemical or biological methods [1]. Industrial SFAEs are currently manufactured by chemical synthesis, which usually requires toxic reagents, base-catalysis at high temperatures, and gives rise to colored by-products [2]. The lipase-catalyzed synthesis in organic medium can be performed under mild conditions, but organic solvents are not useful for dissolving highly polar or hydrophilic substrates. Currently, ultrasound assisted enzyme catalysis is becoming a popular method in biochemistry, since it provides low operational costs and requires neither sophisticated equipment nor extensive

technical training. It has been reported that the application of ultrasound in enzyme solutions produced a positive effect on enzyme activity; however, high-intensity ultrasound caused denaturation [3, 4]. Candida *antarctica* lipase B (CalB) and its commercially available immobilized form, Novozym 435, were used to investigate synthesis of SFAE in this study. The structure of CalB was also examined. Since information on the immobilized Novozym 435 does not contribute to the research on the structure of lipase protein, its structure was not examined. CalB belongs to the α/β hydrolase fold family with a conserved catalytic triad consisting of Ser, His, and Asp/Glu [5]. In contrast to most lipases, CalB has no lid covering the entrance to the active site and shows no interfacial activation [6].With respect to ultrasound assisted enzyme reactions, researchers have suggested that ultrasound can enhance mass transfer of heterogeneous systems [7]. Reports on ultrasound assisted enzyme reactions included changes in enzyme activities and in secondary structure; accordingly, circular dichroism (CD) spectroscopy has been employed to investigate enzyme structure [8-11].Scanning electron microscopy (SEM) also has been used to study the surface of the cellulose and lipases from *Burkholderia cepacia* and *Pseudomonas fluorescens* [11,12].

To our knowledge, activity of lipases from *Candida antarctica* Fraction B has not been studied in and out of ultrasound. In this study, Novozym 435 was primarily studied to catalyze the synthesis of SFAE in and out of ultrasound. Furthermore, we make the first report here that native CalB was studied to understand how ultrasound promotes catalysis, from the viewpoint of secondary structure and morphology. CalB activities in different conditions were also investigated [13].

Materials and methods

2.1 Materials

CalB and Novozym 435, manufactured by Novozymes, Inc. (Franklinton, NC), were purchased from Sigma-Aldrich (St. Louis, MO). CalB was in the form of dried powder, and Novozym 435 refers to CalB that has been physically immobilized onto a macroporous support. Acetone, sucrose, and methyl oleate were purchased from Beijing Chemical Plant and were of analytical grade. All chemicals and solvents were used directly without any pre-treatment.

2.2 Synthesis of SFAE and Yield Measurement

The SFAE synthesis reaction was initiated by adding 40 mg Novozym 435 to 10 mL acetone containing 0.05 mM sucrose and 0.3 mM methyl oleate. The suspension was agitated at 150 rpm (45°C) for 24 h on a shaking table (HZQ-F160, Taicang City Equipment Factory, China). The initial and residual amount of methyl oleate was assayed using a gas chromatograph-mass spectrometer (GC-MS) system (6890N, 5975C inert XL MSD, Aglient Technologies, US). The GC-MS was equipped with a DB-WAX capillary column (30 m × 250 μm × 0.25 μm; Aglient, US) and with a flame ionization detector (FID). The column temperature was held at 150°C for 1 min, increased to 200°C at 10°C/min, held at constant temperature for 1min, increased to 250°C at 3°C/min, then held at constant temperature for 10 min. The conversion ratio from methyl oleate to SFAE was then calculated by the computer.

2.3 Synthesis of SFAE in Ultrasound

The synthesis of SFAE was performed by the same method as in section 2.2, except for the reaction environment. The reaction system was placed in an ultrasonic and thermostatic bath (JXD-02, Beijing Goldstar Ultrasonic Equipment Tech. Corp. Ltd., Beijing, China), including a dual frequency ultrasonic tank with two groups of ultrasonic transducers with different frequencies of 28/40 and 50/135 kHz.

2.4 Assay of CalB Activity

The activity assay was performed in the process of the synthesis of SFAE using CalB to catalyze the process. The initial and residual amounts of methyl oleate were assayed by GC-MS. One unit of CalB activity was defined as the amount of enzyme that consumed 1 μmol of methyl oleate per minute under the assay conditions.

2.5 Circular Dichroism Spectra Analysis

CD spectroscopy is a powerful method in structural biology used to examine proteins, polypeptides, and peptide structures [14]. CD spectra were scanned at the far-UV range from 240–190 nm at room temperature with a circular dichroism spectropolarimeter (Jasco J-810, JASCO Corporation, Tokyo, Japan). The CalB samples was treated with acetone in ultrasound, centrifuged, and dried into powder form, then resuspended into solution at approximately 0.2 mg/mL. CD spectra was used to estimate the relative content of protein secondary structure using reference CD spectra of proteins with known secondary structures.

2.6 SEM Analysis

Samples were suspended in acetone, treated with different ultrasonic irradiation, freeze-dried, placed on the sample holder, and scanned under vacuum. SEM was carried out on a TESCAN VEGA II electron microscope (TESCAN, SRO Corporation, Czech Republic).

2.7 Statistical Analysis

The data obtained were expressed as the mean ± standard deviation (SD) of triplicate determinations. Data were analyzed by an analysis of variance ($p < 0.05$) and the means were separated by Duncan's multiple range test. Statistical analysis was performed using the software SPSS 16.0.

Results and Discussion

3.1 Synthesis of SFAE In and Out of Ultrasound

A comparative study was performed to investigate enzymatic trans-esterification of methyl oleate under ultrasonic irradiation versus shaking in an organic medium. A central composite design was carried out to assess effects of each parameter. The optimal shaking conditions were the following: 45.4°C; the mole ratio of methyl oleate to sucrose = 6.0:1; 4.0 mL acetone; 4.0 mg/mL Novozym 435; and 24.6 h reaction time. The application of ultrasonic irradiation instead of shaking led to improvement in the conversion rate of methyl oleate to SFAE. As shown in Fig.1A, four different ultrasound frequencies ranging from 28–135 kHz at the same intensity (0.15 W/cm^2) displayed different effects during 180 min of irradiation. A marked increase was observed with 50 kHz, in which the conversion rate increased to 46.7% ± 0.7, compared with the control yield of 12.5% ± 0.2. From these results, we could conclude that ultrasonic irradiation accelerated the reaction process. Other recent studies have produced similar results [15, 16]. Medium frequency (50 kHz) ultrasonic treatment produced an excellent acceleration effect. Figure 1B showed the effects of different ultrasonic intensities on the reaction process. A similar trend to frequency was observed for intensity that a medium intensity (0.15 W/cm^2) produced the greatest stimulation of enzyme catalysis, at which the conversion rate was 46.7% ± 0.7, while the yields were 17.3% ± 0.8 and 28.4% ± 1.1 at 0.05 W/cm^2 and 0.35 W/cm^2, respectively. Previous reports concluded that high intensity can inhibit enzyme activity, while mild ultrasonic irradiation, in some cases, could increase the activities of free enzymes [3, 4, 17]. It has been suggested that the ultrasound irradiation might cause cavitations [30], particularly cavitation bubbles [19,20], which could enhance mass transfer in this reaction system. Moreover, ultrasound irradiation might affect the structure of the lipase protein. This change causes a loosening of the protein structure, which favors exposure of the active site and movement of substrates to the accessible active site.

3.2 Assay of CalB Activity In and Out of Ultrasound

A CalB activity assay was performed in the same reaction system as Novozym 435. Four different ultrasound frequencies ranging from 28–135 kHz at the intensity of 0.05 W/cm^2 were discussed (Fig.2A). Catalysis was remarkably stimulated after 30 min of irradiation, with the highest activity of 615 IU ±24.0 at 50 kHz and the second-highest activity of 552 IU ±45.0 at 135 kHz. During longer irradiation times, CalB activity at 135 kHz displayed a sharp decrease, while CalB activity without irradiation decreased more slightly. Thus, it can be concluded that moderate-intensity irradiation enhanced the reaction, but enzyme activity decreased more significantly than the control with prolonged ultrasound treatment.

The results of studies on different intensities are shown in Fig.2B. The same optimal ultrasonic condition was obtained as Novozym 435, which was studied in section 3.1. Within 100 min, CalB activities increased for all ultrasound intensities, compared with the control. With prolonged ultrasound treatment, CalB activity decreased gradually. By comparison, the influence of changing intensities on the activity was less significant than that of changing frequencies.

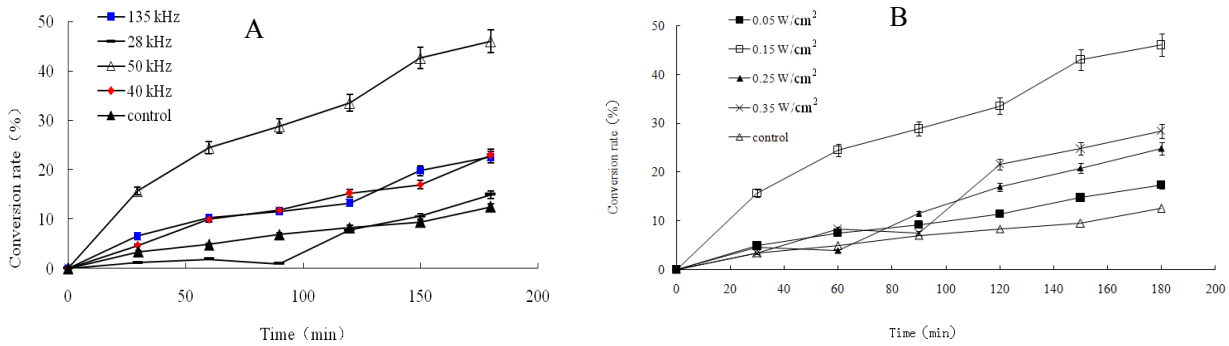

Fig.1 Effect of ultrasonic frequencies on conversion rates of methyl oleate. (A) Different frequencies. (B) Different intensities.

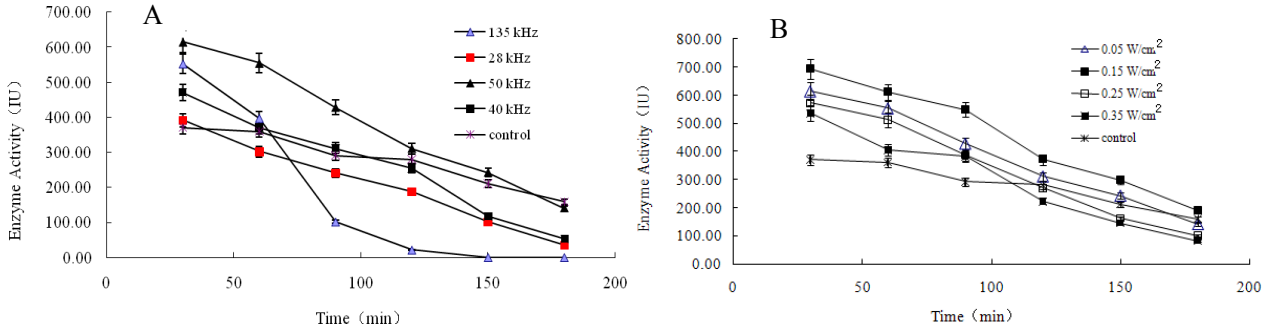

Fig.2 Effects of different ultrasonic frequencies and intensity levels on CalB activity. (A) Different frequencies. (B) Different intensity levels. Values are mean ± SD of at least three duplicate, independent measurements.

3.3 Analysis of CD Spectra

CD analysis was used to detect the secondary structure of CalB. Previous CD studies investigating conformational changes in CalB have established the region of interest in a spectrum is from 190–240 nm, based on the use of optical rotatory activity of α-helix and β-structure, as CD spectra for various structures are known [14,21].

The far-UV CD spectra of α-helical proteins are characterized by three peaks: a negative peak at approximately 222 nm [22], a negative peak of similar intensity at approximately 208 nm, and a stronger positive peak at 192 nm. A peak which appears as a shoulder at 175 nm has been proposed to be due to the charge transfer transitions [23, 24], but, in general, this transition is at a wavelength

that is too low to be detected in a conventional CD instrument. In general, spectra arising from *β*-sheets are characterized by a small negative peak near 217 nm and a positive peak near 195 nm that has approximately half the intensity of the *α*-helix peak in this region [22]. *β* -sheets give rise to considerably less intense signals than helices and show far more variation in spectral characteristics. Intensity of CD peaks reflects the magnitude of ellipticity in the protein [25], which reflects the changes in protein structure.

Figure 3 shows the CD spectra in far-UV regions of CalB treated under different ultrasound conditions (panel B.28, 50, and 135 kHz for 30 min; panel A.50 kHz, 0.15 W/cm^2 for 5, 15, and 30 min), compared to the control without any ultrasonic irradiation. Ultrasound-treated CalB showed significant changes in the CD spectra, which reflected the structural changes in protein secondary structure.

From Fig.3A, the spectra of the control exhibited one weak positive signal at around 190 nm. However, the intensity of positive peak at 190 nm of CalB treated for 15 min was stronger than that without ultrasound treatment. The strongest positive peak belonged to the sample treated for 30 min. These results suggest that an increasing amount of α-helix structure appeared over time. The spectra of CalB irradiated in 50 kHz and 135 kHz presented a more significant positive peak near 195 nm than unsonicated CalB (Fig.3B); nevertheless, there were only a few differences between the control and CalB treated by low frequency (28 kHz). The spectra of three irradiated samples were not significantly different from the control at 227 nm, which is the characteristic region of random coil structures. Taken together, the results indicate that the *α*-helical regions changed but random coil regions were unchanged.

Reportedly, pressure-induced spectral changes were indicative of an increase in the proportion of *α*-helical structure in the protein, which is consistent with the results in this study. The secondary structure in a protein not only depends on the local sequence of amino acids but also on the interactions between different parts of the molecule. It is likely that sonication disrupted these interactions, which might cause the shift from *β*-structure to a preferred *α*-helix structure. Chandrapala *et al.* reported consilient findings in their research[8]. While Stathpulos *et al.* reported a contradictory result that sonicated protein had decreased *α*-content [9].

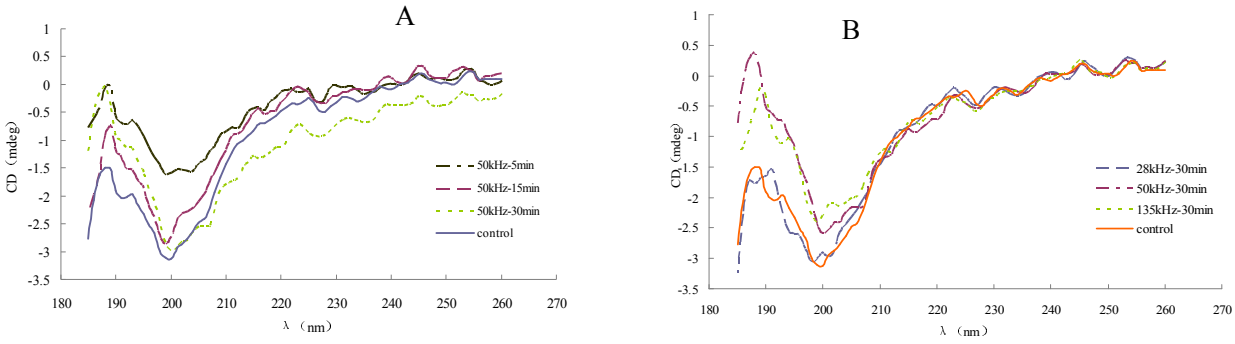

Fig.3 CD spectra, in the far-ultraviolet range, illustrating the effects of ultrasound conditions on CalB. (A) Ultrasound conditions were 50 kHz, 0.15 W/cm^2 for 5 min, 15 min, and 30 min. (B) Ultrasound conditions were 0.25 W/cm^2 for 30 min in different ultrasonic frequencies.

3.4 SEM Analysis

Figure 4 presents the SEM images of treated and non-treated CalB in an ultrasound-assisted system. Definite morphological changes were brought about by ultrasonication. The surface of native CalB was more or less smooth, while after irradiation, small holes were observed on the surface. Shah also found that small spheres or a fine powder appeared on the surface of irradiated *Burkholderia cepacia* lipase, which was quite different from the initial morphology [12]. Therefore, we conclude

that ultrasonic irradiation caused alterations in CalB both in morphology and structure at the molecular level.

Conclusions

The data obtained in the present study indicate that ultrasound irradiation markedly accelerated the preparation of SFAE, catalyzed by Novozym 435. The activity of native CalB from *Candida Antarctica* was also improved under ultrasound conditions. CD measurements demonstrated secondary structure of CalB was changed at some level in the process of ultrasound irradiation. An increasing amount of α-helix structure appeared with prolonged treatment. SEM analysis demonstrated morphological changes after irradiation; moreover, small holes were observed, which indicated an enlarging surface area.

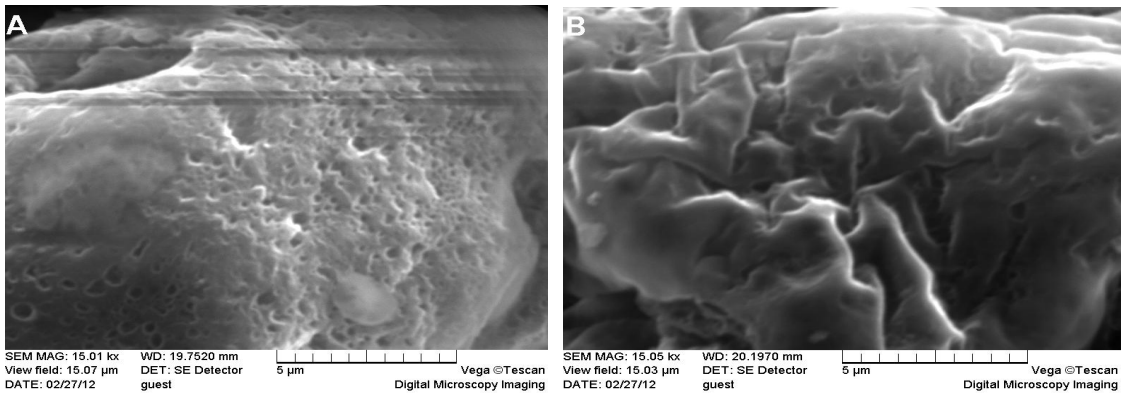

Fig.4 Scanning electron micrographs of CalB. (A) CalB irradiated in ultrasound; (B) CalB without ultrasound. The bar represents 5µm.

Acknowledgements

We acknowledge financial assistance from the National Natural Science Foundation of China (No.31071593, 31301411), the Beijing Natural Science Fund (No.5122008) and the Key Project of Chinese Ministry of Education (No.211101).

References

[1] T. Kobayashi:Biotechnol Lett. Vol.10 (2011), p.1911.

[2] M.J. Ferrer, Soliveri:Enzyme Microb Tech. Vol.36 (2005),p. 391.

[3] J. Wang, Y.P. Cao, B.G. Sun, Y. Mo:Ultrason Sonochem. Vol.18(2011) , p.534.

[4] L.H.M. Vargas, A.C.S. Pião, R.N. Domingos:World J Microbiol Biotechnol. Vol.20 (2004),p. 137.

[5] J. Uppenberg, M.T. Hansen, S. Patkar, T.A. Jones:Structure. Vol. 2(1994),p.298.

[6] M. Martinelle, M. Holmquist, K. Hult:Biochim Biophys Acta. Vol. 1258 (1995),p. 272.

[7] M.T. Zhong, M.X. Wan, S.P. Wang, J.Q. Kang:Ultrason Sonochem. Vol. 11 (2004),p.399.

[8] J. Chandrapala, B. Zisu, M. Palmer, S. Kentish, M. Ashokkumar:Ultrason Sonochem. Vol.18 (2011),p. 951.

[9] P.B. Stathpulos, G.A. Scholz, Y.M. Hwang, J.A.O. Rumfeldt, J.R. Lepock, E.M. Meiering: Pro Sci. Vol.13 (2004),p.3017.

[10] M. Bashari, A. Eibaid, J.P. Wang, Y.Q. Tian:Ultrason Sonochem. Vol.20 (2013),p.155.

[11] Z.B. Wang, X.M. Lin, P.P. Li:Bioresource Technol. Vol.117 (2012),p.222.

[12] S. Shah, M.N. Gupta: Chem Central J. Vol. 2 (2008),p. 1.

[13] E.V. Rokhina, P. Lens, J. Virkutyte:Trends Biotechnol. Vol.27(2009),p. 298.

[14] L. Whitmore, B.A. Wallace: Biopolymers. Vol. 89 (2007),p.392.

[15] K.G. Fiametti, M.K. Ustra, M.L. Corazza:Ultrason Sonochem. Vol. 19 (2012),p.440.

[16] N. Gharat, V.K. Rathod:Ultrason Sonochem. Vol. 20 (2013),p. 900.

[17] M. Sakakibara, D. Wang, R. Takahashi, K. Takahashi, S. Mori:Enzyme Microb Technol. Vol.18 (1996),p.444.

[18] K.S. Suslick, D.A. Hammerton, R.E. Cline: J Am Chem Soc. Vol.108 (1986),p.5641 .

[19] C. Sehgal, R.G. Sutherland, R.E. Verrall:J Phys Chem. Vol. 84 (1980),p.388.

[20] T. Kodama, Y .Tomita, A .Shima:Trans Jpn Sot Mech Eng .Vol.59 (1993),p.1431.

[21] W. Wu, C. Zhang, X. Kong, Y. Hua: Food Chem. Vol. 116 (2009),p.295.

[22] R.W. Woody: Fasman Plenum Press, New York (1996),p.25.

[23] L. Serrano-Andres, M.P. Fülscher: J Am Chem Soc. Vol. 120 (1998),p.10912.

[24] A.T.B. Gilbert, J.D. Hirst:J Molecular Structure Theochem. Vol.675 (2004),p.53 .

[25] N. Sreerama, Y.S. Venyaminov, R.W. Woody: Anal Biochem. Vol. 287 (2000),p.243.

Advanced Materials Research Vols. 881-883 (2014) pp 42-47

doi:10.4028/www.scientific.net/AMR.881-883.42

Analysis on the Main Problems of Industrial Application of the Regenerated Amine Desulphurization Technology

ZHOU Dengfeng[1,2] ,WU Yujiao[1,2*] ,GUO Jianbing[3] ,LU Fanghai[1,2]

[1] School of Materials Science and Metallurgical Engineering, Guizhou Institute of Technology , Guiyang 550003, China,

[2] Special Functional Materials of Guizhou Province, 2011 Collaborative Innovation Center, Guizhou Institute of Technology , Guiyang 550003, China,

[3] National Engineering Research Center for Compounding and Modification of Polymer Materials ,Guiyang ,550014, China

Keywords: regenerated amine ,application of desulphurization technology, corrosion, crystallization , loss of amine

Abstract: In this paper, generation and harm of SO_2 are described. Cansolv SO_2 Scrubbing, a regenerated amine process, is mainly described with respects to its process principle, features and application. This paper analyzed the existing problems such as corrosion , crystallization and loss of amine. Prevention measures were proposed according to the monitoring data, analysis and research.

Introduction

With the improvement of environmental protection requirements, the concentration and total quantity of SO_2 emission have been controlled strictly. Emission standards for the aluminum industry is formulated, SO_2 emission concentration does not exceed 400 mg/Nm^3 since January 1, 2012, selecting desulphurization technology which is economically feasible ,mature and efficient is extremely important that to achieve the emission standards. Regenerated amine adsorption and desorption desulphurization technology has many advantages such as without secondary pollution, recycling by-products sulfuric acid of high commercial value etc, but in industrial application process there are some problems to be solved.

Damage of SO2 in alumina production process

In the alumina production process , the elution step and evaporation step require the use of steam for heating to achieve the desired temperature , the steam is generated with circulating fluidized bed boiler heating soft water. the coal contain sulfur , the sulfur content of coal in Guizhou is up to 3 % to 6% [1],the combustion process generate SO_2, SO_2 emission concentration from coal-fired boiler flue gas is 6000~10000 mg/Nm3 above[4], therefore, the air pollutant SO_2 is mainly come from the combustion of coal-fired boilers.

The air pollutant SO_2 harm human's health and plants, lead to metal corrosion and impact on the ecological environment. SO_2 is a colorless gas with a strong pungent odor, soluble in body fluids and other viscous liquid. The long-term effects can cause a variety of diseases[2], such as: upper respiratory tract infection , chronic bronchitis, emphysema etc. and endanger human health . High concentrations of SO_2 under the influence of plants produce acute hazards, leaf surface necrotic spots and plant leaves withering. Low concentrations[3] of SO_2 under the influence of plant

growth performance is affected, resulting in quantity and quality in decline. Atmospheric SO_2 corrosion is mainly for steel corrosion. Since direct losses caused by metal corrosion is much greater than floods, storms, fires, earthquakes caused by the sum of the loss , and the metal corrosion direct threat to industrial facilities, amenities and transport facilities. SO_2 leading to the formation of acid rain and mist hazards is quite large, mainly for the lakes, groundwater, buildings, forests and ancient artifacts[4]. Meanwhile, the long-term effects of acid rain on soil and water quality will be an immeasurable loss.

Principle and characteristics of amine regeneration desulphurization technology

The regenerated amine desulfurization technology of Cansolv company from Canada mainly consists of two parts: washing - absorption and regeneration (desorption) - purification .

Adsorption solution absorb strong acidic ion, which is the reactions:

$$R_1R_2N\text{-}R_3\text{-}NR_4R_5+HX\rightarrow R_1R_2NH^+\text{-}R_3\text{-}NR_4R_5+X^-$$

X in the formula represents a strong acidic ion , such as : Cl^-, NO_3^- and SO_4^{2-} , etc. in the flue gas. X^- can increase the antioxidant capacity of the absorbing fluid and reduce regeneration energy[5].

The regenerated amine absorb SO_2 from flue gas process:

$$R_1R_2NH^+\text{-}R_3\text{-}NR_4R_5+SO_2+H_2O\rightarrow R_1R_2NH^+\text{-}R_3\text{-}N\ H^+R_4R_5+HSO_3$$

The reaction expressed solution for SO_2 adsorption process, the adsorbent of selective adsorption capacity for SO_2 is much stronger than other types of adsorption solution , making the amine regeneration adsorption and desorption processes on the amount of adsorbed fluid circulation less demanding, greatly reducing system operating energy consumption.

This is adsorption solution regeneration (desorption) Reaction:

$$R_1R_2NH^+\text{-}R_3\text{-}N\ H^+R_4R_5+\ HSO_3\rightarrow R_1R_2NH^+\text{-}R_3\text{-}NR_4R_5+\ SO_2+H_2O$$

Strong adsorption solution in the adsorption of ions produced salts thermally stable, non-volatile, non-heating regeneration. On the one hand reduce the desorption energy consumption, on the other hand ensures high purity of SO_2 byproducts.

Regenerated amine adsorption and desorption technology has many features[6], such as SO_2 adsorption solution without generating strong acidic corrosive medium; simple process and reliable system operation, System without secondary pollution, recycling sulfuric acid byproduct of high commercial value. The desulphurization efficiency can reach more than 95%. The concentration of SO_2 emission after treatment can be lower than 400mg/Nm^3.

Brief introduction of desulphurization and production of sulfuric acid process

An aluminum company use Cansolv's regenerated amine desulfurization technology for SO_2 flue gas desulphurization. the average SO_2 concentration of the aluminum company from the boiler is up to 3000~ 4000ppm. After dust removal and desulphurization the flue gas is into the 150 meters chimney to emission. This project is divided into two systems desulfurization and production of sulfuric acid. Desulphurization and production of sulfuric acid process is briefly shown in Chart 1.

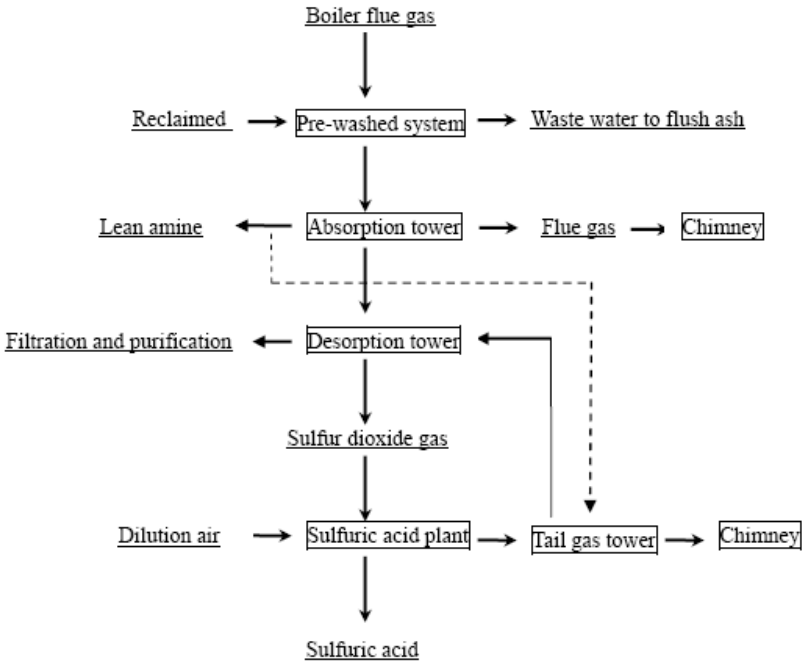

Chart 1 Desulphurization and sulfuric acid production process flow diagram

Problems and analysis of industrial application with regenerated amine desulphurization technology

1 Severe corrosion of absorber and flue

Desulfurization system put into operation in three months later, it is found that filler and lower stainless steel parts has been partially corrosion, especially to the gas venturi inlet. Cause of corrosion analysis is highly acidic flue gas condensate flows from the absorber. The remaining three absorber inspection found that the corrosion under the waterline absorber is obvious, the filler tube also has non-uniform corrosion. The absorber is rinsed by uninterrupted water supply and circulated one hour a day after changing the water filler. and wherein the two filters have been damaged by the construction unit repaired and put into operation more than 30 hours after. combined with corrosion mechanism and part of the sampling results, the system corrosion analysis is as follows:

(1) The existence of Cl^- and F^-in thee circulation system is the root cause of corrosion

It is a typical crevice corrosion from the internal corrosion from the absorber. Crevice corrosion is one form of local corrosion , which may occur in solution, the gap among the stagnation in the surface or shielded. Such gaps may be formed between a metal with a metal or metal and non-metal bonding. According to the sampling analysis results , Cl^- concentration in venturi total circulating water is up to 500-1100mg/l, Cl^- concentration in absorber is up to 500-800 mg/l, based on stainless steel selection data in Table 1, when the Cl^- concentration is greater than 300ppm , it can not use 316 series stainless steel (which is in the pH neutral data). Chloride ions destroy the passivation film of stainless steel, wherein the adsorption theory is described, metal has a strong adsorption capacity to Cl^-[7], the metal is preferentially adsorbed , and the oxygen from the metal surface is drained. Chloride ions and oxygen ions compete for metal adsorption sites on the surface .The formation of a soluble material led to accelerated corrosion at high chloride ion content conditions, stainless steel pitting , crevice corrosion, stress corrosion and corrosion fatigue performance degradation, prone to form intergranular stress corrosion and pitting, and then stress corrosion cracking. When the F- exist, the sodium fluoride which is slightly soluble in water is formed with containing Si substances such as cement, masonry materials ,resulting in the flue,

chimney structure continuous dissolution, while the pressure in the flue and the chimney is positive ,Acid clay used in closed performance is poor, and construction quality control is lax. The flue gas is likely to pass along the structural defects into the cracks between the blocks chimney layer and leak out of wall.

Table 1 Corrosion boundaries of different materials

Tempera-ture/℃	Chloride ion content×10-6（ppm） solution pH =7					
	304 stainless steel		316 stainless steel		Alloy 20,18,6（S31254 or 254SM0）	
	Less than the following non-corrosive	Greater than the following values corrosion	Less than the following non-corrosive	Greater than the following values corrosion	Less than the following non-corrosive	Greater than the following values corrosion
100	12.0	21.0	50	85	450	740
90	15.7	26.7	62	105	668.4	1100
80	20.5	35.0	81	130	1080	1870.7
70	27.0	47.2	105	190	1700	3100
60	37.5	64.7	140	240	3050	5300
50	52.0	86.0	201	330	5400	9300
45	61.0	103.0	250	410	7800	13000
40	71.3	120.0	290	505	10000	18500
35	85.0	150.0	340	615	14000	29000
30	103.0	180.0	410	750	20000	42756.3
25	125.9	210.0	540	950	34000	70000
20	150.0	250.0	650.0	1150		
10	228.0	420.0	1050	2050		

(2) The acidic environment of the system greatly accelerate the corrosion process

According to a large experiment proved that when the pH value is less than 4, the corrosion rate of the metal increase sharply, according to the production site test data, venturi and the absorber pH value is usually 1.3 to 1.5, according to corrosion rate curve in Figure 1, metal corrosion rate 10 to 20 times higher than neutral in this range. Absorber temperature is about 47 ℃, relative to the normal corrosion rate has also been strengthened.

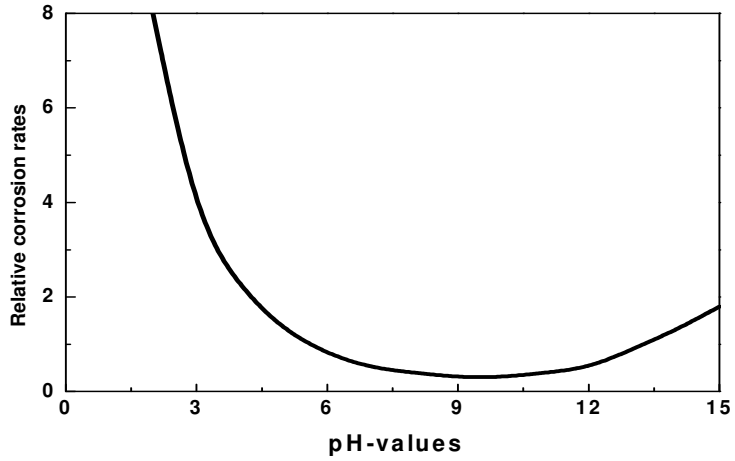

Figure 1 pH- corrosion rates curve

The following two solutions are obtained from the above reasons:

(1) Eliminating corrosion factors

Chloride ions is mainly from industrial water , so increasing a reverse osmosis or desalination equipment of

industrial water will completely stop Cl^- or F^- entering the system and protect the Venturi hydrocyclone .

(2) Transformation of equipment

If removing most of the corrosion factors is impossible , it is necessary to improve the corrosion resistance of the system , especially the desorption tower part , temperatures up to 104 □, is pressurized equipment , preserving more demanding conditions. Replacing the filler with Ha magnetic stainless steel or alloy is feasible .Tower wall also need to change materials relatively, the inner wall can be considered FRP Lining. If it can ensure the strength, plastic and other non-metallic materials also be feasible. Advantage of this scheme can solve the problem completely, without increasing the complexity of the process , drawback is a large one-time investment and long construction period.

2 Sodium ion concentration resulting in amine crystallization

Acid in the desulphurization within the crystalline amine found in particulate matter, as temperatures decrease , but also a large number of crystals desulfurization system , due amine crystallized serious loss flow properties , transfer can not run , leading to a system-wide outage. The crystals were analyzed , the main component of sulfate and sulfite . Desulfurization system in the sulfate ion and sulfite ions fluctuate within a certain range , and only when a large number of sodium ion concentration , the only cause crystallization. After repeated experiments and analysis, due to corrosion, and demineralized water entrained within the flue gas into the metal cation, which is the main factor affecting Fe^{2+}, filtration and purification systems enriched cause resin degradation loss of activity in the backwash resin with sodium hydroxide stage , since the resin loss of activity , can not adsorb sodium ions in the purification stage, a large number of sodium ions into the amine , resulting in crystallization.

Solution is for the whole system replacement amine, amine replacement out after solid-liquid separation recycling ; and for Fe^{2+} add a cationic purification system.

5.3 big loss of Amine solution

According to the design desulfurization systems require supplementary amine solution 37.5 ton per year, after running the actual normal loss is over 100 ton per year, due to the current operation of the amine concentration about 14% is far lower than the design condition 20-25%, otherwise, the loss may reach 200 ton per year. Due to equipment leaks, maintenance and other amine lost during normal operating conditions are normal. In the system during normal operation, air entrainment causes large loss of amine, measures is made to take it, regulate flue gas flow, install the mist eliminator at the top of the absorber, and increase amine recovery equipment in the bottom of the chimney.

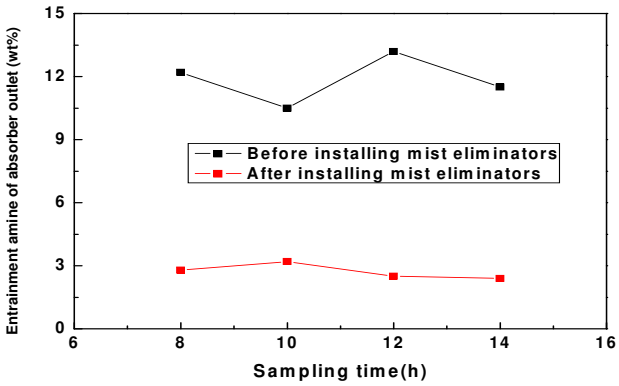

Figure 2 Contrast of entrainment amine of absorber outlet before and after the installation of the mist eliminators

Conclusion

In order to significantly reduce operating costs and ensure stable operation of the desulphurization system, the company had take some measures. such as replacing amine solution in desulfurization system, increasing cation purification system thereby slowing the ion enrichment; increasing reverse osmosis desalination device to control Cl^- and F^- of the system, regulating gas flow and increasing mist eliminator to lower amine entrainment losses. These technological transformation project are implemented for the industrial applications of regenerated amine desulfurization technology which will lay a solid foundation for reaching drainage standard.

References

[1] Xiaoxun Ma, Takao Kaneko, Tsutomu Tashimo,Tadashi Yoshida, Kunio Kato. Use of limestone for SO_2 removal from flue gas in the semidry FGD progress with a powder-particle spouted bed[J]. Chemical Engineering Science,2000,55(3):4643～4652

[2] Chen etc. Sulfuric acid with pyrolusite exhaust governance research and economic evaluation of SO_2[J]. Sulfuric Acid Industry, 1995, (3): 29 ~ 31

[3] Mcinnes R and Royen R V. Desulphurizing Flue Gases[J].Chemical Engineering, 1990,97(9):124～127

[4] Srivastava R, et al. SO2 scrubbing technologies: A review[J]. Environmental Progress, 2001,20(4): 219～227

[5] Jianghan Ying editor. Hydrometallurgical process physical chemistry [M]. Beijing. Metallurgical Industry Publishing Press .1984

[6] Yu Liu. Cansolv renewable amine desulfurization technology Applied Materials Physics and Chemistry PhD thesis in 2000

[7] Gong Min. "Corrosion and Corrosion Control Theory"[M].Chemical Industry Press, March 2009 Gexi

Advanced Materials Research Vols. 881-883 (2014) pp 48-51

doi:10.4028/www.scientific.net/AMR.881-883.48

Effects of strong-acid on performances of copper solvent extraction

Yanjun Liu[1, a], Xiaorong Liu[1, b], Hui Li[2, c], Qing Li[3], Yongsheng Li[1], Chang Su[1] and Jun Tian[3], Yucheng Wang[3]

[1] School of Materials Science and Engineering, Shanghai Institute of Technology, 201418, China

[2] Donghua University, College of environmental science and Engineering, 200051, China

[3] BASF,200137, China

[a]liuyanjun6688@163.com, [b]sharranliu@126.com, [c]feifei7815880@163.com

Keywords: Copper solvent extraction. Phase disengagement. Extraction rate.

Abstract. This paper studied the effect of strong acid---concentrated sulfuric acid---on organic phase physical properties, copper extraction rates as well as phase behaviors in the process of copper solvent extraction. Results demonstrate that with the increase of contact time between organic phase and concentrated sulfuric acid, the organic phase density and viscosity slightly decreased, copper extraction rate linearly decreased from 99.8% to 99.5%, and the average size of organic phase droplet in raffinate cyclically trended to decrease. When the contact time is less than 20 hrs, phase disengagement rate decreased slowly. However, further increasing the contact time the phase disengagement rate decreased rapidly. Organic phase physical properties have little effect on phase disengagement rate.

Introduction

Hydroxyoximes are effective for copper extractant. Among their molecules the working group is oxime group. In extraction process, an atomic hydrogen of the oxime group is replaced by a copper ion, and a chelate ring structure is formed since the nitrogen atom in oxime group has an unpaired electron [1,2]. Copper ions are thus extracted from the aqueous phase. During its long time contact with strong acid oxime extranctant takes Beckmann rearrangement, hydrolysis, and many other chemical reactions. As a result, the oxime functional group is damaged, and substances such as aldehydes and ketones are formed, which result in changes of both physical and chemical properties of the organic phase as well as the extraction performance [3-5]. In addition, being exposed to concentrated acid such a long time accelerates the organic phase degradation, which lowers extraction kinetics, and reduce copper loaded capacity. Ning.et al. [6] found that acidic conditions aggravate the formation of interfacial emulsion materials. Interfacial emulsion materials hinder the interaction between organic phase and aqueous phase, prolong stratification time. They also cause seriously loss of extranctant due to the entrainment of emulsion, thus increase production cost [7,8].

In the present paper, the effect of contact time between organic phase and concentrated sulfuric acid on organic phase physical properties, phase disengagement rate, and copper extraction capacities were studies. The aim of this study is to provide theoretical reference on how to utilize the extractant effectively

Experimental

Experimental material.

The extractant and diluent used in this study were Lix984N and kerosene, respectively. The aqueous phase were made up of 0.25g/L Cu^{2+} and 0.50g/L Fe^{2+}. The pH was adjusted to 2.5. Acid-strip solution was 160g/L H_2SO_4.

Experimental method

The organic phase containing 80% (volume fraction) Lix984N was mixed with 160g /L H_2SO_4 by the volume ratio of 1:1. After a known period of time the mixed solution was diluted to 2.5% Lix984N by kerosene, which was used for extraction experiment later. Two immiscible liquids were stirred 10 min by an electrical stirrer at 450 r/min and the phase ratio O/A was 1:1.

Results and discussion

Effect of contact time on organic phase physical properties

Both density and viscosity of the organic phase have impact on its mixing and clarification properties, therefore, it's of great significance to study the changes of organic phase density and viscosity during its contact with strong acid. The organic phase density and viscosity were characterized after different contact times, and the results are shown in Fig. 1. With the increase of contact time, both the density and viscosity decreased. A reliable explanation is that during the long time contact with concentrated sulfuric acid, the extractant was degraded, forming low molecule degradation products. These degradation products caused the decrease of density and viscosity.

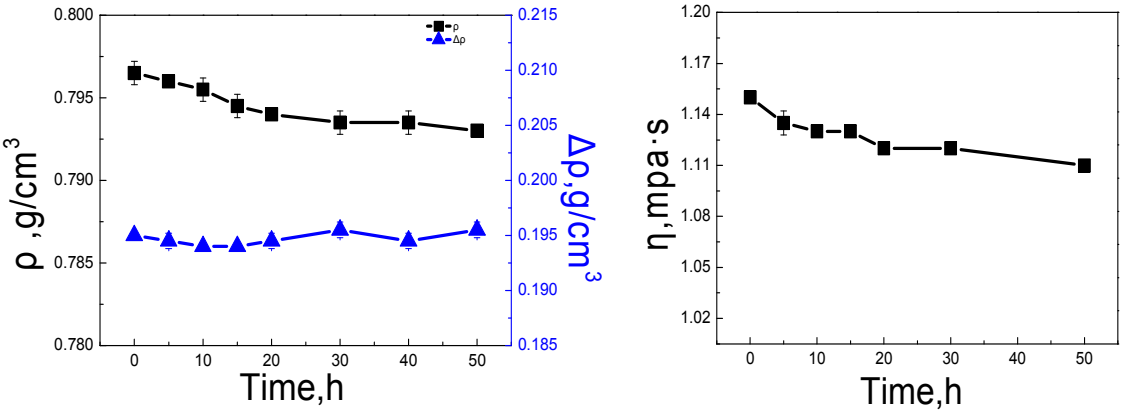

Fig.1 The effect of contact time on organic phase physical properties, e.g. density and viscosity.

Effect of contact time on phase disengagement rate

The coalescence rate of the organic phase in raffinate plays a decisive role on phase disengagement rate. It is mainly affected by chemical compositions, viscosity, surface tension, density and copper content of the organic phase. Since the reaction of copper and extractant occurs on the interface, the surface tension is the dominant factor for phase disengagement [8]. The effect of contact time between organic phase and concentrated sulfuric acid on phase disengagement behavior was studied. As shown in Fig. 2, the organic phase disengagement rate decreased slowly from 0.75 mm/s to 0.5 mm/s in the range 0-20hrs. Further increasing the contact time the phase disengagement rate decreased rapidly from 0. 5 mm/s to 0.05 mm/s. The organic phase reacts with concentrated sulfuric

acid, the resulting degradation products aggregate interface emulsification, and seriously hinder phase disengagement.

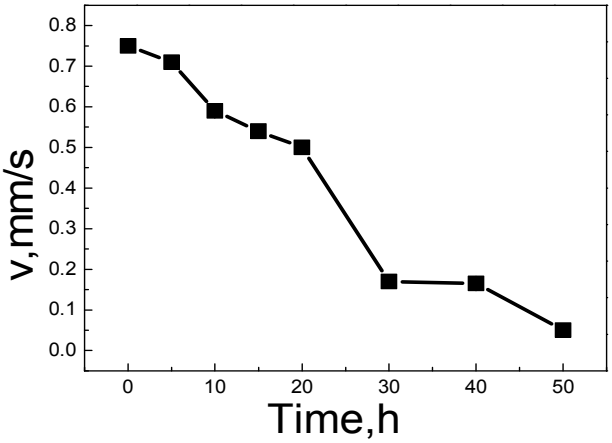

Fig.2 The effect of contacting time on phase disengagement rate

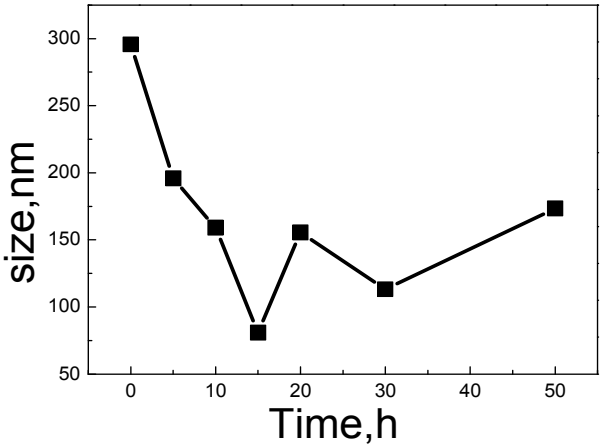

Fig.3 The effect of contact time on the size of organic droplet particle

The particle size of the organic phase in raffinate was also studied. As shown in Fig. 3, increasing the contact time tended to decrease the organic average droplet size. The organic phase average particle size decreases, the interfacial energy is reduced, and the emulsion becomes more stable, all of them are against phase disengagement.

Effect of contact time on copper extraction efficiency

Oxime group is the working group in hydroxy oxime extractant. In the process of copper extraction, copper ion forms chelate structure with oxime group by replacing a hydrogen atom in the oxime functional group, thereby copper is extracted from the solution [9]. As shown in Fig. 4, with the increase of contact time, copper extraction efficiency shows a decreasing trend, though not very much. During the long time contact with concentrated strong acid, the oxime group was destroyed, and the effective concentration of extractant was then reduced. Consequently, the extraction kinetics rate slowed down, the organic phase loading capacity decreased, and the extraction efficiency thus decreased. Therefore, controlling the contact time between organic phase and strong acid is of great significance to keep high extraction efficiency.

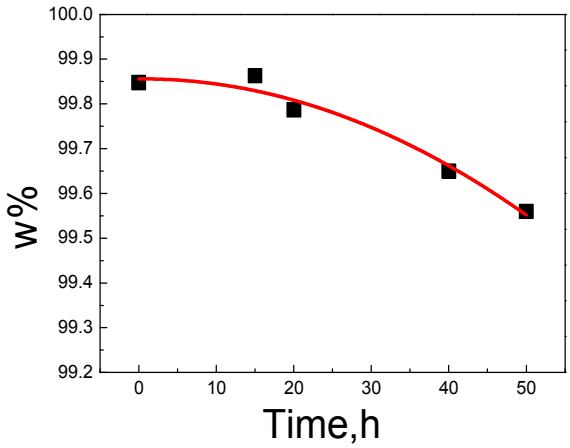

Fig.4 The effect of contact time on copper extraction rates

Conclusions

1) With the increase of contact time between organic phase and concentrated sulfuric acid, both density and viscosity of the organic phase slightly decreased. However, the difference density between organic phase and raffinate did not change much.
2) The organic phase disengagement rate decreased slowly from 0.75 mm/s to 0.5 mm/s in the range 0-20hrs. Further increasing the contact time the phase disengagement rate decreased rapidly from 0. 5 mm/s to 0.05 mm/s. Copper extraction rate decreased slightly from 99.8% to 99.5%
3) With the increase of contact time, the average size of the organic phase droplet in raffinate cyclically trended to decrease.

Acknowledgements

This work was financially supported by the National Natural Science Foundation of China (51074107), and the Key Discipline Construction of Shanghai (J51504).

References

[1]W.Chen. Study on the synthesis of hydroxyoxime extractant Lix63 and its analog's design and synthesis.2007,03 (In Chinese)
[2]K.R. Barnard, D.W. Shiers: Hydrometallurgy Vol.104 (2010), p.268
[3] S.Vaishnavi，J.K.Verma，N.S.Shenoy: Miner. Eng. Vol. 23 (2010), p.454
[4] K.R. Barnard and N.L. Turner: Hydrometallurgy Vol. 109 (2011), p.245
[5] X.R. Liu, G.Z. Qiu, Y.H.Hu, J.S. Liu and L. Li: Trans. Nonferrous Met. Soc. China, Vol. 10 (2000), p. 97
[6] P.G. Ning，H.B. Cao, C.M. Liu, Y.P. Li and Y. Zhang: Hydrometallurgy Vol. 97 (2009) p.131
[7] R.P. Sperline, Y. Song and H.Freiser: Hydrometallurgy Vol. 50 (1998) p.1
[8] X.R. Liu, G.Z. Qiu, Y.H. Hu, J. Yang and M.L. Jin: Trans. Nonferrous Met. Soc. China Vol. 13 (2003), p.963

Advanced Materials Research Vols. 881-883 (2014) pp 52-56

doi:10.4028/www.scientific.net/AMR.881-883.52

Visual Study on the Effect of Osmotic Pressure on the Morphology of Emulsion Liquid Membrane

Sunjun Li[1,a], Hongjing Liu[2,b]

[1]School of Petrochemical Engineering, Shenyang University of Technology, Liaoyang , China

[2]School of Petrochemical Engineering, Shenyang University of Technology, Liaoyang , China

[a]email: lisujun006@163.com, [b]email: liuhongjing@aliyun.com

Keywords: emulsion liquid membrane, morphology, osmotic pressure

Abstract. The purpose of this paper is to investigate the effect of osmotic pressure on the morphology of emulsion liquid membrane (ELM) by the visual way. The experimental results show that osmotic pressure has great effect on the globules of emulsion liquid membrane through water diffusion between two water phases. When under isotonic pressure, the water transport trend cannot be observed. When osmotic pressure is less than zero, water transfers from the internal phase to the external phase. But when osmotic pressure is larger than zero, water transports from the external phase to the internal phase first by diffusion, then water transports from the internal phase to the external phase by the coalescence. Therefore, it is possible to tailor osmotic pressure between two water phases to keep the stability of emulsion liquid membrane when ELM is used to separate some component.

Introduction

Water-in-oil-in-water ($W_1/O/W_2$) emulsion liquid membrane consists of dispersed oily globules containing smaller aqueous droplets. The smaller aqueous droplets are called the internal phase (W_1), continuous phase is called the external phase (W_2), and the layer of oil membrane separating W_1 and W_2 is called oil phase (O). Internal phase provides a reservoir for encapsulating sensitive substances so that the encapsulated substances can be released under the way of sustained release through this layer of oil phase [1-2]. In the past 20 years, emulsion liquid membrane has been studied in detail because they have potential applications in many fields, such as purification of compounds from industrial waste water, cosmetics, agroalimentary industry, especially in sustained-release of drugs [3-7]. Sachio Matumoto confirmed that the water transport under osmotic pressure gradient between the inner aqueous phase and the outer aqueous phase greatly influenced the viscosity of a series of diluted $W_1/O/W_2$ emulsions[8]. Osmotic pressure is an important factor accelerating or inhibiting the water transport, some researchers have investigated the effect of osmotic pressure on the release rate and stability of multiple emulsions [9-11].

This paper is to investigate the effect of osmotic pressure on the morphology of emulsion liquid membrane by visual way. The morphology of emulsion liquid membrane will be observed under different osmotic pressures. The morphology change of individual emulsion globule reveals the mechanism controlled by osmotic pressure. The study is significant to keep the stability of emulsion liquid membrane.

Material and Method

2.1 Raw Material

Paraffin was chosen as oil phase to prepare the $W_1/O/W_2$ multiple emulsion. The hydrophobic surfactant Span-80 (Dalian University of Technology Chemical Factory, China), and hydrophilic

surfactant Tween-80 (Longxi chemical factory, China), were used to stabilize the $W_1/O/W_2$ globules. The reagents mentioned above are all of C.R. grade. Potassium chloride and glucose are used to adjust the osmotic pressure difference, and they are A.R grade.

2.2 Method

2.2.1 Preparation

Preparation of W_1/O primary emulsion: internal aqueous phase was gradually added into the stirred oil phase with span-80 whose concentration is 4wt%, according to some ratios of oil solvent to water at 50℃, and the system was stirred by JRJ-300-1 shear machine (Shanghai Biaoben Factory) at 3500 rpm for 15 minutes.

Preparation of $W_1/O/W_2$ multiple emulsions: freshly prepared primary emulsion (W_1/O) was added to external aqueous phase with tween-80 whose concentration is 3wt%. The mixture was stirred gently for 10 minutes at room temperature at the speed of 400 rpm by a mixing machine JJ-1 (Changzhong Guohua Electric Machine Limited Corporation). The volume fraction of the primary emulsion was always 0.33.

2.2.2 Microscopic observation

A single multiple emulsion globule was observed by a XSP-BM microscope (Shanghai Shangguang limited corporation) equipped with a Nikon CooopPIX4500 camera (Nikon corporation, Japan). The change of morphology with time was taken photos under different osmotic pressures.

2.2.3. Stability studies

The drop size is observed using a optical microscope equipped with a camera. The mean diametere were calculated, calculated by D (3，2),

$$D(3,2) = \frac{\sum_i N_i D_i^3}{\sum_i N_i D_i^2} \quad (1)$$

Where Ni is the total number of droplets with diameter Di.

Results and Discussion

3.1Effect of osmotic pressure on the morphology of emulsion liquid membrane

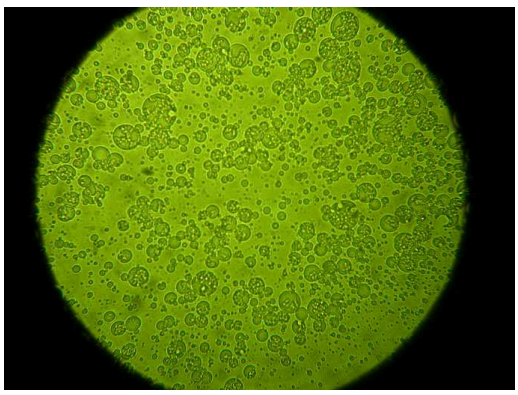

Fig. 1 The picture of ELM with deioned water both in the internal and external phase

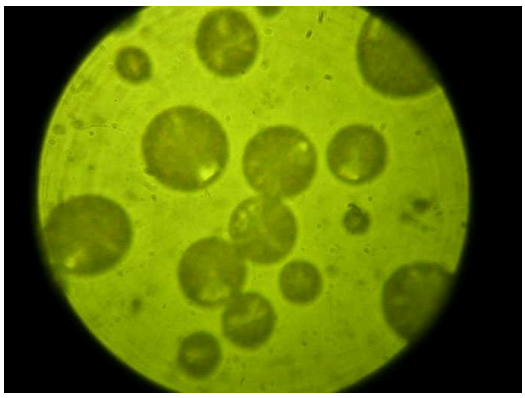

Fig. 2 The picture of ELM with 0.1mol/l KCl in the internal phase

When the internal phase and external phase are all deionized water, the morphology of emulsion liquid membrane is shown in Fig.1. When the internal phase is 0.1 mol/l KCl solution and the external phase is deionized water, the morphology of emulsion liquid membrane is shown in Fig.2. It is clearly that the droplet size from Fig.2 is larger than that from Fig.1. Two possible factors may lead to the above phenomenon: the addition of KCl has influence on the morphology of emulsion droplet, and osmotic pressure caused by the water transfer has effect on emulsion morphology.

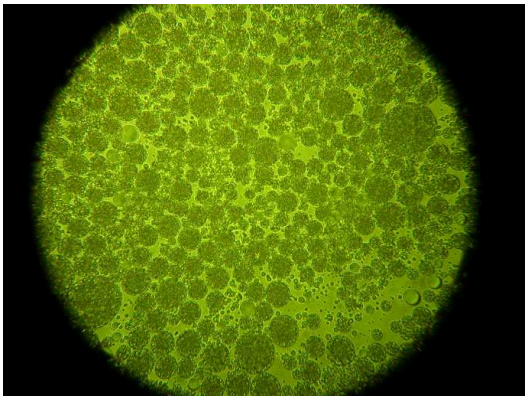

Fig. 3 The picture of ME with 0.1mol/lKCl in the internal phase while 0.2mol/l glucose is used to balance osmotic pressure

To illustrate the effect of osmotic pressure, ELM were prepared that the internal phase is 0.1 mol/l KCl solution and the external phase is glucose solution balanced the osmotic pressure between the two water phases. Fig. 3 shows the morphology of emulsion membrane system has no obvious change. So the effect of osmotic pressure causing water mass transfer should be the main reason for the change of morphology.

3.2 Effect of osmotic pressure on the morphology of individual globule

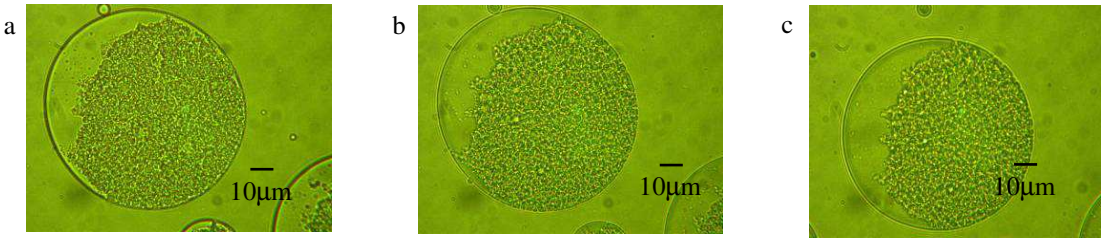

Fig. 4 The morphological change of a single ME globule with time when 0.01mol/l KCl both in the internal phase and in the external phase a.0min b.110min c.210min

In order to investigate the influence of osmotic pressure on water transfer in emulsion liquid membrane, a single globule is observed by visual method over time.

Fig.4 show the morphology of globule in which 0.01 mol/l KCl is added both in the internal and external phase, namely no osmotic pressure difference at this case. As we can see from the Fig.4, the droplet size changed little within 210 min. Therefore, the result proves that the present of osmotic pressure leads to water transfer so as to change the morphology of emulsion globule.

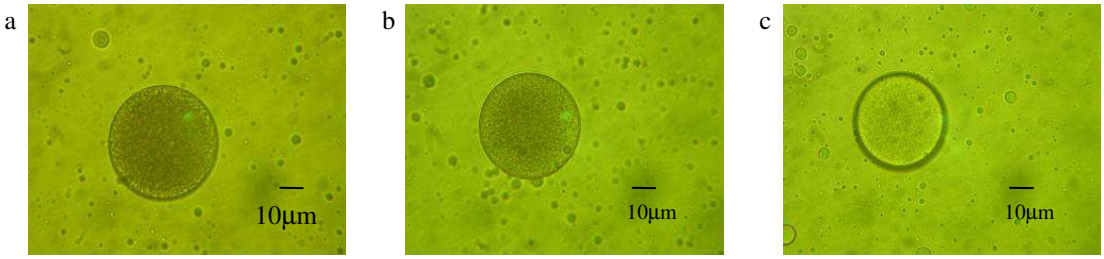

Fig. 5 The morphological change of a single ME globule with time when 0.005mol/l KCl in internal phase and 0.025 mol/l KCl in external phase a.0min b.20min c.120min

Fig.5 show the morphology of emulsion globule in which 0.005 mol/l mol/l KCl was added in the internal and 0.025 mol/l KCl was added in the external phase. Based on the van 't hoff osmotic pressure equation, $\Delta\pi = (C_{i0} - C_{e0})RT$, the osmotic pressure was calculated and $\Delta\pi < 0$, namely osmotic pressure less than zero at this case. As we can see from the Fig.5, the droplet size changed significantly within 120 min. The result proves that water can transfer from the internal phase to the external phase, and leading to the disappearance of water in the internal phase. As a result, multiple emulsion changes into simple emulsion.

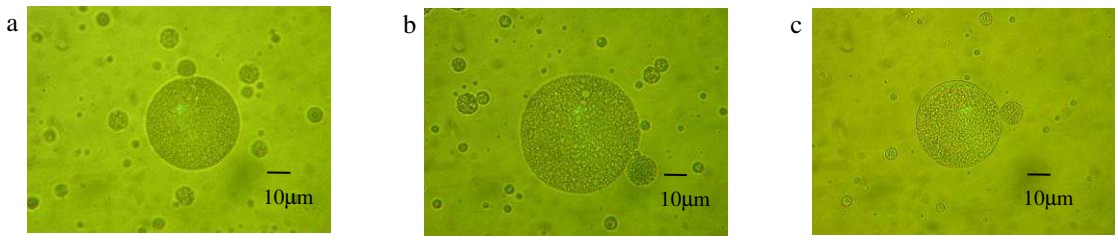

Fig. 6 The morphological change of a single globule with time when 1mol/l KCl in internal phase a.0min b. 70min c. 240 min

Fig.6 show the morphology of a globule in which 1 mol/l mol/l KCl was added in the internal. According to the van 't hoff osmotic pressure equation, $\Delta\pi = (C_{i0} - C_{e0})RT$, the osmotic pressure was larger than zero. As we can see from the Fig.6, the droplet size swells first, then the droplet size decrease within 240 min. Therefore, the result proves that water can transfer from the external phase to the internal phase, leading to the swelling in the internal phase. The increase of droplet size is due to swelling, and the reduction in droplets size was caused by the rupture with the swelling. In the process of observation, the coalescence of internal phase droplets and the suddenly disappearance can be observed.

Summary

The experimental results show that osmotic pressure has great effect on the morphology of globules through water transfer between the internal phase and the external phase. When under isotonic pressure, the water transport trend cannot be observed. When osmotic pressure is negative, water transports from the internal phase to the external phase. But when osmotic pressure is positive, water transports from the external phase to the internal phase first by diffusion, then transports from the internal phase to the external phase by coalescence. Therefore, it is possible to tailor osmotic pressure between two water phases to keep the stability of emulsion liquid membrane when it is used to separate some component.

Literature References

[1] Fechner, A., Knoth,A., Scherze,I., Muschiolik, G.. Food Hydrocolloids, Vol.21 (2007), P.943.

[2] Cournarie, F., Savelli, M. P., Rosilio, V., Bretez, F., Vauthier, C.,Grossiord, J. L., et al. European Journal of Pharmaceutics and Biopharmaceutics, Vol. 58(2004), P.477.

[3] J.L. Grossiord, M. Seiller, A. Silva-Cunha, in: M. Seiller, J.L. Grossiord (Eds.), Editions de Sant´e, Paris, 1998, P.57.

[4] Michael P. Aronson, Michael F. Petko, J. Colloid and interf Sci,1993, Vol. 159(1993),P.134.

[5] Silva-Cunha, J.L. Grossiord,F.Puisieux, International Journal of Pharmaceutics,Vol.158(1997), P.79.

[6] Paul Kent, Brian R.Saunders. J. Colloid interf Sci, Vol.242(2001), P.437.

[7] O.S. Matsumoto, J.Text. Stud. Vol.17(1986), P.141.

[8] J. Yan, R. Pal. J. Membr. Sci. Vol.190(2001), P.79.

[9] Jun Yan, Rajinder Pal. Journal of Membrane Science. Vol.213(2003) ,P.1.

[10] Li Weixuan, Dai Xing, Shi Yajun, S. Membrane Sci. and Tech. Vol.14(1990), P.40.

[11] Lixiong Wen. Kyriakos D.apadopoulos. Colloids and Surfaces A.Vol.174(2000),P.159.

Advanced Materials Research Vols. 881-883 (2014) pp 57-60

doi:10.4028/www.scientific.net/AMR.881-883.57

Stereo-controlled total synthesis of leodomycins A and B

ZHU Cheng-Lin [a,b] ZHANG Jian-Ting [a] CHEN Shi-Peng[a] FENG Jun-Min[a]
WANG Gao-Peng[a] LI Yu-Ping[b] HUANG Shuang-Ping [a*] WANG Xiao-Ji[a*]

[a] School of Pharmacy, Jiangxi Science and Technology Normal University, Jiangxi 330013, China;
[b] School of Life Science, Jiangxi Science and Technology Normal University, Jiangxi 330013, China

Keywords: synthesis, leodomycins, epoxidation

Abstract: A highly convergent formal synthesis of Ieodomycins A and B was achieved in 7 steps. The key features involved in the synthetic sequence of Ieodomycins A and B are the Sharpless asymmetric epoxidation and the Mukaiyama aldol reaction[1]. The synthesis of C-3 epimer of Ieodomycins A and B was also accomplished in good yields, but now just Heptyl diene aldehyde was getted thought 4 steps. Use Geraniol as meterials to make the corresponding aldehyde **(1)** via Swern oxidation. Though epoxidation, Wittig reaction and HIO_4 oxidation to get the intermediate . Useing it though few steps, the target molecule can be getted.

Ieodomycin A and B are active secondary metabolites of marine microorganisms[2].They have shown potent antimicrobial activity against Bacillus subtilis and Escherichia coli with minium inhibitory concentrations (MICs) of 32-64 μg/mL[3,4]. Since several pathogens are developing a resistance to antibiotics; there is an urgent need for new antimicrobial agents to combat the threats imposed by antibiotic-resistant pathogenic bacteria[5,6]. Recently, Koul, Videsh T. Salunkhe, Sandeep Bhosale,and Prasad Punde reported on the synthesis of leodomycin A and B starting from D-glucose in 15 steps. After that, Emmadi Narender Reddy , Atmakur Krishnaiah , Tadikamalla Prabhakar Rao make the stereoselective total synthesis of Ieodomycins A and B starting from geraniol in 12 steps. Now Heptyl diene aldehyde was getted by 4 steps. Each steps have high yield. The last intermediate molecular can be used to synthesis Ieodomycins A and B.

Change geraniol into the corresponding aldehyde **(1)** in 80% yield via Swern oxidation. The obtained aldehyde **(1)** was epoxidised with m-CPBA in DCM at 0˚C to give a racemic mixture of compound **(2)** in 85% yield.In the next step, the compound **(2)** was subjected to a Wittig reaction by treatment with methyltriphenyl phosphonium bromide in the presence of n-BuLi in dry THF to afford conjugated alkene **(3)** in 75% yield. Next, compound **(3)** was cleaved by using sodium periodate/periodic acid in aqueous THF solution at 0˚C to get the aldehyde **(4)** in 84% yield. Then though few steps Ieodomycin A and Ieodomycin B were getted. The studies outlined below demonstrate the feasibility of this approach in a synthesis of Ieodomycins A and B. Ieodomycin B was also obtained by intramolecular lactonization of leodomycin A, which was derived from Mukaiyama aldol reaction of compound **(7)**. **(7)** was prepared from aldehyde **(4)**, which was further obtained from genaniol.

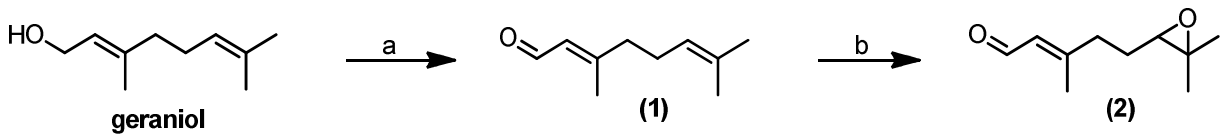

geraniol **(1)** **(2)**

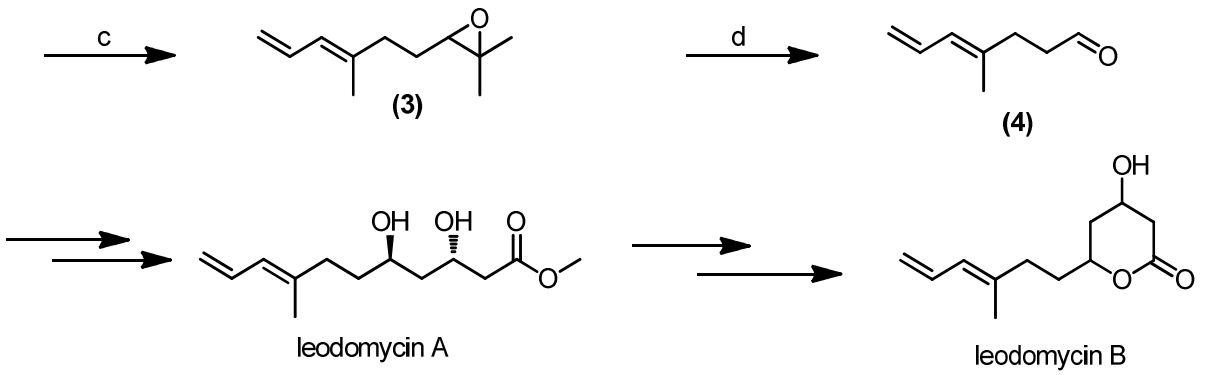

(a) $(COCl)_2$, DMSO, Et_3N, DCM, -78˚C to 0˚C , 80%; (b) m-CPBA, DCM, 0˚C , 0.5 h, 85%; (c) $Ph_3P{=}CH_2$, n-BuLi, THF, 0˚C , 75%; (d) HIO_4, THF:H_2O(5:3), 0˚C , 0.5 h, 84%.

Scheme 1

Experimental

Reaction were conducted under N_2 in anhydrous solvents such as DCM and THF. All reactions were monitored by TLC (silica-coated plates and visualizing under UV light). Light petroleum ether (bp 60-90˚C) was used. Yield refer to chromatographically and spectroscopically (^1H, ^{13}C NMR) homogeneous material. NMR spectra were recorded on Bruker AV-400MHz spectrometers. The solvents and reagents were purified and dried according to standard procedures: CH_2Cl_2, Et_3N, and TMSCl. Air-sensitive reagents were transferred by a syringe or double-ended needle. Evaporation of solvents was performed at reduced pressure on a EYELA totary evaporator.^1H and ^{13}C NMR spectra of samples in $CDCl_3$ were recorded on Bruker UXNMR FT-400MHz spectrometers. Chemical shifts (δ) are reported relative to TMS (δ = 0.0) as the internal standard. Mass spectra were recorded in ESI spectrometers, All high resolution mass spectra were recorded on QSTAR XL hybrid ms/ms system (Applied Bio systems/MDS sciex, foster city, USA), equipped with an ESI source (IICT, Hyderabad). Column chromatography was performed on silica gel (200-300 mesh) supplied by Qingdao Marine chemical factory, China. TLC was performed on Merck 60 F-254 silica gel plates. Optical rotations were measured with a JASCO DIP-370 Polarimeter at 25˚C .

1.1 aldehyde (1)

A well stirred solution of $(COCl)_2$ (9 mL, 97.24 mmol) in dry DCM (120 mL) was treated dropwise with DMSO (14 mL, 194.49 mmol) in dry DCM (50 mL) at -78 ˚C . The mixture was stirred for 15min before a solution of geraniol (10.0 g, 64.83 mmol) in dry DCM (60 mL) was slowly added. Stirring was continued at the same temperature for 30min and a solution of Et_3N (66 mL, 374.72 mmol) in dry DCM (80 mL) was added. The reaction mixture was stirred at -78˚C for 1 h and then the solution was allowed to warm to 0 ˚C overnight. Quenched by HCl solution (30 mL, 1 M). After shaking, the phases were separated, and the aqueous layer was extracted with Et_2O (3 × 100 mL). Combined organic layer was dried over anhydrous Na_2SO_4, filtered and concentrated in rotavapor. Residue was purified by silica gel column chromatography (n-hexane: EtOAc = 15:1) to afford the desired compound **(1)** as a colorless oil in 80% yield. ^1H NMR (400 MHz, $CDCl_3$): δ 9.98 (d, J = 8.0 Hz, 1H), 5.87 (d, J = 8.0 Hz, 1H), 5.07 (s, 1H), 2.25-2.18 (m, 4H), 2.16 (s, 3H), 1.68 (s, 3H), 1.62 (s, 3H).^{13}C NMR (400 MHz, $CDCl_3$): δ 190.022，162.545, 131.859， 126.659，122.048， 39.836， 25.073， 24.849， 16.885.

1.2 3,7,7-Epoxy octenal (2)

To a solution of **1** (7.88 g, 51.76 mmol) in DCM (300 mL) was added m-CPBA (12.51g, 75%, 54.35 mmol) over a period at 0 ˚C while stirring. After the addition, stirring was continued at the same temperature for 30 min to complete the reaction as indicated by TLC. The Reaction mixture was then quenched by the addition of a saturated $NaHCO_3$ solution (35 mL), and extracted with

DCM (3 × 80 mL). The organic layer was washed with brine and dried over anhydrous Na_2SO_4. The solvent was removed under vacuum, and the residue was purified by silica gel column chromatography (n-hexane: EtOAc = 20:1) to give **2** (7.40 g) in 85% yield. ^{1}H NMR (400 MHz, $CDCl_3$): δ 9.99 (d, J = 8.0 Hz, 1H), 5.90 (d, J = 8.0 Hz, 1H), 2.71 (t, J = 3.6 Hz, 1H), 2.41-2.33 (m, 2H), 2.19 (s, 3H), 1.78-1.68 (m, 2H), 1.30 (s, 3H), 1.28 (s, 3H). ^{13}C NMR (400 MHz, $CDCl_3$): δ 192.904, 164.702, 128.732, 64.780，59.045，38.967，24.732, 23.241，19.251, 18.964.

1.3 Epoxy -1,3-dioctylene (3)

Methyltriphenyl phosphonium bromide (19.24 g, 98%, 52.78 mmol) was dissolved in dry THF (89.5 mL) at room temperture under a nitrogen atmosphere. Then n-BuLi (50.59 mmol, 20.2 mL of a 2.5 Mol solution in cyclohexane) was added slowly to the stirred solution at 0 ˚C for 1 h. Subsequently compound **(2)** (7.40 g, 43.99 mmol) in dry THF (14.8 mL) was treated dropwise at -78˚C . Then the solution was allowed to warm to room temperature overnight. The reaction mixture was quenched with water (20 mL), and extracted with DCM (3 × 80 mL). The organic layer was washed with brine and dried over anhydrous Na_2SO_4. Filtered and concentrated in rotavapor. Residue was purified by silica gel column chromatography (DCM: Petrolem ether = 1:30) to get the light yellow oil (**3**) (5.49 g) in 75% yield. ^{1}H NMR (400 MHz, $CDCl_3$): δ 6.56 (ddd, J = 6.4, 10.4, 10.4 Hz, 1H), 5.88 (d, J = 10.8 Hz, 1H), 5.10 (d, J = 16.8 Hz, 1H), 5.00 (d, J = 10.0 Hz, 1H), 2.71 (t, J = 6.2 Hz, 1H), 2.24-2.16 (m, 2H), 1.77 (s, 3H), 1.70-1.63 (m, 2H), 1.30 (s, 3H), 1.25 (s, 3H). ^{13}C NMR (400 MHz, $CDCl_3$): δ 138.053， 133.073， 125.984， 115068， 64.205， 63.771， 36.386， 27.229， 24.788， 18.875.

1.4 Heptyl diene aldehyde

A solution of epoxide **3** (5.40 g, 32.48 mmol) in THF:H_2O (5:3, 86.4 mL) was treated at 0˚C with HIO_4 (8.97 g, 99%, 38.98 mmol). The resultant biphasic mixture was stirred at 0˚C for 30 min to complete the reaction as indicated by TLC. The reaction mixture was quenched with a saturated aqueous $NaHCO_3$ solution (20 mL), and extracted with DCM (3 × 60 mL). The combined organic layer was washed with brine, dried over anhydrous Na_2SO_4, The solvent was evaporated under reduced pressure, and the residue was purified by silica gel column chromatography (n-hexane: DCM = 5:1) to give a light yellow oil (**4**) (3.38 g) in 84% yield. ^{1}H NMR (400 MHz, $CDCl_3$): δ 9.78 (s, 1H), 6.54 (ddd, J = 10.8, 16.8, 10.4 Hz, 1H), 5.86 (d, J = 10.4 Hz, 1H), 5.12 (d, J = 16.8 Hz, 1H), 5.03 (d, J = 10.8 Hz, 1H), 2.56 (t, J = 8.2 Hz, 1H), 2.39 (t, J = 7.4 Hz, 1H), 1.77 (s, 3H). ^{13}C NMR (400 MHz, $CDCl_3$): δ 201.992， 136.948， 132.878， 126.189， 115.746， 41.906， 31.772， 16.686.

Acknowledgement

We thank the Natural Science Foundation of Jiangxi Province (No. 2010GZH0042), Scientific Research Fund of Jiangxi Provincial Education Department (No. KJLD12036).

References

[1] (a) Blunt, J. W.; Copp, B. R.; Munro, M. H. G.; Northcote, P. T.; Prinsep, M. R. Nat. Prod. Rep. 2004, 21, 1-49; (b) Faulkner, D. J. Nat. Prod. Rep. 2002, 19, 1-48; (c) Blunt, J. W.; Copp, B. R.; Munro, M. H. G.; Northcote, P. T.; Prinsep, M. R. Nat. Prod. Rep. 2005, 22, 15-61; (d) Blunt, J. W.; Copp, B. R.; Munro, M. H. G.; Northcote, P. T.; Prinsep, P. R. Nat. Prod. Rep. 2006, 23, 26-78; (e) Tsuda, M.; Mugishima, T.; Komatsu, K.; Sone, T.; Tanaka, M. J. Nat. Prod. 2003, 66, 412-415.

[2] Högberg, L. D.; Heddini, A.; Cars, O. Trends Pharmacol. Sci. 2010, 31, 509-515.

[3] Mojid Mondol, M. A.; Kim, J. H.; Lee, M. A.; Tarep, F. S.; Lee, H. S.; Lee, Y. J.; Shin, H. J. J. Nat. Prod. 2011, 74, 1606-1612.

[4] Salunkhe, V. T.; Bhosale, S.; Punde, P.; Bhuniya, D,; Koul, S.; Tetrahedron Lett. 2013, 54, 2489-2491.
[5] Reddy, E. N.; Krishnaiah, A.; Rao, T. P.; Tetrahedron: Asymmetry. 2013.
[6] (a) Huang, H. J.; Yang, W. B. Tetrahedron Lett. 2007, 48, 1429-1433; (b) Wegner, R.; Schulz, S. Tetrahedron 2002, 58, 315-320.

Advanced Materials Research Vols. 881-883 (2014) pp 61-64

doi:10.4028/www.scientific.net/AMR.881-883.61

Optimization of HS-SPME for GC-MS analysis of volatiles compounds in roasted sesame oil

Zhaoxi Fang[1, a], Guoqin Liu[1,2, b,*],Xuede Wang[2, c], Lijuan Han[1, d], Bingge Liu[2, e]

[1] College of Light Industry and Food Science, South China University of Technology, Guang zhou 510630, China

[2] College of Food Science and Engineering, Henan University of Technology, Zheng zhou 450001, China

[a]fangzhaoxi@163.com, [b]liuguoqin2009@126.com, [c]wangxuede1962@126.com, [d]hanlijuan.scut@gmail.com, [e]binggegeer@126.com

Keywords: Headspace SPME-GC-MS, Roasted sesame oil, DVB-CAR-PDMS fibre

Abstract: This paper was to develop a simple and rapid headspace solid-phase microextraction (HS-SPME) method coupled with gas chromatography–mass spectrometry (GC-MS) for the determination of volatiles compounds from the roasted sesame oil (RSO). A HP-5MS capillary column (30 m × 0.25 mm I.D. × 0.25 mm film thick) was used for GC-MS, and a 50/30 μm divinylbenzene/carboxen/polydimethylsiloxane (DVB/CAR/PDMS) fiber was used to extract volatiles compounds. The condition was optimized by varying the sample-to-headspace ratio (0.5-2.5 g/15 ml), extraction time (10-50 min) and Splitless time (0.5-4 min). The results showed that the optimal operating conditions occurred at (extraction temperature:40℃, sample-to-headspace ratio: 1.5 g/15 ml, extraction time: 40 min, Splitless time: 1 min) for the analyze method.

Introduction

Roasting sesame seeds and then pressing the seeds are common process for the production of sesame oil in Asia. The sesame oil has more characteristic aroma and taste than other vegetable oils. The characteristic aroma and taste of RSO is the most important element for Asian and more and more people has chosen it as natural salad oil, cooking oil, or seasoning ingredient [1]. Its aroma and taste is characterized by various volatile compounds which are low molecular weight compounds (less than 300 Da). However, the RSO is more expensive than other vegetable oils such as soybean oil, so the adulteration of RSO with other cheap edible oils is motivated by some edible oil industries [2]. Indubitably, the detection of adulteration is crucial for protecting consumer's rights and interests. In recently years, adulteration has become more sophisticated. An easily, rapidly, sensitivity, selectivity and accuracy analytical methodology is required for detecting adulterations [3]. Aiming to contribute to the current knowledge, using some volatile compounds as adulteration's markers of RSO may be an effective way to detect the adulteration.

HS-SPME has been proved to be a fast and convenient sampling method to define volatile compounds. It also has been successfully applied to study wine varieties [4], the adulteration of olive oil [5] and *etc.* Therefore, based on HS-SPME, the aim of this study was to optimize a HS-SPME method for monitoring volatile compounds of RSO and provide a scientific basis for further volatiles compounds research.

Materials and methods

Materials. RSO was prepared for method optimization from sesame seeds roasted at 200℃ for 20min and then pressed it.

Method optimization. Parameters investigated to optimize the SPME method were extraction temperature, sample-to-headspace ratio, extraction time and Splitless time. The sample-to-headspace ratio was optimized using 0.5, 1, 1.5, 2 and 2.5 g RSO weighed into reactivials (Supleco, 15 mL).

Optimal extraction time was determined using 10, 20, 30, 40 and 50 min extraction at constant temperature (40 ^{O}C). Splitless time was tested using 0.5, 1.0, 2.0, 3.0 and 4.0 min while the fibre was left in the injection port for 5 min.

HS-SPME-GC-MS. The fibre used for the extraction of the volatile components was divinylbenzene/carboxen/polydimethylsiloxane (DVB/CAR/PDMS) 50/30 um obtained from the Supelco Company, which has been used for many experiments to extract volatiles compounds [6]. The fibre was conditioned before use, as recommended by the manufacturer. Oil sample was placed into a 15 ml vial closed by PTFE/silicone septum. SPME needle inserted through the septum and then the fibre was exposed at 40 ℃ for 40 min with magnetic string(100 rpm). Then, the fibre was left into the injection port for 5 min. The injector of GC-MS was set at 240 ℃ and operated in the splitless mode for 1 min [7].

An Agilent 7890A GC coupled with an Agilent 5975C MS was used to perform the analysis. A HP-5MS capillary column (30 m×0.25 mm I.D.×0.25 mm film thick; Agilent Technologies, USA) was equipped, with purified Helium as the carrier gas, at a constant flow rate of 6 ml/min. The oven temperature was held at 40 ℃ for 2 min and then increased to 240 ℃ at a rate of 10℃/min, and finally held at 240 ℃ for 10 min. The MS interface temperature and ion source temperature were set at 250 ℃ and 200 ℃ respectively, and MS was scanned at 70 EV over 40-450 a.m.u. The mass spectrometer was operated in the full scan, and the area of each peak was determined by ChemStation software (Agilent Technologies). All samples were run in twice.

Data analysis. Optimization of extraction conditions was done using both total area counts from the Mass spectrum, and the ratio of total area counts to total number of peaks which was described by Kalua [8]. Duncan's multiple range test of the SPSS 13.0 (SPSS Inc., Chicago, USA) was performed to analyze the differences among samples. The significance level was 5%.

Results and discussion

Extraction temperature. 40 ℃ is widely used to extract volatiles compounds in the analysis of volatile compounds from olive oil [8,9]. RSO and olive oil both have been used as natural salad oil and seasoning ingredient. So we also chose 40 ℃ as the extraction temperature in the following study. In addition, as 40 ℃ is close to body temperature and it may be could simulate the similar headspace volatile profile of oil during human consumption [9]. Some articles showed that high temperatures such as 50 ℃ can accelerate the decomposition of natural substance and generate new oxidation products [10].

Sample-to-headspace ratio. In this study, the optimization of sample-to-headspace ratio was decreased by increasing the mass of RSO. From the results of Fig.1 (a), total peak area counts and the ratio of total area to number of peaks were showed no significant difference ($P < 0.05$) at 0.5g, 1g, 1.5g, 2g, 2.5g. The results might be different from some articles [11] which have reported that changing the Sample-to-headspace ratio may lead to differences in extraction efficiency. HS-SPME is an equilibrium extraction that involves the partitioning of analytes from aqueous phase to the gas phase and into the polymeric phase according to their partition coefficients. The equilibrium conditions can be simply described by Eq. (1) [12].

$$n = C_o K_{fs} V_f \tag{1}$$

where n is the extracted amount of the analyte, C_o is the initial concentration of the target analyte in the sample, V_f is the fibre coating volume, K_{fs} is the distribution coefficient of the analytes between the fibre coating and the sample.

In this equation, the amount of extracted analyte will correspond directly to sample's concentration, independing on the sample volume. It has an agreement with this article's results. In addition, the point at 1.5g has a smaller variance than others, so that we chose 1.5 g for the subsequent investigations.

Extraction time. The influence of extraction time on the area of peaks and the ratio of total area counts to total number of peaks has been shown in Fig.1 (b). Fig.1 (b) presents that total peak area counts increased until a maximum was reached at 40 min and then remained constant ($P < 0.05$). The ratio of total area to number of peaks showed no significant difference ($P < 0.05$) at 30, 40 and 50 min but these points were significantly different ($P < 0.05$) from the point at 10 min to the point at 30 min. However, the ratio of total area to number of peaks increased until the extraction time reached at 30 min. Considered total peak area counts and the ratio of total area to number of peaks, an extraction time of 40 min was chosen for subsequent investigations.

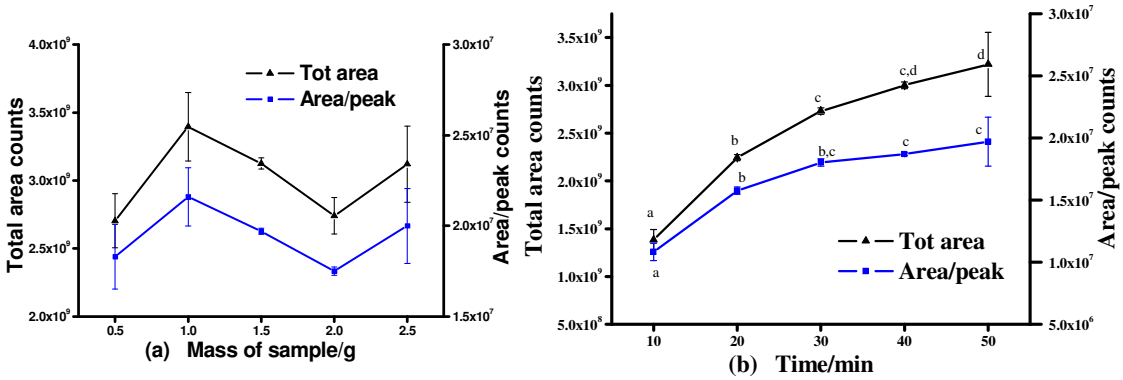

Fig. 1 Plot of total peak area and ratio of total peak area-to-number of peaks as a function of sample-to-headspace ratio (a) and extraction time (b), respectively.

Splitless time. The splitless time affects the efficiency of desorption process by controlling the amount of hydrocarbons into the capillary column. The influence of splitless time on the area of peaks and the ratio of total area counts to total number of peaks has been shown in Fig.2 (a). From Fig.2 (a), it could be observed that the total area counts showed no significant difference ($P < 0.05$) at 0.5, 1 and 2 min, but the point at 3 min was significantly different ($P < 0.05$) from others. The ratio of total area to number of peaks' tendency was closed to the total area counts. But, compared with the splitless time equal or less than 1 min, the massspectrometry of splitless time equal or more than 2 min had a higher baseline (Fig.2 (b)). So we can conclude that when splitless time equal or more than 2 min, more impurities desorbed into the capillary column and affected the test. In summary, a splitless time of 1 min was chosen for subsequent investigation.

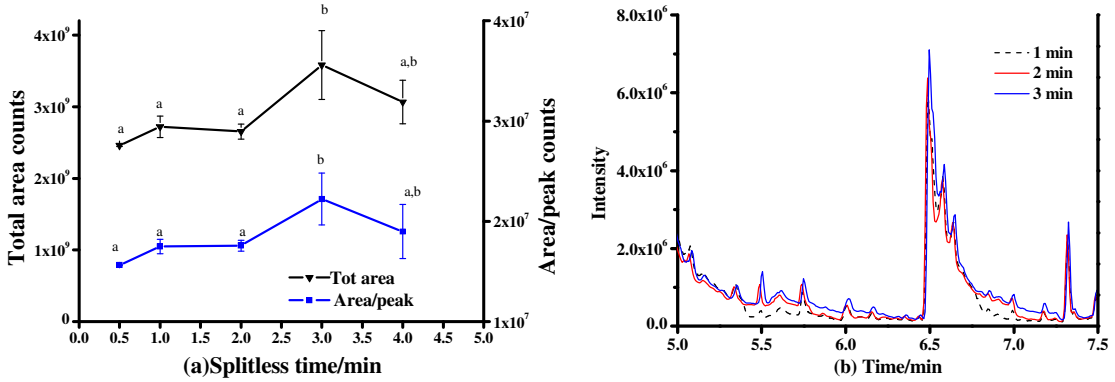

Fig. 2 Plot of total peak area and ratio of total peak area-to-number of peaks as a function of splitless time (a) and mass spectrum of splitless time optimization (b).

Summary

A total of volatile compounds extracted using a CAR/DVB/PDMS fibre was successfully identified using GC-MS. The paper optimized conditions of HS-SPME for the extraction of volatiles compounds in RSO and it using a single factor experimental design to study the variables of SPME, namely, extraction temperature, sample-to-headspace ratio, extraction time and splitless time. In this paper, both total area counts from the mass spectrum and the ratio of total area counts to total number of peaks were used to the optimization of extraction conditions. The optimal operating conditions

obtained were 40 ℃of extraction temperature, 1.5 g/15 ml of sample-to-headspace ratio, 40 min of extraction time and 1 min of splitless time.

Acknowledgements

We would like to gratefully thank the financial support from the National Natural Science Foundation of China (Project No. 31271885,31271884) , Key Projects in the National Science & Technology Pillar Program during the Twelfth Five-year Plan Period (Project No. 2012BAD37B01), and Public Welfare (Agriculture) Research Project (201303072).

References

[1] Lee, S. W., Jeung, M. K., Park, M. H., Lee, S. Y., & Lee, J… Effects of roasting conditions of sesame seeds on the oxidative stability of pressed oil during thermal oxidation. Food chemistry, 118(3) (2010), 681-685.

[2] Garcia, R., Martins, N., & Cabrita, M. J… Putative Markers of Adulteration of Extra Virgin Olive Oil with Refined Olive Oil: Prospects and Limitations. Food Research International (2013).

[3] García-González, D. L., & Aparicio, R… Research in olive oil: challenges for the near future. Journal of agricultural and food chemistry, 58(24) (2010), 12569-12577.

[4] Zhang, J., Li, L., Gao, N., Wang, D., Gao, Q., & Jiang, S… Feature extraction and selection from volatile compounds for analytical classification of Chinese red wines from different varieties. Analytica chimica acta, 662(2) (2010), 137-142.

[5] Mildner-Szkudlarz, S., & Jeleń, H. H... The potential of different techniques for volatile compounds analysis coupled with PCA for the detection of the adulteration of olive oil with hazelnut oil. Food Chemistry, 110(3) (2008), 751-761.

[6] Lee, E., & Choe, E... Changes in oxidation-derived off-flavor compounds of roasted sesame oil during accelerated storage in the dark. Biocatalysis and Agricultural Biotechnology, 1(1) (2012), 89-93.

[7] Cecchi, T., & Alfei, B... Volatile Profiles of Italian Monovarietal Extra Virgin Olive Oils via HS-SPME-GC-MS: Newly Identified Compounds, Flavors Molecular Markers, and Terpenic profile. Food Chemistry (2013).

[8] Kalua, C. M., Bedgood Jr, D. R., & Prenzler, P. D... Development of a headspace solid phase microextraction-gas chromatography method for monitoring volatile compounds in extended time–course experiments of olive oil. Analytica chimica acta, 556(2) (2006), 407-414.

[9] Contini, M., & Esti, M... Effect of the matrix volatile composition in the headspace solid-phase microextraction analysis of extra virgin olive oil. Food chemistry, 94(1) (2006), 143-150.

[10] Panseri, S., Soncin, S., Chiesa, L. M., & Biondi, P. A... A headspace solid-phase microextraction gas-chromatographic mass-spectrometric method (HS-SPME–GC/MS) to quantify hexanal in butter during storage as marker of lipid oxidation. Food chemistry, 127(2) (2011), 886-889.

[11] Keszler, Á., & Héberger, K… Influence of extraction parameters and medium on efficiency of solid-phase microextraction sampling in analysis of aliphatic aldehydes. Journal of Chromatography A, 845(1), (1999) 337-347.

[12] Pawliszyn, J. (Ed.)… Applications of solid phase microextraction (Vol. 5). Royal Society of Chemistry(1999).

Advanced Materials Research Vols. 881-883 (2014) pp 65-69

doi:10.4028/www.scientific.net/AMR.881-883.65

The Resonance Rayleigh Scattering Spectrum Characteristic of Tb^{3+}-GMFX-AR and the Determination of Gemifloxacin

XI Hui-ping[1, 2 a*], FANG Xiu-wei [2 b] ,

[1.] School of Resource and Environmental Engineering, Wuhan University of Technology, Wuhan ,China

[2.] He'nan Quality Polytechnic, Pingdingshan, henan ,China

[a.]Xihuiping1@163.com [b.] fangxiuwei@sohu.com

Keywords: Gemifloxacin; terbium (III); Alizarin Red; Resonance Rayleigh Scattering

Abstract: A new method for the determination of Gemifloxacin (GMFX) by using Resonance Rayleigh scattering was put forward. In HAc-NaAc buffer solution of pH 5 - 6, terbium (III) and antibiotics GMFX could form cationic complexes, which coulf further form 1 :2 : 1 (Tb3+ : GMFX :AR) ternary ion association complexes by the reaction with Alizarin Red (AR) anion through electrostatic and hydrophobic interaction. The new Resonance Rayleigh scattering (RRS) spectra would appear, and the two scattering peaks were located at 370nm and 590 nm. At 370 nm, the scattering enhancement (ΔI) was proportional to GMFX of certain concentration and its linear range and detection limit (3σ) were 0.005 ~ 4.00 μg.mL^{-1} and 14.5 ng.mL^{-1}. This method is simple, fast, with good selectivity and reproducibility, and it can be used for determination of GMFX drug in various body fluids.

Introduction

Gemifloxacin (GMFX) is the fourth-generation fluoroquinolone antibacterial drug developed jointly by the LG company of Korean and the GSK company of the United Kingdom, approved by the Food and Drug Administration (FDA) on sale in America and approved by the State Food and Drug Administration (SFDA) in China in July 2006. The formula of GMFX is shown in Figure 1. GMFX can simultaneously act on bacterial DNA gyrase and DNA topoisomerase IV, in improving the antimicrobial activity while reducing drug resistance. The activity of GMFX resistant to Streptococcus pneumoniae is stronger than ciprofloxacin, sparfloxacin, grepafloxacin, moxifloxacin and so on, as 30 to 60 times ciprofloxacin, 15 to 30 times levofloxacin. Its antibacterial activity of different strains pneumonia resistant to penicillin and erythromycin is 16 to 64 times ciprofloxacin and its effect against Haemophilus influenzae, Moraxella catarrhalis, Escherichia coli, Klebsiella pneumoniae is better than ciprofloxacin and levofloxacin. Currently the determination methods of this drug are high performance liquid chromatography [1-2], capillary electrophoresis[3], LC-MS/MS method [4], fluorescence quenching method [5].

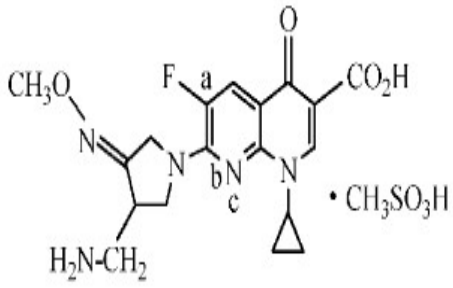

Fig.1 The chemical structure of GMFX

This study showed that, in HAc-NaAc buffer solution of pH5.50, GMFX antibiotics and Tb (Ⅲ) could form chelate cations, which could further form 1 :2 : 1 (Tb3+ : GMFX :AR) ternary ion association complexes by the reaction with Alizarin Red (AR) anion through electrostatic and hydrophobic interaction. This resulted in Resonance Rayleigh Scattering (RRS) significantly enhanced and new **RRS** spectra emergence. Based on it the new method using the resonance Rayleigh Scattering Spectroscopy to determinate GMFX was established, the linear range and the detection limit (3σ) of this method respectively 0.0 05 ~ 4.00 μg.mL^{-1} and 14.5 ng.mL^{-1}. The method was rapid, sensitive, and with good selectivity for the sample analysis, the average recovery was 100.25%, with an average relative standard deviation (RSD) 1.29%.

Experimental

2.1 Apparatus and Reagents

A RF-5301PC fluorescence spectrophotometer (Shimadzu Corporation, Japan) was used for recording fluorescence spectra and making fluorescence measurements. The absorption spectra were made on a Lab-Tech-1000 UV-visible spectrophotometer (Beijing, China). The pH was measured with a Model pHs-3CT meter (Shanghai, China).

The standard solution of Gemifloxacin (GMFX mesylate, Shanghai Institute of Organic Chemistry, purity ⩾ 99%): Weigh accurately the standard 0.1000g in a 50ml beaker, dissolve with water and transfer to a 100 ml brown volumetric flask, dilute with water to the mark, shake, formulate into 1.000 mg • ml^{-1} stock solution, place it in the refrigerator at 5 ℃ from light. Add water as needed to the desired concentration when used.

Tb^{3+} stock solution (1.0×10^{-2} mol·L^{-1}): Weigh 0.7477g Tb_4O_7 (Shanghai Sinopharm Chemical Reagent Co., Ltd., batch number: F20090116) in a 50 ml beaker, drop 1:1 HCl to it, heat in boiling water bath to dissolve, continue heating to evaporate, and add water until the steam nearly neutral to remove the excess acid, and then transfer to 100 ml brown volumetric flask, dilute with water to the mark, shake, store it in the refrigerator at 5 ℃ . Dilute to 1.0×10^{-3} mol • L^{-1} as the working fluid when used.

HAc-NaAc buffer solution: 0.20 mol · L^{-1}, pH = 5.5

Alizarin Red solution: 1.0x10^{-3} mol · L^{-1}.

All reagents were of analytical reagent grade without further purification. Water used throughout was doubly distilled water.

2.2 Experimental Methods

1.0 ml 1.0×10^{-3} mol • L^{-1} Tb^{3+} solution, 0.8 ml 1.0×10^{-3} mol • L^{-1} the AR solution, the appropriate quantity of GMFX standard solution and 1.0 ml HAc-NaAc buffer solution of pH5.50 were added into a 10.0 ml colorimetric tube in turn, diluted with water to the mark, thoroughly mixed and placed for 5 min. Then RRS intensity of the Tb3 +-GMFX -AR ternary ion-association complex (I)

and the blank solutions (I_0) were measured with the following settings of the spectrofluorimeter: excitation wavelength, λex = 370 nm, emission wavelength, λem = 370 nm, excitation and emission band-passes, 5 nm. And then calculate $\Delta I = I-I_0$.

Results and discussion

3.1 Resonance Rayleigh Scattering Spectral characteristics

Resonance Rayleigh scattering spectra of Tb3+-GMFX-AR system was shown in fig. 2. As shown in Fig. 2, the Resonance Rayleigh Scattering of GMFX, Tb^{3+} and AR respectively or two system of their composition was very weak, but when Tb3+-GMFX-AR three yuan ion association complex formed, the Resonance Rayleigh scattering of system significantly was enhanced, and the new Resonance Rayleigh scattering spectra appeared. The largest emission peak was at 370 nm, a smaller scattering peak near 590 nm. At 370 nm, Δ I value increased linearly with the concentration of GMFX, so it could be used for the quantitative determination of drug.

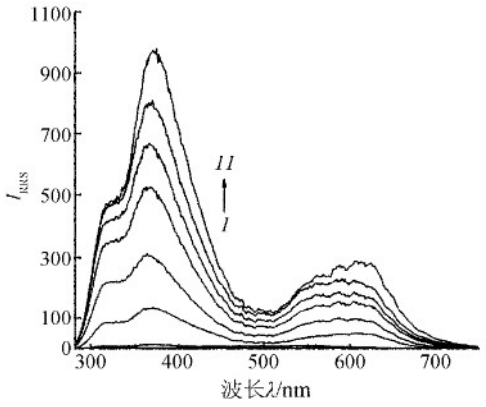

Fig. 2 RRS spectrum of Tb3+-GMFX-AR System
1：Tb^{3+}；2：AR；3：GMFX-AR；4：GMFX；
5：Tb^{3+}-GMFX；6：Tb^{3+}- AR；7-11：Tb^{3+}-GMFX-AR
$C_{Tb3+}=1.0\times10^{-4}$ mol·L^{-1}；$C_{AR}=8.0\times10^{-5}$ mol·L^{-1}；
C_{GMFX}（1，5，6）$=1.0\times10^{-6}$ mol·L^{-1}；C_{GMFX}（7-11）/$\times10^{-6}$:1.0，
4.0，6.0，8.0，10.0 mol·L^{-1}；pH= 5.50。

3.2 Effect of buffer solution and pH value

The effect of buffer medium on the scattering intensity of system was investigated. The results showed that, when the Britton-Robinson (B-R) buffer solution was used, PO_4^{3-} and Tb^{3+} in B-R buffer would form precipitate; while using HAc-NaAc medium, the sensitivity and the stability of the system were the best, and the suitable reaction acidity was pH 5.00-6.00. So HAc-NaAc solution of pH 5.50 was used as buffer solution, the optimal dosage was 0.60-1.50mL, the selection of volume was 1.00 mL in this experiment.

3.3 Dosage selection of Tb (Ⅲ) and Alizarin Red

For 2.0 μg/10 mL of GMFX, when 1.0×10^{-3} mol • $L^{-1}Tb^{3+}$ solution and 1.0×10^{-3} mol • L^{-1}AR dosage range respectively were 0.80-1.30 mL and 0.65-1.00 mL, the ΔI value of system was largest and substantially constant. So the amount of Tb (Ⅲ) and Alizarin Red used were respectively 1.00 mL and 0.80 mL.

3.4 Effect of ionic strength

The effect of ionic strength on the RRS intensity of system was investigated by adding strong electrolyte NaCl. The results showed that NaCl had no effect on RRS intensity of blank reagent, and it had basically no effect on RRS intensity of the three element system at NaCl concentrations below 0.02 mol • L^{-1}, but when the concentration of NaCl was further increased, it could cause ΔI values decrease gradually.

3.5 The order of reagents adding and stability of the system

The effect of the order of reagents adding on RRS intensity of system was studied. It was indicated that that for this system, when Tb3 +, AR, GMFX, HAc-NaAc buffer solution were added in turn, the ΔI values of system was max, and when ternary ion-association complex was formed, its RRS intensity at least was stable within 12h.

3.6 Calibration curve

A calibration curve was drawn by taking different amounts of GMFX standard solution according to experimental methods, the results indicated that the relative RRS intensity (ΔI) of system showed a linear relationship to the concentration of GMFX within the range of 0.005 ~ 4.00 μg • mL^{-1}, the linear regression equation was ΔI = 215C + 45.2 (C: μg • mL^{-1}), the correlation coefficient r = 0.9991, the detection limit (3σ) was 14.5 ng • mL^{-1}.

3.7 The influence of coexisting substances

The effects of coexisting substances on determination were studied too. The results showed that, for 2 μ g • mL^{-1} GMFX, with relative error less than ± 5%, the following substances (Times) did not interfere with the determination: maltose (1500), glucose, lactose, sucrose (1000), soluble starch, urea (750), L - phenylalanine L DL-, histidine, aspartic acid, Amari (15), niacin (8), NO_3^-, Zn^{2+} (100), Ca^{2+}, NH_4^+, SO_4^{2-}, Cl^- (80), Mn^{2+} (50), K^+ (35), I^- (20), Mg^{2+} (15). The smaller amount of Cu^{2+}, Al^{3+} and Fe^{3+} ions was allowed in system, but if 0.83mL 3.0mg • mL^{-1} thiourea solution was added to mask, the allowable amount of Cu^{2+} could increase to 5 times; 0.8mL 1.0mg • mL^{-1} solution of NH4F added , the allowable amount of Al^{3+} and Fe^{3+} could increase to 5 times. It was found that this method had good selectivity.

3.8 Determination of GMFX in tablets

The mesylate GMFX sample was dissolved in the water to appropriate concentration, filtered drily, the primary filtrate was discarded and then the continued filtrate was collected as sample solution. The sample solution was measured on the best experimental conditions with the working curve method, and the results were compared with high performance liquid chromatograph. The measurement results were shown in Table 1.

Table 1 The measurement results of GMFX in tablet (equivalent to the labeled amount%)

sample	This method			HPLC method						
	Measured values	mean	RSD	measured values					mean	RSD
Tablet 1	128.47 128.25 128.45 128.59 128.26	128.40	0.15	128.84	128.47	128.36	127.80	127.64	128.22	0.38
Tablet 2	113.36 113.35 113.35 113.35 113.36	113.35	0.01	113.16	113.14	112.84	112.95	113.53	113.12	0.21

3.9 Recovery test

The appropriate amount of GMFX reference solution was added in the sample solution, and the recovery was determined (Table 2). The average recovery rate was 100.25%, the average RSD was 1.29%.

Table 2 Recovery test (n = 5)

added amount (mg)	measured values (mg)					recovery (%)					mean recovery (%)	RSD (%)
100	98.24	103.14	103.14	103.14	103.14	98.24	103.14	103.14	103.14	103.14	102.16	2.2
150	149.69	148.62	151.47	150.34	150.02	99.79	99.08	100.98	100.23	100.01	100.02	0.68
200	193.88	196.47	198.47	198.47	198.47	96.94	98.24	99.24	99.24	99.24	98.58	1.0

Summary

A new method was proposed for the determination of Gemifloxacin (GMFX) indirectly by using Resonance Rayleigh scattering. At 370 nm, the scattering enhancement (ΔI) is proportional to GMFX of certain concentration. In addition to its stability, reproducibility and rapidity, this method had a wide linear range and low detection limit and it could be used for determination of GMFX drug in various body fluids.

References

[1] Sharif S， Khan I U， Sheikh T A， et al. Acta Chromatographica，2011，23（1）：95
[2] Nagavali D，Abirami G，Karar S K. Journal of Pharmary Research，2011，4（6）：1701
[3] Elbashir A A，Saad B，Ali A S M，et al. Journal of Liquid Chromatography，2008，31:1465
[4] Nageswara Raoa R，Gangu Naidua Ch，Guru Prasada K，et al. Biomedical Chromatography，2011，25:1222
[5] ZHONG Wen-Qing，WANG Yan，HUANG Bin，et al. China Academic Journal Electronic Publishing House，2012，32（6）：1570
[6] CHEN Guo-zhen，HUANG Xian-Zhi，ZHENG Zhu-Xin，et al. Fluorescence Analysis [M], Beijing：Science Press，1990：122
[7] LI Xiao-Yan，LI Shu-Wei，ZENG Ming，et al. Chinese Journal of Analysis Laboratory，2006，25（4）：38
[8] FU Li，LIU Bao-Sheng，CAO Dong-Lin，et al. Metallurgical Analysis，2007，27 （7 ）：26